CR-102776

INVESTIGATION INTO NUMERICAL SOLUTION OF

PARTIAL DIFFERENTIAL EQUATIONS

Final Report for Contract NAS 8-20136

June 1970

N70-74565

Final Report

Investigation into Numerical Solution of Partial
Differential Equations

Contract NAS8-20136

June 1970

Prepared For

The National Aeronautics and Space Administration

George C. Marshall Space Flight Center

Huntsville, Alabama

Tulane University

New Orleans, Louisiana

FOREWORD

This report was prepared by the Chemical Engineering Department with the cooperation of the Computer Laboratory of Tulane University, New Orleans, Louisiana, to report on the "Investigation into the Numerical Solution of Partial Differential Equations," of Contract NAS8-20136.

CONTENTS

Section I

Summary of Investigation

SUMMARY OF INVESTIGATION

Introduction. During the period from May 25, 1965, through
June 30, 1970, numerical solutions for four different classes
of problems described by partial differential equations have
been investigated under Contract NAS8-20136. The work per-
formed under terms of this contract will be described in this
final report.

The first section of this report is a summary of the
results of the work and a list of sources for a complete
description of the work. Each of the last four sections of
this report is a more detailed description of the work on one
class of problems. In most cases, these last four sections
are comprised of technical papers published in journals or of
excerpts from doctoral dissertations.

It should be noted at this point that new techniques were
needed for the numerical solutions of these problems and that
several of the methods developed may be useful in solving other
problems. The originality of the work performed under the
terms of this contract is attested to by the publication of
four papers in technical journals and the completion of five
doctoral dissertations on this work. In addition, two more
doctoral dissertations will be completed on work begun under
the contract, and there may be other papers published.
A complete listing of the publications and dissertations

SUMMARY OF INVESTIGATION

Introduction. During the period from May 25, 1965, through
June 30, 1970, numerical solutions for four different classes
of problems described by partial differential equations have
been investigated under Contract NAS8-20136. The work per-
formed under terms of this contract will be described in this
final report.

The first section of this report is a summary of the
results of the work and a list of sources for a complete
description of the work. Each of the last four sections of
this report is a more detailed description of the work on one
class of problems. In most cases, these last four sections
are comprised of technical papers published in journals or of
excerpts from doctoral dissertations.

It should be noted at this point that new techniques were
needed for the numerical solutions of these problems and that
several of the methods developed may be useful in solving other
problems. The originality of the work performed under the
terms of this contract is attested to by the publication of
four papers in technical journals and the completion of five
doctoral dissertations on this work. In addition, two more
doctoral dissertations will be completed on work begun under
the contract, and there may be other papers published.
A complete listing of the publications and dissertations

resulting from this contract is presented at the end of Section I of this report.

Major Classes of Problems Studied. The original problem studied under terms of this contract was a two-dimensional moving boundary problem. Analytic solutions for this type problem cannot be obtained, and very few attempts at numerical solutions have been successful. A successful numerical solution was obtained for this problem and resulted in the doctoral dissertations by Killeen and Stack.

As a part of one of the unsuccessful attempts at a solution for the moving boundary problem it was necessary to solve, numerically, for the velocity field in an ideal fluid. Numerical solutions for this problem in terms of the potential are well known, but a solution was desired in terms of the velocity components directly. This solution was obtained and published in the paper by von Rosenberg. As a result of this work, a more efficient method was developed by Gates, and his dissertation and the paper by Gates and von Rosenberg describe this work. The methods were so successful for solution of the unsteady-state potential flow problem (the elliptic-problem) that an attempt was made to apply this new method to the unstea state (parabolic) problem. The results of this work are described in the dissertation by Mount which was completed in May 1970.

resulting from this contract is presented at the end of Section I of this report.

Major Classes of Problems Studied. The original problem studied under terms of this contract was a two-dimensional moving boundary problem. Analytic solutions for this type problem cannot be obtained, and very few attempts at numerical solutions have been successful. A successful numerical solution was obtained for this problem and resulted in the doctoral dissertations by Killeen and Stack.

As a part of one of the unsuccessful attempts at a solution for the moving boundary problem it was necessary to solve, numerically, for the velocity field in an ideal fluid. Numerical solutions for this problem in terms of the potential are well known, but a solution was desired in terms of the velocity components directly. This solution was obtained and published in the paper by von Rosenberg. As a result of this work, a more efficient method was developed by Gates, and his dissertation and the paper by Gates and von Rosenberg describe this work. The methods were so successful for solution of the unsteady-state potential flow problem (the elliptic-problem) that an attempt was made to apply this new method to the unsteady state (parabolic) problem. The results of this work are described in the dissertation by Mount which was completed in May 1970.

Work had been started at Tulane on the development of numerical solutions for first-order hyperbolic equations before this contract was initiated. The continuation of this work was partially supported under this contract during the development of the solution for a transient, compressible flow problem including a moving shock. This work is described in the dissertation by Watts and the paper by Watts and von Rosenberg. Work is continuing to refine this method and extend it. This work will result in a dissertation by Royo.

At the request of a group in the Propulsion and Vehicle Engineering Laboratory at Huntsville, a mathematical model of the molecular sieve bed for the control of carbon dioxide in the environment of a space capsule was developed. This model was then solved numerically on the computer. Actually, three mathematical models of varying complexity were developed. The simplest one, which took much less computing time, was ·checked against the more complex models and found to be sufficiently accurate for purposes of predicting behavior of the bed. This work will be described in a dissertation by Schof.

Moving Boundary Problem. The physical problem studied is that of the draining of a liquid film from the walls of a tank. The co-ordinates were changed so that the governing equations are essentially the Navier-Stokes equations. These equations for the isothermal problem are

$$\frac{\partial w}{\partial z} + \frac{\partial v}{\partial y} = 0 \tag{1}$$

and

$$\frac{\partial w}{\partial t} + w\frac{\partial w}{\partial z} + v\frac{\partial w}{\partial y} = -g\frac{\rho_L - \rho}{\rho_L} + \frac{\mu}{\rho}\frac{\partial^2 w}{\partial y^2} \tag{2}$$

with the equation of the moving boundary given by

$$\frac{\partial \delta}{\partial t} + w\frac{\partial \delta}{\partial z} - v = 0 \tag{3}$$

where $\delta(z,t)$ is the width of the boundary. The other variables are defined at the end of this section. The complete non-isothermal problem which is more complicated, is discussed in Section II of this report. Only the method of solving the isothermal problem will be touched on in this summary.

Two problems are involved in obtaining a numerical solution to this problem. First, the location of the boundary at each new time level must be found from eqn. (3). Next, the velocity components, w and v, must be found from eqns. (1) and (2) in the entire liquid region. A two-dimensional grid of points was set up, and the values of w and v were determined at some of these discrete points.

In order to determine the location of the boundary of the liquid at the new time level, a finite difference analog to eqn. (3) was written for each row of points. Each of these equations contains the values of δ at two rows at the new time level. These equations were solved simultaneously with a material balance relationship so that the additional amount of

liquid at the new time level was set equal to the amount of fluid which flowed into the liquid region at the z = 0 boundary during the time interval between two successive time steps. Values of the velocity components at the old time level were used in these equations so that no iteration was required.

The values of the velocity components, w and v, were determined at the new time step for one new row of points at a time. An iterative procedure was used for the finite difference analogs which were centered in time. The values of w and v used in the coefficients in eqn. (2) were one iteration behind those determined at each iteration. Eqns. (2) and (1) were used alternately to determine first the w's and then the v's at the new time level.

Potential Flow Problems. In some of the early work on the moving boundary problem, it was necessary to determine the velocity field in the vapor, which was considered an ideal or inviscid fluid. For this fluid, eqn. (1) applies, but since the fluid has no viscosity, eqn. (2) does not apply. Instead, the requirement that the flow is everywhere irrotational is the second needed equation. This relation is

$$\frac{\partial w}{\partial y} - \frac{\partial v}{\partial z} = 0 \tag{4}$$

A numerical method for solving eqns. (1) and (4) simultaneously was developed. For the first method developed,

both w and v were determined at all the intersection points of a finite grid of horizontal and vertical lines. An iterative method was needed since the boundary conditions are given on all four sides of the region. Several efficient algorithms were developed for which the equations from several rows of points were solved simultaneously.

In the development of several of these multi-row methods, it was discovered that one-fourth of the equations containing one-fourth of the unknown values of w and v formed an independent set. In this set the values of w and v were located on different points in the grid, and the points at which w and v were located were arranged in a checkerboard pattern. Therefore, a new method was developed for the numerical solution of eqns. (1) and (4). This new method is clearly superior to the original method. In fact, for some grid sizes it is possible to obtain a direct solution to the finite difference equations with no iteration.

With such an efficient method available for the steady-state problem, it was decided to attempt the development of a "checkerboard" method for unsteady-state potential flow. Equation (4), the irrotationality condition, still applies to the unsteady state case, but eqn. (1), the continuity relation, must be modified by the addition of an accumulation term for the unsteady state case. This relation becomes

$$\frac{\partial w}{\partial z} + \frac{\partial v}{\partial y} = -\frac{\partial T}{\partial t} \tag{5}$$

where T is the flux potential which is temperature in the case of heat conduction. The flux components can be defined from the potential as

$$w = -\frac{\partial T}{\partial z} \tag{6}$$

and

$$v = -\frac{\partial T}{\partial y} \tag{7}$$

For this problem values of T at one-fourth the points of the original grid must be determined at each time, as well as values for w and v. Finite difference analogs to eqns. (4) and (5) and either (6) or (7) are necessary to determine the unknowns. A successful procedure was developed for this problem, and it apparently has some advantages over previously developed numerical methods for highly anisotropic problems.

Compressible Flow Problems. The differential equations for transient flow of a compressible fluid cannot be solved analytically and only recently have numerical or graphical methods been developed for these problems. Any type of solution is greatly complicated by shocks or discontinuities which move through the flow field. For this problem, a method had been developed for the numerical solution which worked very well until the development of a shock. The

development of a method of introducing and following the shock was continued under this contract.

The equations governing transient discharge of a compressible fluid from a duct of constant cross-section are

$$\frac{\partial b}{\partial t} = -u\frac{\partial b}{\partial x} - \frac{\partial u}{\partial x} \tag{8}$$

$$\frac{\partial u}{\partial t} = -u\frac{\partial u}{\partial x} - \exp\left[b(\gamma-1)\right]\frac{\partial b}{\partial x} \tag{9}$$

These equations apply for isentropic conditions and can be used even when a shock is present if the entropy change across the shock is small.

A centered finite difference method had been used to solve these equations numerically with excellent results up until the development of a shock. The shock forms and moves into and then out of the duct. All flow variables are discontinuous across the shock. Therefore, at the formation of the shock, a pair of moving points was introduced into the fixed grid. The values of the dependent variables on the two sides of the shock were assigned to these moving points, and these points were allowed to move through the fixed grid with the speed of the shock. Excellent results were obtained for this problem.

For shocks of higher strength the entropy change is too large for the isentropic equations to be used; so a third equation must be included in the mathematical model. Also, in

computing the position of the shock, the characteristics of the system were used. Therefore, in a continuation of this work, the equations in terms of these characteristics are the ones solved numerically. The characteristics are defined as

$$P = \frac{2}{\gamma-1} A + u \qquad (10)$$

$$Q = \frac{2}{\gamma-1} A - u \qquad (11)$$

and the governing differential equations in terms of these variables are

$$\frac{\partial P}{\partial t} + (u+A) \frac{\partial P}{\partial x} - A^2 \frac{\partial S}{\partial x} = 0 \qquad (12)$$

$$\frac{\partial Q}{\partial t} + (u-A) \frac{\partial Q}{\partial x} + A^2 \frac{\partial S}{\partial x} = 0 \qquad (13)$$

$$\frac{\partial S}{\partial t} + u\frac{\partial S}{\partial x} = 0 \qquad (14)$$

for a duct of constant cross-section.

At the present time, eqns. (12), (13), and (14) have been solved numerically. There is apparently some advantage over solving the equations in terms of the physical variables. A method is now being developed for introducing the shock into the solution of these equations. The conditions at a weak shock are much simpler in terms of the characteristics than in terms of the physical variables; so a definite advantage is expected in this case. The work on this problem will continue after termination of the contract.

<u>Molecular Sieve Adsorption Problem</u>. Carbon dioxide must be continuously removed from the environment of any manned space craft. For longer flights a molecular sieve adsorption bed is preferred over the lithium hydroxide cannisters currently used. The carbon dioxide can be desorbed from the molecular sieve bed which can then be reused to adsorb more carbon dioxide.

Several mathematical models of this adsorption bed were developed, and computer programs were written for the numerical solution of these models. The simplest model was sufficiently accurate for purposes of the laboratory and could be used to predict behavior of the bed in a very short time. This simple model will be discussed below; discussions of the more exact models are given in Section V of this report.

The heat effects of adsorption are included in the simplest model, but the temperatures of the gas and solid are assumed to be equal at any position in the bed. Furthermore, the loading of the carbon dioxide on the solid, w_s, is assumed to be constant throughout the solid pellet. Both these assumptions were justified from the results of the more exact models studied. Variations in the gas density caused by changes in pressure and temperature are also neglected, but these variations can be shown to be small by analysis. The resulting differential equations are

$$\frac{\partial w_s}{\partial t} = E_E \ (p - p_{ks}) \tag{15}$$

$$-u\frac{\partial p}{\partial x} - \frac{\partial p}{\partial t} = E_F \ \frac{\partial w_s}{\partial t} \tag{16}$$

$$u\frac{\partial T}{\partial x} + (1 + E_G) \ \frac{\partial T}{\partial t} = E_H \ \frac{\partial w}{\partial t} \tag{17}$$

In addition to these relations, an equilibrium condition is needed to relate w_s, the loading on the solid, to p_{ks}, the equilibrium partial pressure of the carbon dioxide in the gas phase. This equilibrium condition is a function of T, the temperature of the solid.

Finite difference equations analogous to eqns. (15) and (16) were written, and the unknown value of p was eliminated. This procedure resulted in a single relation between w_s and p_{ks} which was solved simultaneously with the equilibrium relation. The amount of iteration is minimized, and the solution proceeds very rapidly even though small increments in x and t must be used.

A model of the vacuum desorption case has also been developed. This model accounts for density variations in the gas since the pressures are extremely low. However, the results obtained from the computer runs show that the gas is removed from the bed as rapidly as it is desorbed.

During development of the adsorption model, a new analog for the partial pressure in the mass transfer term was utilized.

This diagonal analog was then applied to the equations for the counter-current heat exchanger which had been solved some years before. The results were so much improved that a publication resulted.

Nomenclature

A - dimensionless velocity of sound

b - $\ln(\rho/\rho_0)$

E_E - dimensionless mass transfer coefficient

E_F - ratio of capacitance of solid to gas for mass

E_G - ratio of heat capacity of solid to gas

E_H - ratio of heat of adsorption to heat capacity of gas

g - acceleration of gravity

p - partial pressure of carbon dioxide

p_{ks} - equilibrium partial pressure of carbon dioxide

P - $\frac{2}{\gamma-1} A + u$

Q - $\frac{2}{\gamma-1} A - u$

S - dimensionless entropy

t - time

T - temperature

u, v, w - velocity or flux components

w_s - loading of carbon dioxide on solid

x, y, z - co-ordinate directions

δ - co-ordinate of moving boundary

γ - ratio of heat capacities

μ - viscosity

ρ - density of gas

ρ_L - density of liquid

ρ_0 - reference density of gas

List of Dissertations and Papers

Dissertations

Killeen, Daniel B., August 1966

"Numerical Solution of Equations Describing An Unsteady Draining Process"

Watts, J. W., III, July 1967

"Numerical Solution of Partial Differential Equations Describing Compressible Flow From a Duct"

Stack, John E., Jr., August 1967

"Numerical Solution of Two-Dimensional Moving-Boundary Problem"

Gates, William J., June 1968

"Numerical Solution for Flux Components in Potential Flow"

Mount, Darrell E., April 1970

"Numerical Solution of Transient Potential Flow Equations"

Royo, Carlos M., in preparation

"Numerical Solution of Characteristic Equations for Transient, Compressible Flow"

Schof, David E., Jr., in preparation

"Numerical Solution of Microscopic-Macroscopic Systems and Related Potential Flow Problems"

Papers

von Rosenberg, D. U. "Numerical Solution for Flux Components in Potential Flow Problems." Mathematics of Computation, 21, (October 1967) pp. 620-28

Watts, J. W., and D. U. von Rosenberg. "A Numerical Solution of a Transient Shock Wave Problem." Chem. Eng. Sci., 24, (January 1969) pp. 49-56

von Rosenberg, D. U., and D. E. Mount. "Improved Numerical Solution of a Countercurrent Heat Exchanger." Chem. Eng. Sci., 24, (March 1969) pp. 619-20

Gates, W. J., and D. U. von Rosenberg. "An Improved Method of Numerical Solution for Flux Components in Potential Flow." Chem.Eng. Sci., 25, (March 1970) pp. 535-47

Section II

Moving Boundary Problem

PROBLEM DEFINITION

The physical system studied is that of a reservoir whose surface is at rest at time zero with vapor above the surface at a temperature higher than that of the liquid. As the liquid is drained out of the reservoir, a film forms on the wall and vapor condenses on the liquid surface simultaneously. The total vapor space above the liquid is relatively small so that condensed vapor on the dry wall above the initial liquid surface need not be considered in the problem.

The equations describing this process may be derived using basic physical laws. The result is that four partial differential equations are obtained. The equations relating the variables and their rates of change within the liquid are the continuity, momentum, and energy equations. In addition there is a partial differential equation involving the position of the boundary. This last equation is actually one of the boundary conditions. There are also other boundary conditions, both at the wall and at the liquid-vapor interface.

This type of problem has been analytically investigated by Sparrow and Gregg (11), Chung (2), and O'Laughlin (8). Killeen (7) developed a finite difference solution to the isothermal drainage problem with certain restrictions in the model. The discussion of an expanded model for the isothermal case will be presented in the next chapter.

The actual equations and boundary conditions are given by Chung (2). In Figure 3-1, a sketch of the physical picture of the film is shown.

$x = 0$

y

x

$T = T_s$

$T = T_b$

v

u

$y = \delta (x, t)$

$x = St$

$T = T_b$

S
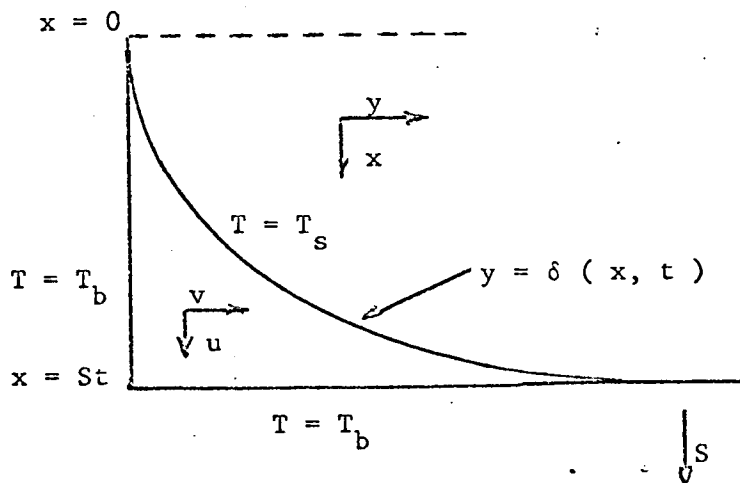
Figure 3-1 - Film for Drainage with Condensation

The equations describing this system are:

Continuity

$$\frac{\partial u}{\partial x} + \frac{\partial v}{\partial y} = 0 \qquad (3.1)$$

Momentum

$$v \frac{\partial u}{\partial y} + u \frac{\partial u}{\partial x} + \frac{\partial u}{\partial t} = E_2 + E_3 \frac{\partial^2 u}{\partial y^2} \qquad (3.2)$$

Energy

$$v \frac{\partial T}{\partial y} + u \frac{\partial T}{\partial x} + \frac{\partial T}{\partial t} = E_1 \frac{\partial^2 T}{\partial y^2} \qquad (3.3)$$

Boundary Conditions

at $y = 0$; $u = 0$, $v = 0$, $T = T_w$ (all x and t)

at $y = \delta\,(\,x,\,t\,)$; $\dfrac{\partial u}{\partial y} = 0$, $T = T_s$; $\dfrac{\partial \delta}{\partial t} + \dfrac{u}{} \dfrac{\partial \delta}{\partial x} - v =$

$$E_4 \frac{\partial T}{\partial y} \qquad\qquad\qquad (\,3.4\,)$$

x and y are independent variables representing distance

t is an independent variable denoting time

u is the x-component of velocity

v is the y-component of velocity

T is the temperature

S is the constant drainage velocity at which the surface of

the bulk of the liquid is being lowered. At this surface

where $x = St$, additional boundary conditions are:

$$u = u\,(\,y,\,t\,) \text{ and } T = T_b$$

The physical constants E_1, E_2, E_3, and E_4 are given as

follows:

$$E_1 = k\,/\,\rho c$$

$$E_2 = g\,(\,\rho - \rho v\,)\,/\,\rho$$

$$E_3 = \mu\,/\,\rho$$

$$E_4 = k\,/\,\lambda\,\rho$$

It is clear that in solving this problem, consideration must

be given to the energy and mass transfered at the interface.

This problem is studied in two parts. First an attempt is

made to develop a better model for the isothermal drainage problem

as presented by Killeen (7). Then this expanded model is to be

used to solve the general problem.

DISCUSSION OF THE ISOTHERMAL DRAINAGE PROBLEM

The unsteady drainage problem represents a much simpler physical problem than the one presented in the previous chapter. There is no mass or energy transfer at the interface. Thus the energy equation and the energy term in the boundary equation are omitted. The set of equations reduces to:

Continuity

$$\frac{\partial u}{\partial x} + \frac{\partial v}{\partial y} = 0 \qquad (4.1)$$

Momentum

$$v \frac{\partial u}{\partial y} + u \frac{\partial u}{\partial x} + \frac{\partial u}{\partial t} = E_2 + E_3 \frac{\partial^2 u}{\partial y^2} \qquad (4.2)$$

Boundary Conditions

at $y = 0$; $u = 0$, $v = 0$ (all x and t)

at $y = \delta (x, t)$; $\frac{\partial u}{\partial y} = 0$; $\frac{\partial \delta}{\partial t} + \frac{u}{} \frac{\partial \delta}{\partial x} - v = 0$

$$(4.3)$$

at $x = 0$; $u = u (y, t)$

Since much of the work done in solving this set of equations numerically is closely connected with the work on the non-isothermal problem, it is felt necessary to present a general outline of the steps used by Killeen (7) in his solution. In his solution, use

14

was made of the fact that the film formed by the draining of a
liquid is the same as the film formed on a plate which is withdrawn
from the liquid. This equivalence was shown by Van Rossum (13).
The equations given above are transformed so that distance is
measured upward from a reference plane on the surface of the bulk
liquid which moves downward with a velocity S. The transformed
distance is z = St - x. In addition, a new variable representing
the velocity upward with respect to this moving reference plane is
defined as w = S - u. The various transformations are given by
Killeen (7). The result is that the equations have the form:

Continuity

$$\frac{\partial w}{\partial z} + \frac{\partial v}{\partial y} = 0 \qquad\qquad (4.4)$$

Momentum

$$v\,\frac{\partial w}{\partial y} + w\,\frac{\partial w}{\partial z} + \frac{\partial w}{\partial t} = -E_2 + E_3\,\frac{\partial^2 w}{\partial y^2} \qquad (4.5)$$

Boundary Conditions

at y = 0; w = s, v = 0

at y = δ (z, t); $\frac{\partial w}{\partial y} = 0,\quad \frac{\partial \delta}{\partial t} + \frac{w\,\partial \delta}{\partial z} - v = 0$

$$(4.6)$$

at z = 0; w = w (y, t)

Dimensionalization of the variables was then made by Killeen
(7).

His method follows:

1. All lengths divided by δ_o, the thickness of the film

   at z = 0.

2. All velocities divided by S, the drain velocity.

3. All time divided by δ_o / S.

The boundary conditions then become:

at y = 0; v = 0, w = 1

at y = δ; $\dfrac{\partial w}{\partial y} = 0$

at z = 0; δ = 1, w = w (y, t)

The dimensionalization of course redefines the actual values of the

constants E_1 and E_2. They are now given as follows:

$$E_2 = \delta_o \, g \, (\rho - \rho v) \; / \; S^2 \rho$$

$$E_3 = \mu \; / \; \rho S \delta_o$$

To solve the problem, a velocity profile at z = 0, typical of

boundary layer flow was chosen as:

$$w_o = 1 - \frac{3}{2} y + \tfrac{1}{2} \, y^3$$

In the actual numerical solution, analogs centered about half-

time levels were written for the momentum equation. For a given row,

there may or may not have been liquid at the old time step near the

boundary. A four-row averaging technique was employed if there was

liquid at the old time step, and a three-row averaging method was

used when liquid was not present at the old time step. Centered-

difference equations were written at the new time level to solve the

continuity equation for v. The procedure for locating the boundary at each time step was an important part of the solution. Analogs for the boundary equation were written between successive rows, starting with the second and third and continuing to the last two. Each of these equations contains the length of two rows. These were used in conjunction with an overall mass balance. In this balance, the mass entering the system during one step at $z = 0$ is equated to the sum of the changes in mass in each row during that time step. This relation contains the lengths of all of the rows and together with the other boundary equations gives a sufficient number of equations for solution.

In his model, Killeen used the assumption that the liquid layer at $z = 0$ is of length δ_o at $t = 0$ and remains constant thereafter. This assumption seemingly caused the eventual breakdown of the solution. Eventually a situation is reached in which there is not enough fluid entering at $z = 0$ to be distributed among the rows which are present. It is here that a further study of this model has been principally concentrated.

The computer program listing for the numerical solution is shown in the work of Killeen (7). It consists of a main program and four subroutines. Since $\Delta y = \Delta z$, the solution is set up so that the number of rows increases by one during each succeeding time step. In starting up, the main program is used to calculate the number of fluid increments in the second row after one time step. The WF subroutine is used to calculate w's at this new row, and the VF subroutine is used to calculate the v's. These calculated

velocity components are then used in the GETJB subroutine to

compute the number of fluid increments at the second and third rows

after the next time step. The velocity subroutines are then used

to calculate new velocity values at these rows. The entire procedure

is then repeated for as many time steps as possible.

The momentum equation is used in the WF subroutine to compute

the values. Values of w and v which appear as coefficients in this

equation are obtained by an averaging and iteration procedure. After

the values of w have been calculated, they are used in the continuity

equation to compute the v's. The boundary equation analogs together

with the overall mass balance are used in the GETJB subroutine to

calculate new values of the boundary. This solution was carried out

for a variety of increment sizes and ratios. It was found that the

best ratio of Δz to Δy was unity and the ratio of Δy to either of

these varied between four and sixteen. This essentially concludes

the discussion of the numerical solution by Killeen (7).

Before attempting to develop a better model, a preliminary

study of various aspects of the existing solution was made. First,

the errors generated in the iteration procedure used in the calcula-

tion of the velocity components were investigated.

Investigation of Iteration Procedures

In Figure 4-1, the points where the w's and v's are calcu-

lated are shown:
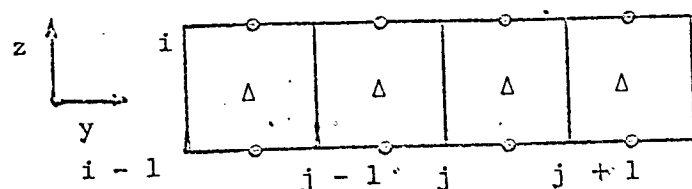

Figure 4-1 - Grid for Velocity Calculations

The w's are calculated at the I th row at the 0-points from the momentum equation and the v's at the Δ-points from the continuity equation. The momentum equation analogs are centered about the Δ-points at the half-time level and the w's and v's are thus needed at these points. For the first iteration, the values used are:

$$w(i - \tfrac{1}{2}, j - \tfrac{1}{2}, n + \tfrac{1}{2}) = \tfrac{1}{2}\left[w(i - 1, j - \tfrac{1}{2}, n) + w(i, j - \tfrac{1}{2}, n)\right] \qquad (4.7)$$

$$v(i - \tfrac{1}{2}, j - \tfrac{1}{2}, n + \tfrac{1}{2}) = v(i - \tfrac{1}{2}, j - \tfrac{1}{2}, n) \qquad (4.8)$$

After these have been used in the calculation of the w's at the I th row and the v's at the I $-$ $\tfrac{1}{2}$ row, the new values of the coefficients are:

$$w(i - \tfrac{1}{2}, j - \tfrac{1}{2}, n + \tfrac{1}{2}) = \tfrac{1}{4}\left[w(i - 1, j - \tfrac{1}{2}, n) + w(i, j - \tfrac{1}{2}, n) + w(i - 1, j - \tfrac{1}{2}, n + 1) + w(i, j - \tfrac{1}{2}, n + 1)\right] \qquad (4.9)$$

$$v(i - \tfrac{1}{2}, j - \tfrac{1}{2}, n + \tfrac{1}{2}) = \tfrac{1}{2}\left[v(i - \tfrac{1}{2}, j - \tfrac{1}{2}, n + 1) + v(i - \tfrac{1}{2}, j - \tfrac{1}{2}, n)\right] \qquad (4.10)$$

These values are used to obtain new estimates of w's and v's from the momentum and continuity equations. This procedure is continued until the values converge.

It is possible that errors which occur from incomplete convergence during the first few time steps could greatly affect the calculations for w and v at late time steps, especially those at the uppermost rows.

These runs were made with a $\Delta y / \Delta z$ ratio of 16 with $\Delta y = 1/48$ and $\Delta z = 1/768$ for a period of about 35 time steps. The values of the velocity components obtained were the same to four decimal places for 5 iterations. A series of runs were made in which 3, 5, 7 and 10 iterations were made at each time step before the calculations proceded to the next time level. Simular results were obtained for other increment sizes and ratios.

The computed values which should be most affected by errors are those at the uppermost row after many time steps, since these values are necessarily affected by all previous calculations in both time and space. It is significant that the use of a relatively small number of iterations such as five, produces the same results to four decimal places as does the use of a large number of iterations. This result indicates that the analogs used have good stability and convergence properties.

Study of Boundary Location Procedures

In the determination of the location of the fluid boundary at each row at every time step, the variable used the computation by Killeen was the discrete number of fluid increments, not the actual distance. This variable is defined as:

$$\delta (I) = \left[JB (I, 2) - 1 \right] \left(\Delta y \right) \qquad (4.11)$$

In the solution for the JB's at a new time level, the values of JB at the old time level are involved. These new values of the JB's are obtained in decimal or floating point form and converted to integer form for use as an index. In this procedure, the fractional

part of the value is truncated. In Killeen's procedure, integer

values were used in the calculation of JB's at the next time level.

Decimal values at the old time level were used in the compu-

tation of the boundary at the new time. The result was altered

slightly, but not enough to be a significant improvement in the

solution.

In the boundary equation analogs, w and v appear as coeffi-

cients. In his solution, Killeen (7) used the values at the Δ-

point at the old time level as indicated in Figure 4-2.
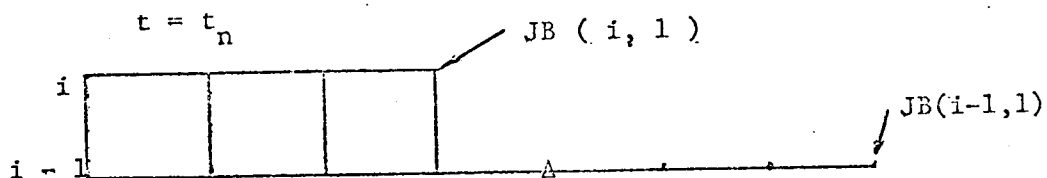
Figure 4-2 - Grid for Velocity Coefficients at the Boundary

The Δ -point has the value:

$$\Delta \text{ -point} = \frac{JB\ (\ i,\ 1\ )\ +\ JB\ (\ i\ -\ 1,\ 1\ )\ -\ 1}{2} \qquad (\ 4.12\ )$$

A study of the way in which these coefficients are chosen

indicates that slightly better results are obtained if the values

of w nearest the boundary at the I th and I - 1 rows at the old

time level are averaged and used in the equations. A simular

procedure is used for the v coefficient.

Expanded Model for Isothermal Drainage

The preliminary work on the original model by Killeen (7) was done in order to facilitate studies for other models of this process. In addition to the above work, the computer program for the numerical solution was more compact by eliminating unneeded storage space of data. In the original program, storage was provided for all the values of w and v at both the old and new time levels. During the calculation procedures at the new time level for w at the I th row, the only values needed at the old time level are those at the I and I - 1 rows. This makes it possible to use only two subscripts for w, thereby reducing storage considerably. Only one row of v's at the old time level are needed so the dimensions for v may also be reduced by one.

As stated earlier, the probable cause of the eventual break-down of the numerical solution occurs because not enough fluid enters during a time step to be distributed among the rows after their number becomes large. Therefore the nature of the boundary layer flow at z = 0 needs to be investigated.

The boundary layer flow near a submersed plate which is suddenly set in motion has been studied by Schlichting (10) and others. It was found that the thickness of the boundary layer can be expressed as a function of time. The relation is:

$$\delta (t) = 4 \sqrt{\nu t} \qquad (4.13)$$

where ν is the kinematic viscosity.

The boundary layer flow at z = 0 in the drainage problem may
also be viewed as that made by a submersed plate suddenly set in
motion. Referring to Figure 4-3 it is seen that at z = 0, there is
a continuous body of fluid above that point.
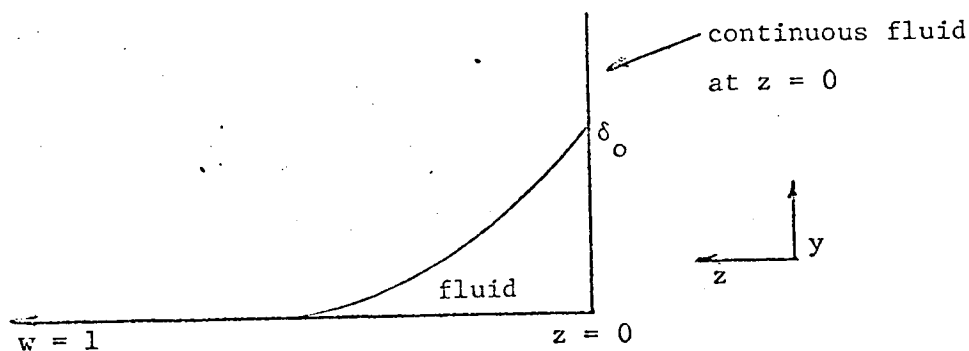
Figure 4-3 – Boundary Layer Flow at z = 0

Since the two processes are very much alike physically, the expression
for δ may be used at z = 0 to obtain a more realistic and better
numerical solution.

In working with this problem, it was decided to redimension-
alize the variables as follows:

1. All lengths divided by ν / S

2. All velocities divided by S, the drain velocity.

3. All time divided by ν / S^2

The form of the equation is not changed, but the values of the
constants are redefined. These new values are:

$$E_2 = g \nu (\rho - \rho v) / \rho S^3$$

$$E_3 = 1$$

Mathematically, the equation for δ_o at $z = 0$ takes on a simplified form. This is shown in the following series of steps. All primed quantities represent dimensionless variables. The variables which are dimensionalized in the equation are δ and t. The relations are:

$$\delta' = \delta / (\nu / S) \quad \text{and} \quad t' = \frac{t}{\nu / S^2} \qquad (4.14)$$

or

$$\delta = \frac{\nu}{S} \delta' \quad \text{and} \quad t = \frac{\nu}{S^2} t' \qquad (4.14a)$$

Substituting into the expression $\delta = 4\sqrt{\nu t}$

$$\frac{\nu}{S} \delta' = 4 \sqrt{\frac{\nu \nu}{S^2} t'} \qquad (4.15)$$

or

$$\delta' = 4 \sqrt{t'} \qquad (4.15a)$$

Thus a very simple relation for δ' in dimensionless form is obtained. In the actual numerical solution, the original symbols, δ and t, are retained.

The procedure used to adapt this relation for use in the numerical solution is shown in the following steps:

1. At any time t, $t = (IM - 1) (\Delta t)$ since $IM = 1$ at $t = 0$ and one extra row of fluid is obtained for each time step.

2. $\delta_o = \left[JB(1,2) - 1 \right] \left[\Delta y \right]$ where the subscript 1

represents the first row and the subscript 2 indicates

the new time level.

3. After substitution the equation has the form:

$$\left[JB(1,2) - 1 \right] \left[\Delta y \right] = 4 \sqrt{(IM-1)\Delta t} \qquad (4.16)$$

or

$$JB(1,2) = 1 + 4 / \Delta y \sqrt{(IM-1)\Delta t} \qquad (4.16a)$$

This relation for JB (1, 2) may then be used directly in the
solution for all the JB's.

In the solution for the location of the boundary, the first
step necessary is to develop an expression for the mass balance by
using the new relation for δ_o.

The mass balance representing the amount of fluid entering
the system at z = 0 during one time step has the form:

$$\sum_{I=2}^{IM} \left[\rho (JB(I,2) - 1) \Delta y \Delta z - \rho (JB(I,1) - 1) \Delta y \Delta z \right]$$

$$= \int_{t}^{t+\Delta t} \int_{y=0}^{y=\delta_o} w_o (y, t) \, dy \, dt \qquad (4.17)$$

The same boundary layer velocity profile as before is used, but is now fitted to a growing δ_o. The relation is:

$$w_o\ (\ y,\ t\ ) = 1 - 3/2\ (\frac{y}{\delta_o}) + \tfrac{1}{2}\ (\frac{y}{\delta_o})^3 \qquad (\ 4.18\ )$$

The mass balance then becomes:

$$\rho\ \Delta\ y\ \Delta\ z\ \sum_{I\ =\ 2}^{IM}\ \left[JB\ (\ I,\ 2\ ) - JB\ (\ I,\ 1\ )\right] \qquad (\ 4.19\ )$$

$$= \rho \int_{t}^{t\ +\ \Delta\ t} \int_{y\ =\ 0}^{y\ =\delta_o} \left[1 - 3/2\ (\frac{y}{\delta_o}) + \tfrac{1}{2}\ (\frac{y}{\delta_o})^3\right]\ dy\ \ dt$$

Integrating with respect to y the equation is:

$$\Delta\ y\ \ \Delta\ z\ \sum_{I\ =\ 2}^{IM}\ \left[\ JB\ (\ I,\ 2\ ) - JB\ (\ I,\ 1\ )\ \right]$$

$$= \int_{t}^{t\ +\ \Delta\ t} \left[\ y - \frac{3}{2\delta_o}\ \frac{y^2}{2} + \frac{1}{2\delta_o^3}\ \frac{y^4}{4}\ \Big|_{o}^{\delta_o}\ \right]\ dt$$

$$= \int_{t}^{t\ +\ \Delta\ t} 3/8\ \delta_o\ \ dt \text{ with } \delta_o = 4\sqrt{t} \qquad (\ 4.20\ )$$

Since δ_o is known as a function of t, this expression may be integrated to give a relation involving the time at the beginning and end of the time step. If however, the value of the integral is approximated by averaging the value of the integrated at the two

limits and multiplying by Δt, a much simpler expression results. The equation then has the form:

$$\Delta y \, \Delta z \sum_{I=2}^{IM} \left[JB(I,2) - JB(I,1) \right]$$

$$= 3/8 \, \Delta t \left[\frac{\delta_o \big|_{t+\Delta t} + \delta_o \big|_t}{2} \right] \qquad (4.21)$$

Since $\Delta z = \Delta t$, these may be cancelled on both sides of the equation. Substituting the expression for δ_o at both times, the equation becomes:

$$\Delta y \sum_{I=2}^{IM} \left[JB(I,2) - JB(I,1) \right] \qquad (4.22)$$

$$= 3/8 \left[\frac{(JB(1,2)-1)\Delta y + (JB(1,1)-1)\Delta y}{2} \right]$$

or

$$\sum_{I=2}^{IM} \left[JB(I,2) - JB(I,1) \right] = 3/16 \left[JB(1,2) - JB(1,1) - 2 \right] \qquad (4.22a)$$

It is seen from the above relation that the overall mass balance now allows for an increasing amount of fluid entering at $z = 0$ during a time step. The use of the modified mass balance and

the expression for δ_o should enable the numerical solution to be carried out for a higher number of time steps. The velocity profile at $z = 0$ is calculated in the same manner using the dimensionless profile w_o.

In using the new relations for the numerical solution, the initial approach is to let JB (1, 2) = 1 at $t = 0$ and then calculate JB (1, 2) after each succeeding time step from the formula. This approach is reasonable because it lets $\delta_o = 0$ at $t = 0$ and then grow directly according to the boundary layer relation. This is more physically realistic than the method used in the original solution by Killeen (7). The procedure for the rest of the solution remains the same except for use of the modified mass balance in the boundary determination.

The first work done incorporating the above relations into the numerical solution demonstrated that the values assigned to w on the first row by the boundary conditions greatly affected the results. Consequently, it was here that the investigation centered.

Initially $w = 0$ at $z = 0$ for all y. At $t = 0^+$, w has nonzero values for a few increments. Several different values of the velocity profile at $z = 0$ were used to start the numerical solution. These were:

1. $w = 0$ at $z = 0$

2. $w = 0.5$ at $z = 0$

3. $w = 1.0$ at $z = 0$

4. A linear velocity profile

None of these produced significantly better results than using the original velocity profile w_o. All of this seemed to indicate that an established velocity profile for a significant number of increments during the first time step was needed. Since the relation for the number of increments, $JB(1, 2) = 1 + 4/\Delta y \sqrt{(IM - 1) \Delta t}$ progresses relatively slowly if $JB(1,2)$ is equal to unity initially, it was evident the model needed to be modified.

After a thorough study of the various possibilities, the following model was proposed:

1. Let $JB(1, 2)$ have a sizeable number of increments initially.

2. Keep $JB(1, 2)$ equal to this value until enough time steps have elapsed so that $JB(1, 2)$ would equal to this value if calculated by the equation,

$$JB(1, 2) = 1 + (4/\Delta y) \sqrt{(IM - 1) \Delta t}$$

3. Then use the expression for $JB(1,2)$ thereafter.

This model then requires that a boundary layer of significant distance be formed almost immediately and after a short period of time, it begins to grow. This is more physically realistic than the original model in which a boundary layer of significant thickness is formed quickly and remains constant for all time.

The number of increments to which $JB(1, 2)$ is initially set is of course dependent somewhat on the size of the increments used. This has to be determined for each individual case but the magnitude of δ_o is roughly the same.

As the boundary layer begins to grow, the solution can be carried out much further than was originally possible. The problem of insufficient fluid for distribution among the rows does not appear in the amount of time which elapses before the enlargement of the boundary layer starts.

In the original numerical solution, another problem which limited the solution was the calculation of values of v from the continuity equation near the interface. This problem is one characteristic of boundary layer flow. Discussion of this may be found in Schlichting (10), Rouse (9), and others. The values of v are computed from the differences in the values of w on two adjacent rows, and each succeeding value includes all the differences at lower values of y. As a result, values of v near the boundary become abnormally large. The transformation of the equations by using potential and stream functions to obtain a second order equation does not produce significantly better results. It is not possible to determine exactly the limits of the magnitude of v near the boundary. However, looking at the original drainage problem, it is evident that there is more of a tendency for fluid to move in the x-direction than in the y-direction. Hence it is reasonable to assume that the greatest value of v would probably not exceed the greatest value of w which is unity. Certainly the absolute value of v would be no greater than the dimensionless value of two for this problem.

The first place these erroneous values of v begin to affect the solution is in the momentum equation calculations for w. These errors are then carried into the boundary calculations.

In the system of equations developed for the WF subroutine which is solved using the Thomas Algorithm, the values of v appear in some of the algebraic expressions which are coefficients of the unknown w's. In these expressions where v's appear, the terms involving the v's are usually small compared to the other terms and do not significantly affect the calculations at all. If however, the values of v become very large, then the whole calculation procedure for the w's becomes erroneous. Since relatively small values of v, whether correct or not, do not significantly affect the calculations to a great degree, a procedure was used in which very large values of v near the boundary were limited to series of values ranging up to two. While it is realized that these values of v are not necessarily correct, the purpose is to allow a further study of the numerical solution. Without doing this, it would be difficult to determine the real limits of the solution.

These "clamped" values of v were used in the original numerical developed by Killeen (7) and a slight improvement resulted. The solution could be carried out for a few additional time increments. This adjustment however, showed that the real source of trouble was not erroneous values of v near the interface, but was the problem of insufficient fluid entering the system.

It was felt necessary to limit these values of v near the
boundary from being too large in any subsequent work in order to
determine the limits of the numerical solution for the revised
model.

The above discussion essentially covers the development of
the expanded model with regard to the derivation of relations used
and numerical techniques for solution. The results of this model
along with a comparison with the model of Killeen (7) are
presented in Chapter V.

RESULTS OF THE ISOTHERMAL DRAINAGE PROBLEM

There were two major objectives involved in the study of the
isothermal drainage problem. First, several areas of the original
solution by Killeen (7) were investigated. This included a study
of iteration procedures in the momentum equation and the choice of
the velocity coefficients in the momentum and boundary equations.
After this was done, the feasibility of applying boundary layer
theory to obtain a better model was determined. The general result
of both of these studies was to obtain a solution which approximates
the position of the boundary more closely and which lasts for longer
periods of time, depending on the particular set of conditions.

The study of the original solution was discussed in Chapter
IV. The major improvements over the original solution were:

1. Elimination of much unneeded storage space for data in
   the computer solution.

2. Determination of the lower limit of the number of itera-
   tions required for the calculations of the velocity
   coefficients.

3. A better choice of the velocity coefficients in the
   boundary equation.

4. Determination of the actual limits of the numerical
   solution without interference from erroneous values of
   v near the boundary.

In addition, a new algorithm was developed to solve the boundary system of equations. This is discussed in Chapter VI and Appendix A.

As discussed in Chapter IV, the major revision in the model is to let the value of δ_o be fixed initially and grow according to a boundary layer relation after a certain number of time steps. The lower limit to which δ_o can be set initially was an important part of this study. This limit depends both on the size of the increments, Δy and Δz, and their ratio. The value used in the original solution was $\delta_o = 1$, so that JB (1, 2) $= 1 + 1 / \Delta y$. This value was used as an upper limit for the initial size of δ_o in the new model. For any choices of increment sizes, the solution was investigated for a wide range of values of δ_o from unity to zero. Three different sets of conditions which are typical are used to present these results. The values of the JB's were obtained as computer output. The form of these is the same as those presented by Killeen (7). This output is presented for several runs in Appendix B. For each of the sets of conditions, the results for the upper limit, $\delta_o = 1$, and the lower limit are presented graphically. These runs are as follows;

Run	y	z	$\Delta y / \Delta z$	Initial JB (1)
1	1/24	1/384	16	10
2	1/24	1/384	16	26
3	1/48	1/384	8	20
4	1/48	1/384	8	49
5	1/48	1/768	16	15
6	1/48	1/768	16	49

In Figures 5-1 to 5-6, the position of the boundary at several different time steps is presented for each of the runs. In each case, the curve labeled with the highest number of time steps represents the extent of the solution for those conditions.

Figure 5-1 - Run # 1

$\Delta y = 1/24$

$\Delta z = 1/384$

JB (1 , 2) = 26

for 25 Δ t

$t = 40 \Delta t$

$t = 25 \Delta t$

$t = 10 \Delta t$

Initial JB (1, 2) = 26

Increments of $\Delta z \rightarrow$

Increments of $\Delta y \rightarrow$

Figure 5-2 – Run # 2

$\Delta y = 1/48$

$\Delta z = 1/384$

$JB (1, 2) = 21$

for $4 \Delta t$

Initial JB $(1, 2) = 21$

$t = 48 \Delta t$

$t = 21 \Delta t$

$t = 4 \Delta t$

Increments of $\Delta y \rightarrow$

Increments of $\Delta z \rightarrow$

Figure 5-3 — Run # 3

$\Delta y = 1/48$

$\Delta z = 1/384$

$JB'(1, 2) = 46$

for $22 \Delta t$

$t = 35 \Delta t$

$t = 22 \Delta t$

$t = 10 \Delta t$

Increments of $\Delta y \rightarrow$

Increment of $\Delta z \rightarrow$

Figure 5-4 -- Run # 4

$\Delta y = 1/48$

$\Delta z = 1/768$

$JB (1, 2) = 15$

for $4 \Delta t$

$t = 79 \Delta t$

$t = 40 \Delta t$

$t = 4 \Delta t$

Increments of $\Delta z \rightarrow$

Increments of $\Delta y \rightarrow$

Figure 5-5 - Run # 5

$\Delta y = 1/48$

$\Delta z = 1/768$

$JB (1, 2) = 49$

for $48 \Delta t$

$t = 58 \Delta t$

$t = 40 \Delta t$

$t = 4 \Delta t$

Increments of $\Delta z \rightarrow$

Increments of $\Delta y \rightarrow$
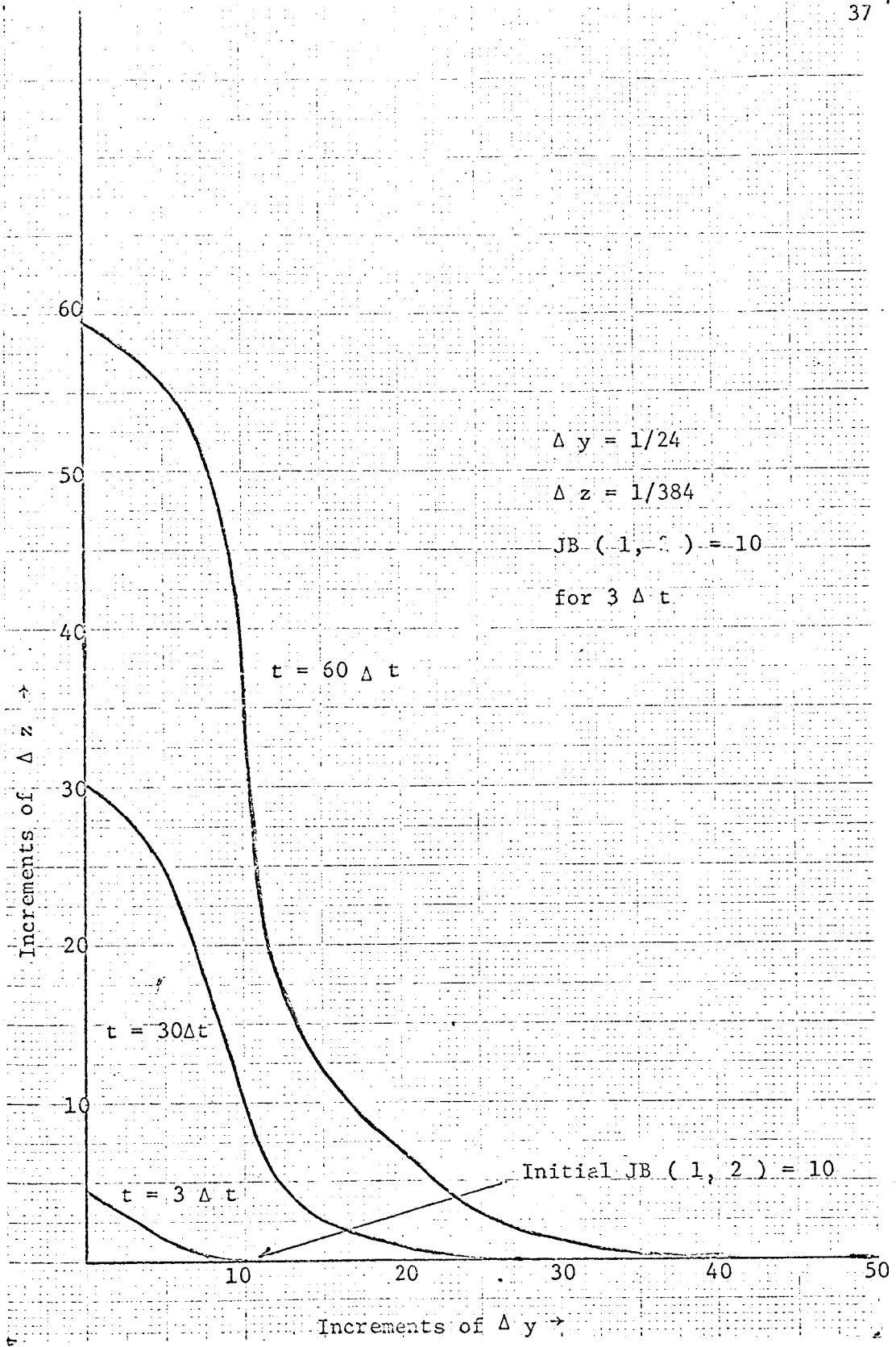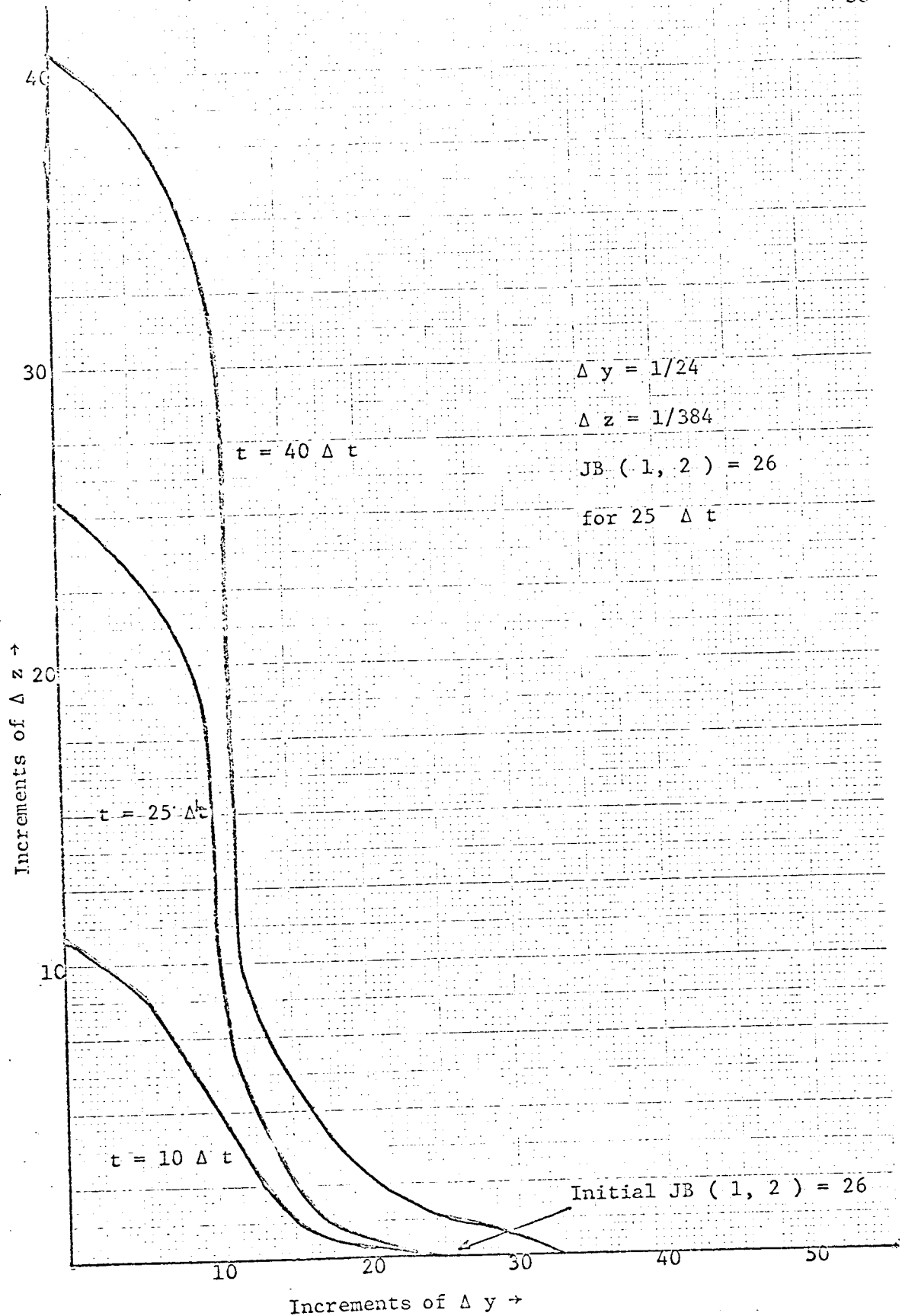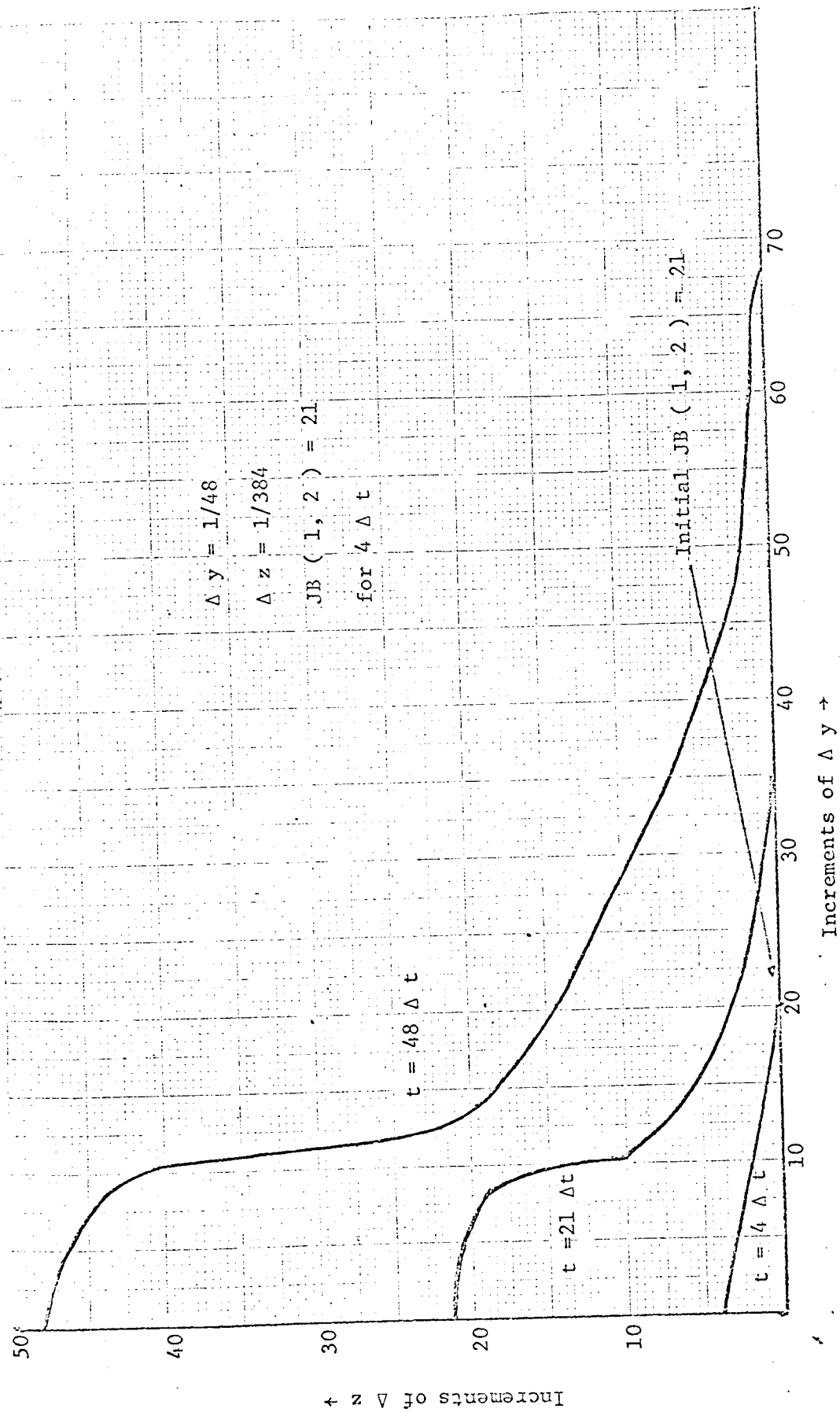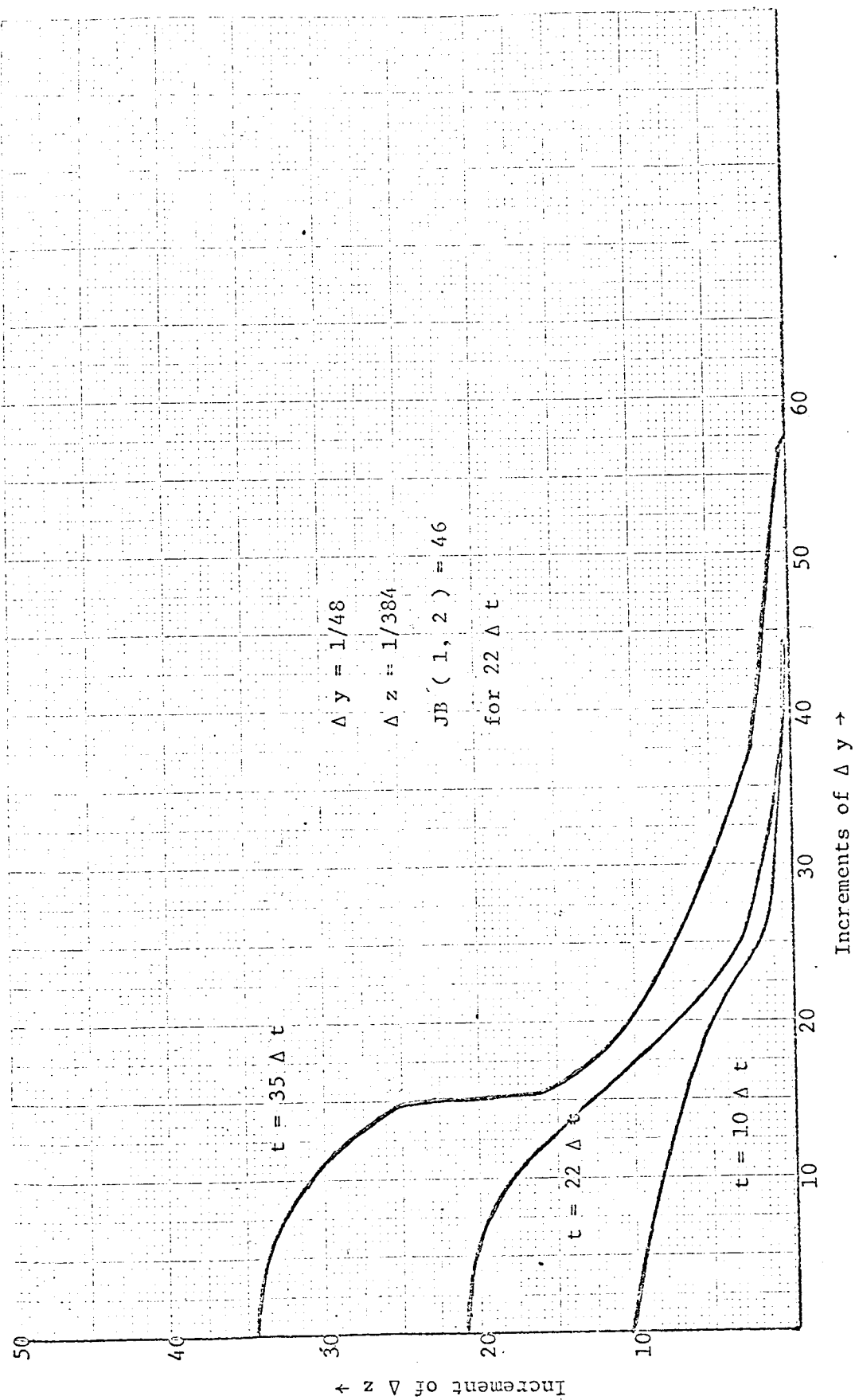
Figure 5-6 — Run # 6

It can be seen from the graphs that the solutions with a lower value of δ_0 at $t = 0$ are substantially better than those at the higher values. These lower values of δ_0 are also more physically realistic since the boundary layer is very small at $t = 0^+$. 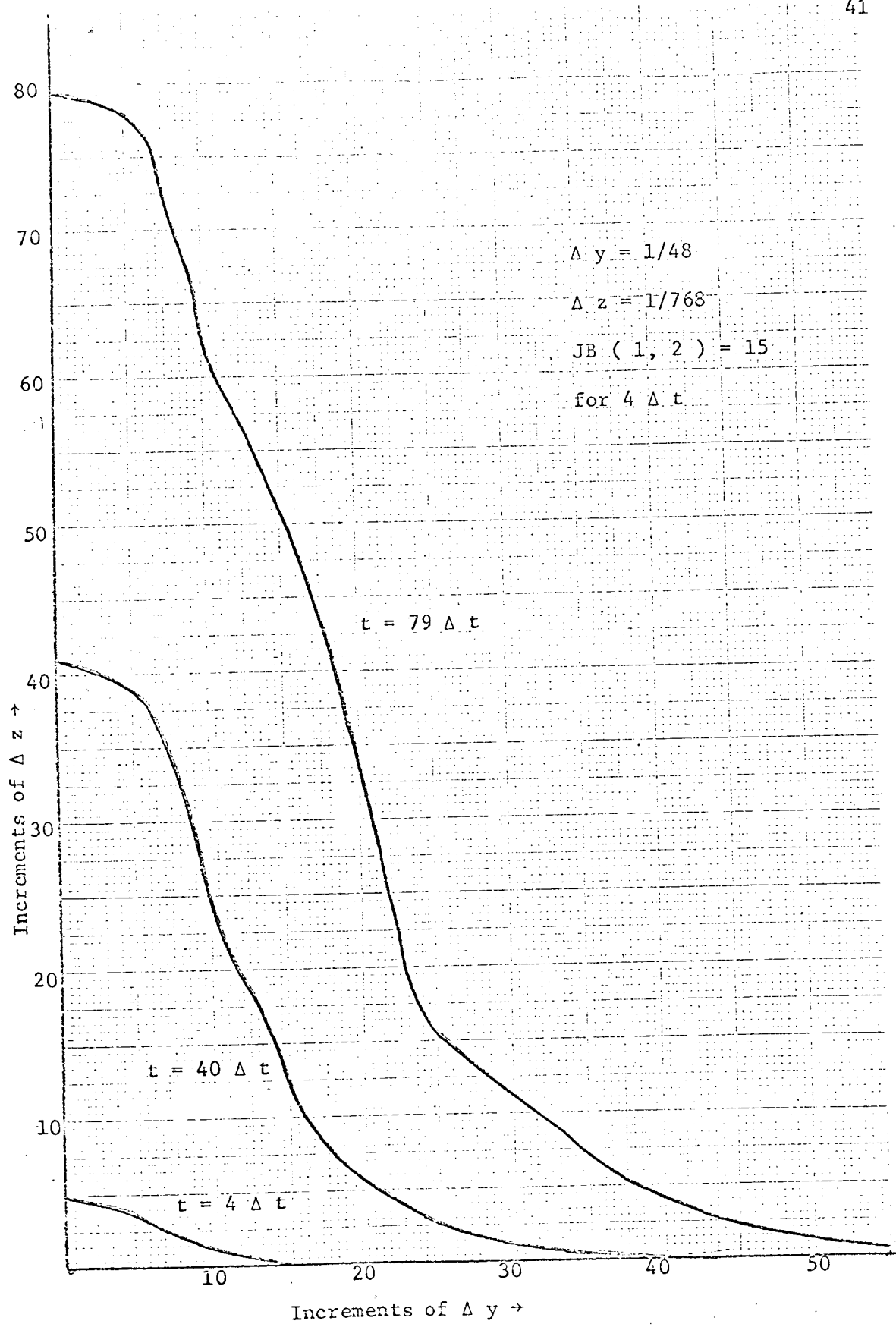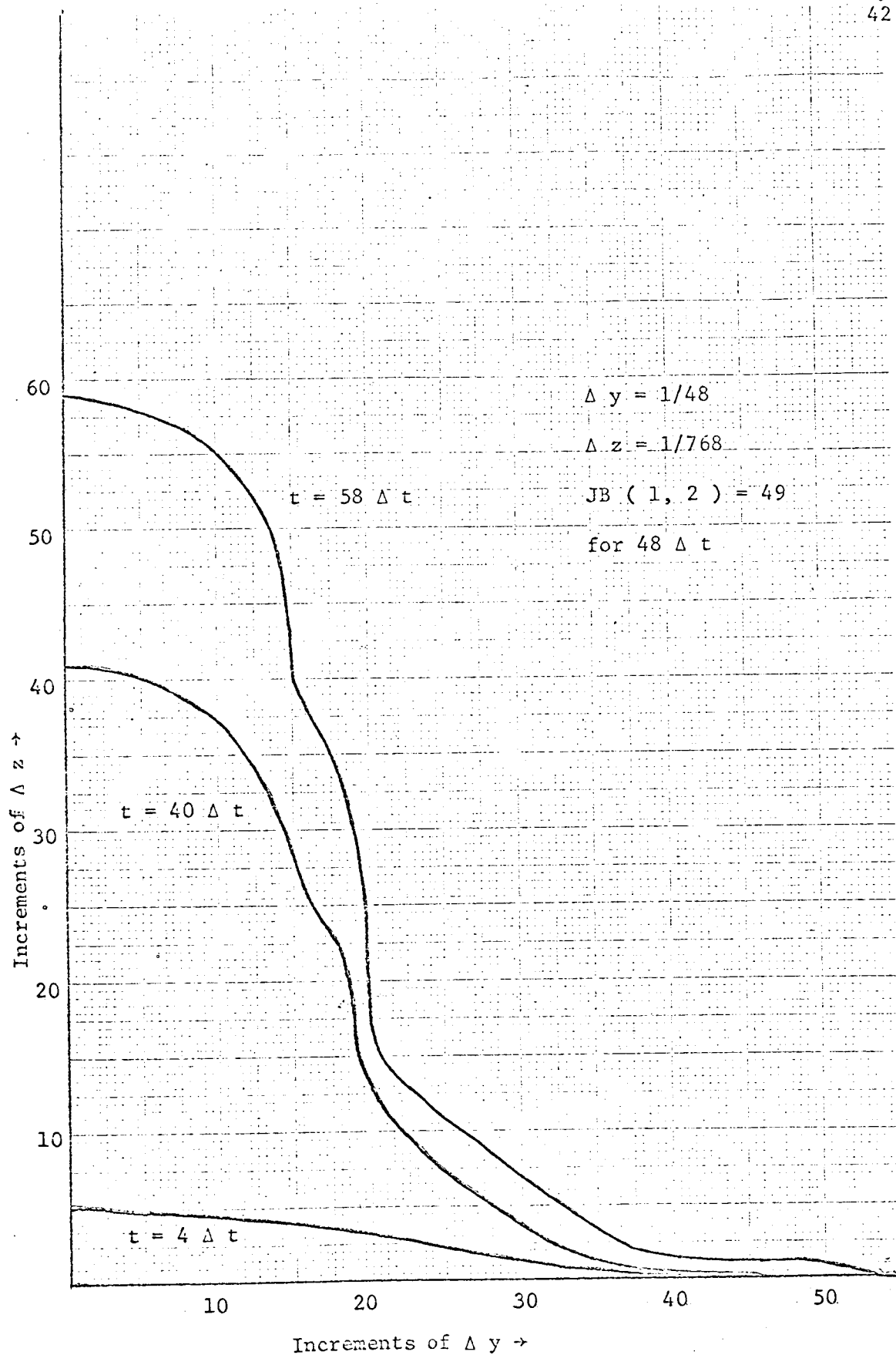In almost all of the studies made, it was found that the number of time steps for which δ_0 is constant ranged from about three to five. These are relatively small numbers so that the boundary layer equation is applied very quickly. It is also seen that there is a general consistency as to the initial size of δ_0 for the different sets of conditions. For example, JB (1, 2) is 10 with $\Delta y = 1/24$ for Run # 1 and JB (1, 2) is 21 with $\Delta y = 1/48$ in Run # 3.

In Figures 5-7 to 5-9, a comparison of the results of the new solution and those of the original solution is made. The curves for the original solution are those for runs made with "clamped" values of v near the boundary. Thus the extent of the original solution without interference from erroneous values of v near the boundary can be seen. These graphs show the improvement in the isothermal solution with the new model. The boundary is more accurately described, particularly at the lower time levels because the initial size of δ_0 has a significant effect during the first part of the solution. Also, the extent of the solution is roughly doubled in most of the runs.
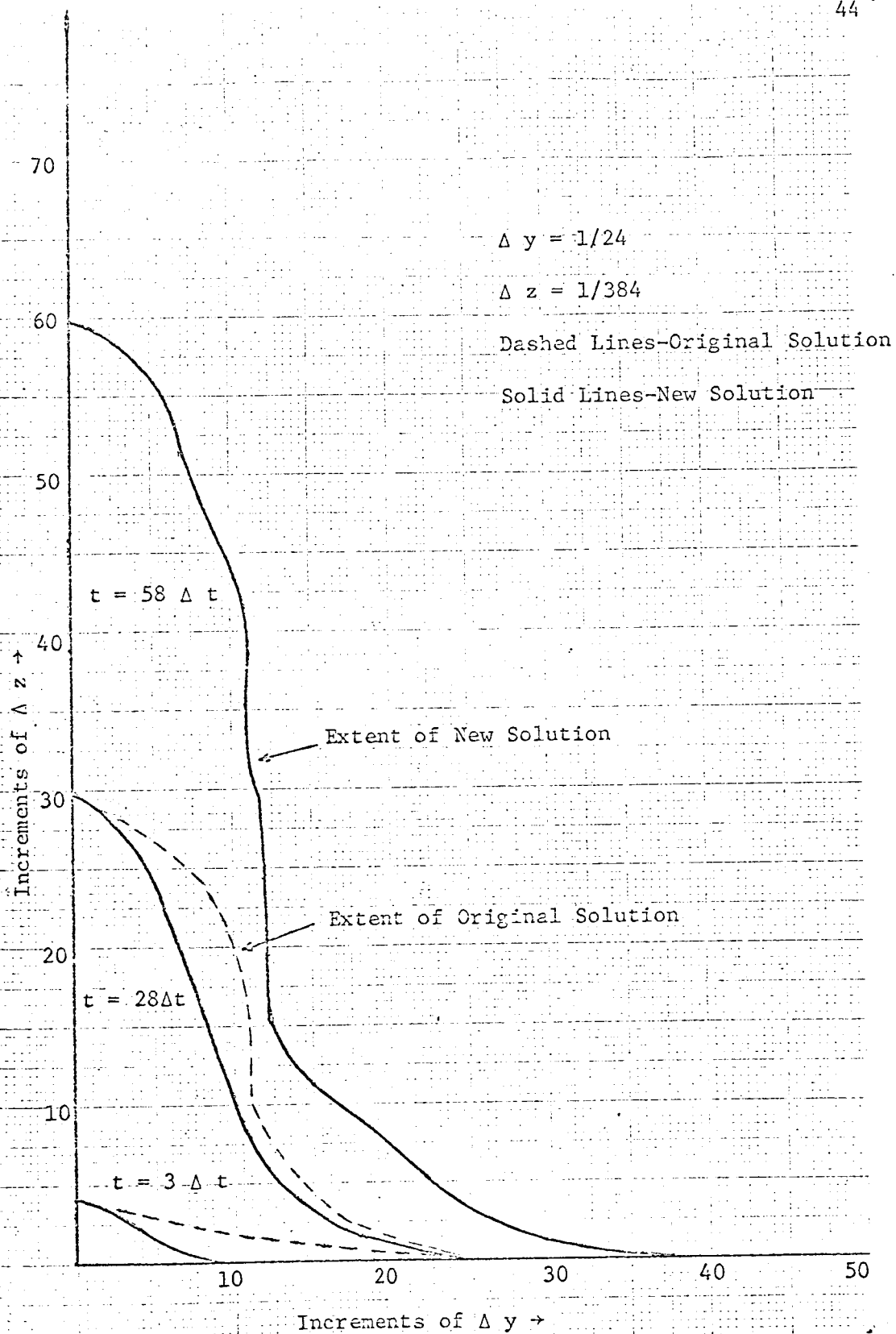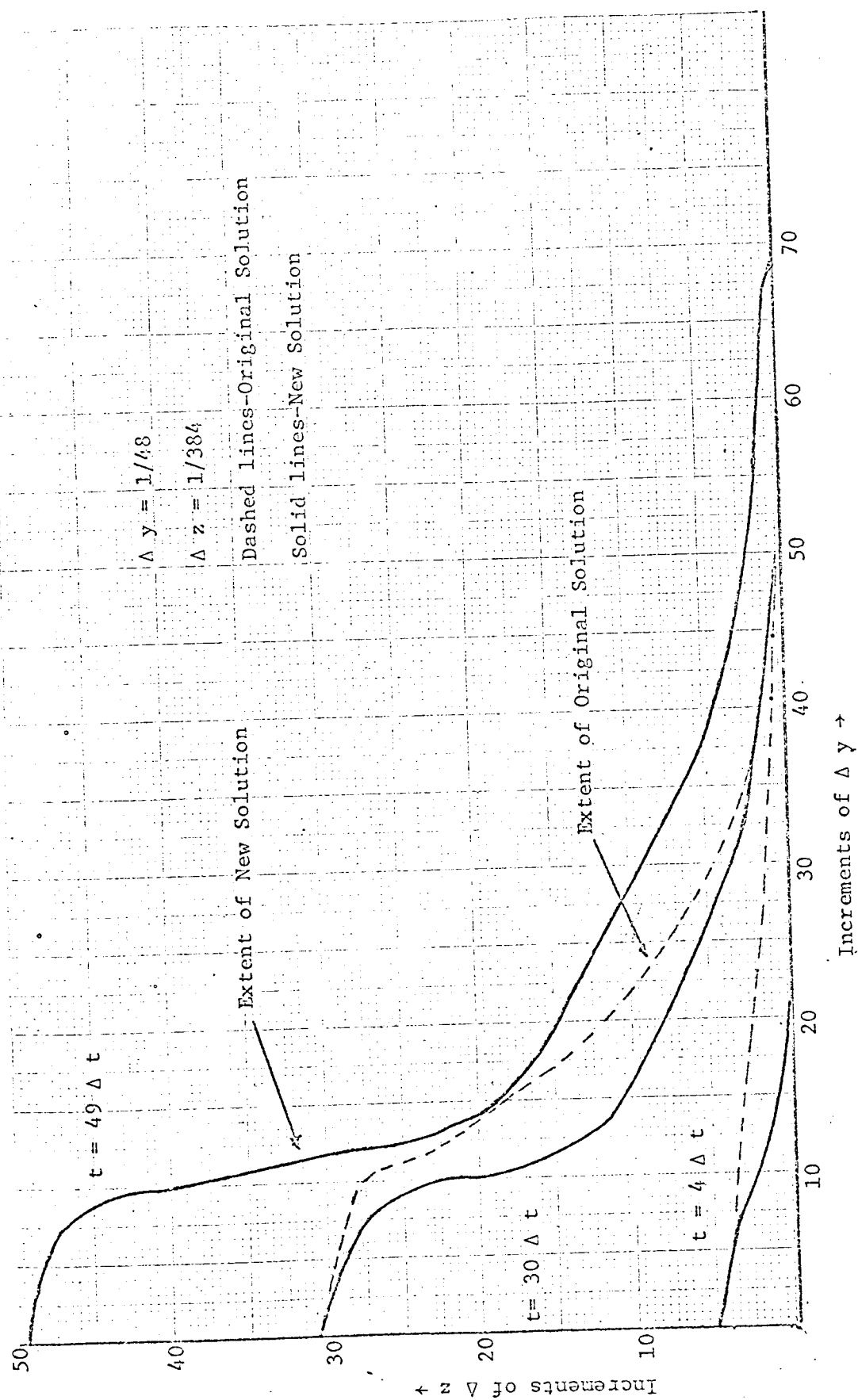
Figure 5-7 - Isothermal Boundary Comparison No. 1

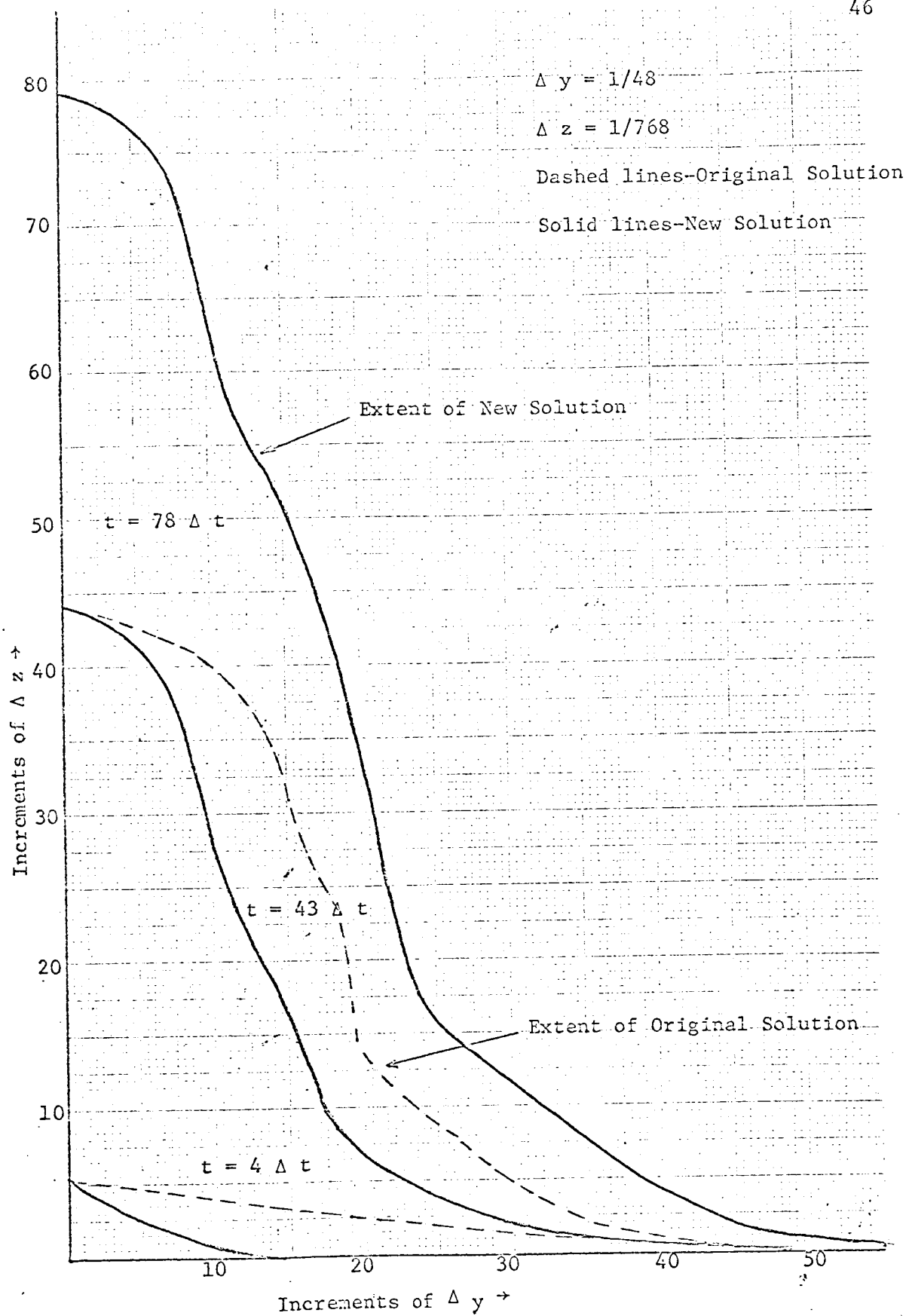Figure 5-8 - Isothermal Boundary Comparison No. 2

Figure 5-9 - Isothermal Boundary Comparison No. 3

RESULTS OF THE GENERAL PROBLEM

The study of the nonisothermal drainage problem consisted of two main parts. First the energy equation was added to the system and then the mass added to the system due to vapor condensation was included in the overall mass balance to obtain the general solution.

Addition of the Energy Equation to the System

The numerical techniques used to include the energy equation to the solution were discussed in Chapter VI. This equation includes the combined effects of energy transport by conduction and by bulk flow. The temperature profiles obtained are thus a complex function of both of these effects.

At any particular row at any time, the value of the temperature is equal to T_s at the interface and decreases to T_b at the wall. The type of profile obtained was found to depend mainly on the direction of flow in the y-direction. The velocity in the z-direction affects only the magnitudes of the temperatures at any row as a whole since the fluid flow in the z-direction is always positive.

It was found that if almost all of the values of v at any particular row were of the same sign, a monotonically decreasing temperature profile was obtained. However when a range of positive values of v occurred for part of a row and were followed by a series of negative values for the remainder of the row, in many cases perturbations in the temperature profile around the point of change resulted. This is explained physically in the following manner.

If the velocities in the y-direction at any row are all of the same sign indicating all of the transverse flow is in one direction, then the type of profile mainly depends on conduction effects and thus decreases in a regular manner from the value of T_s at the surface to the value of T_b at the wall. When the velocities are positive for part of the row and negative for the remainder, there is a tendency for energy to be stored at and around the points where the fluid flow from both directions meets. This is reflected in higher temperatures at such points.

In Table VII-1, typical values of the temperatures at an arbitrary row are shown together with the corresponding values of v. In this case, since there are not ranges of velocities which are opposite in sign, the temperature profile is of the monotonically decreasing type.

In Table VII-2 the temperature values together with the values of v are shown for the case of opposite flows in the y-direction. It is seen that the point where the temperature discontinuity occurs corresponds to the point where a significant range of positive and negative velocities meet. It was found in general that this type of discontinuity occurred when there were at least four or five successive points with velocities of negative sign, indicating a significant flow toward the wall at those points.

JB (I) = 10

J	T (I, J)	v (I, J)
1	0.8000	0.0006
2	0.8000	0.0175
3	0.8000	0.0549
4	0.8000	0.1035
5	0.8000	0.1509
6	0.8000	0.1801
7	0.8002	0.1593
8	0.8024	0.1161
9	0.8225	0.4182

Table VII-1 - Temperatures and Velocities for a Monotonically

Decreasing Temperature Profile

JB (I) = 21

J	T (I, J)	V (I, J)
1	0.8000	0.0034
2	0.8000	0.0435
3	0.8000	0.1019
4	0.8000	0.2310
5	0.8000	0.3499
6	0.8000	0.5251
7	0.8000	0.5617
8	0.8001	0.5001
9	0.8008	0.3853
10	0.8049	0.1755
11	0.8221	-0.1288
12	0.8034	-0.3628
13	0.8005	-0.4329
14	0.8001	-0.3945
15	0.8000	-0.3750
16	0.8001	-0.4053
17	0.8006	-0.4263
18	0.8028	-0.5373
19	0.8126	-.08523
20	0.8530	-0.4896

Table VII-2 - Temperatures and Velocities for a Temperature

Profile with Perturbations

General Solution for Drainage with Condensation

The method used for approximating the amount of vapor condensed during any time step was discussed in Chapter VI. In the solution for the location of the boundary, the equation most affected was the overall mass balance which relates all of the unknown boundary values. It was found that the system of boundary equations as a whole is very sensitive to changes in the overall mass balance.

After testing the solution for the same range of values of increment size and ratio that were used in the isothermal solution, two general changes were noted.

First it was found that in many cases a higher initial value of δ_o had to be used. The value of δ_o had to be changed more for higher values of the ratio $\Delta y / \Delta z$. The other general result was that the solution did not last quite as long for any of the sets of conditions. This was probably due to the many additional calculations involved which produced additional errors due to truncation, etc.

Computer output showing boundary values for several sets of conditions is shown in Appendix B. These are of the same form as those presented for the isothermal case.

In Figures 7-1 to 7-3, the position of the boundary at different times is presented graphically. The conditions of increment size are the same as those in Chapter V for the isothermal case. The corresponding isothermal boundary positions are given along with the various curves so that they can be easily compared.

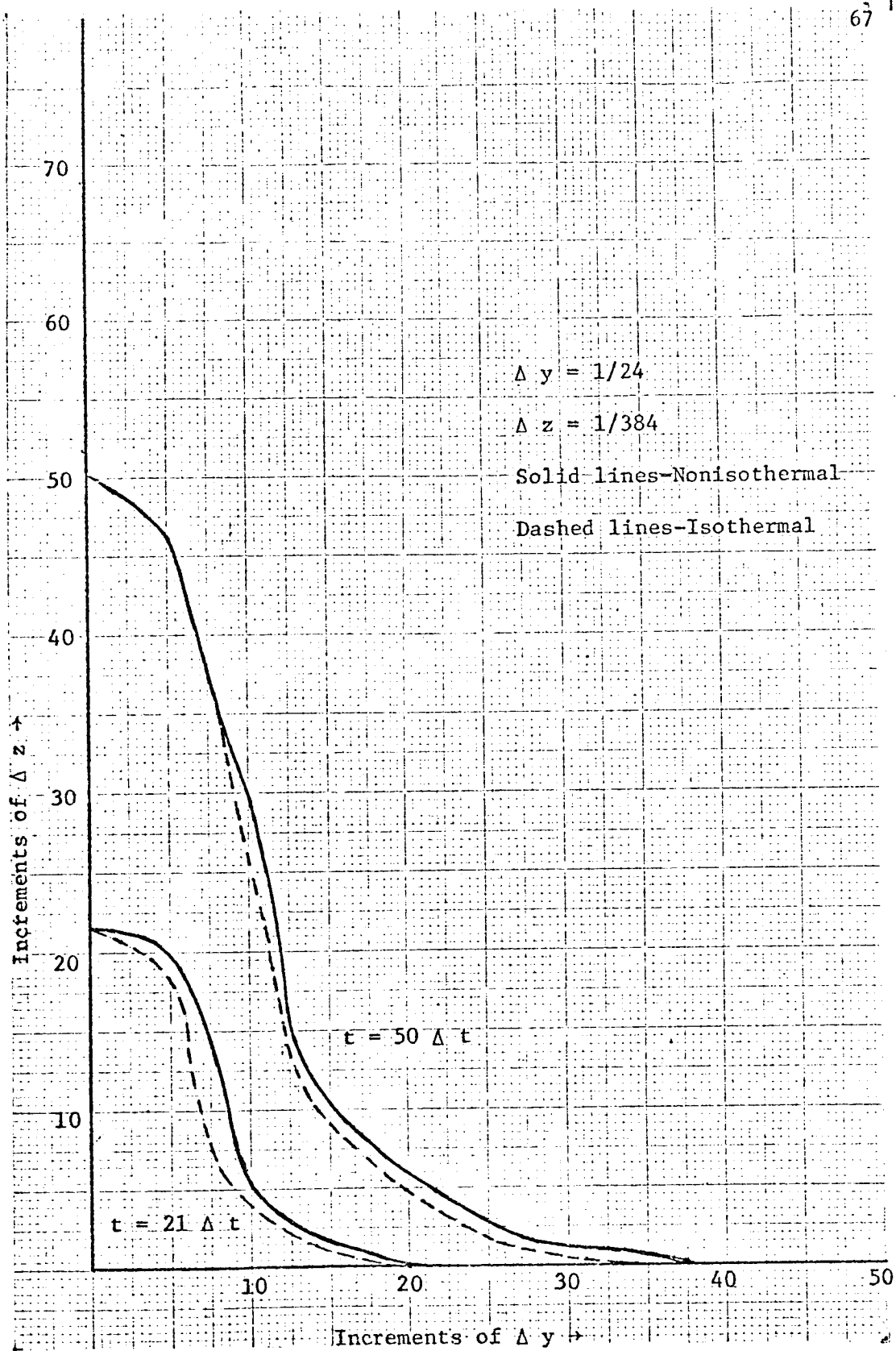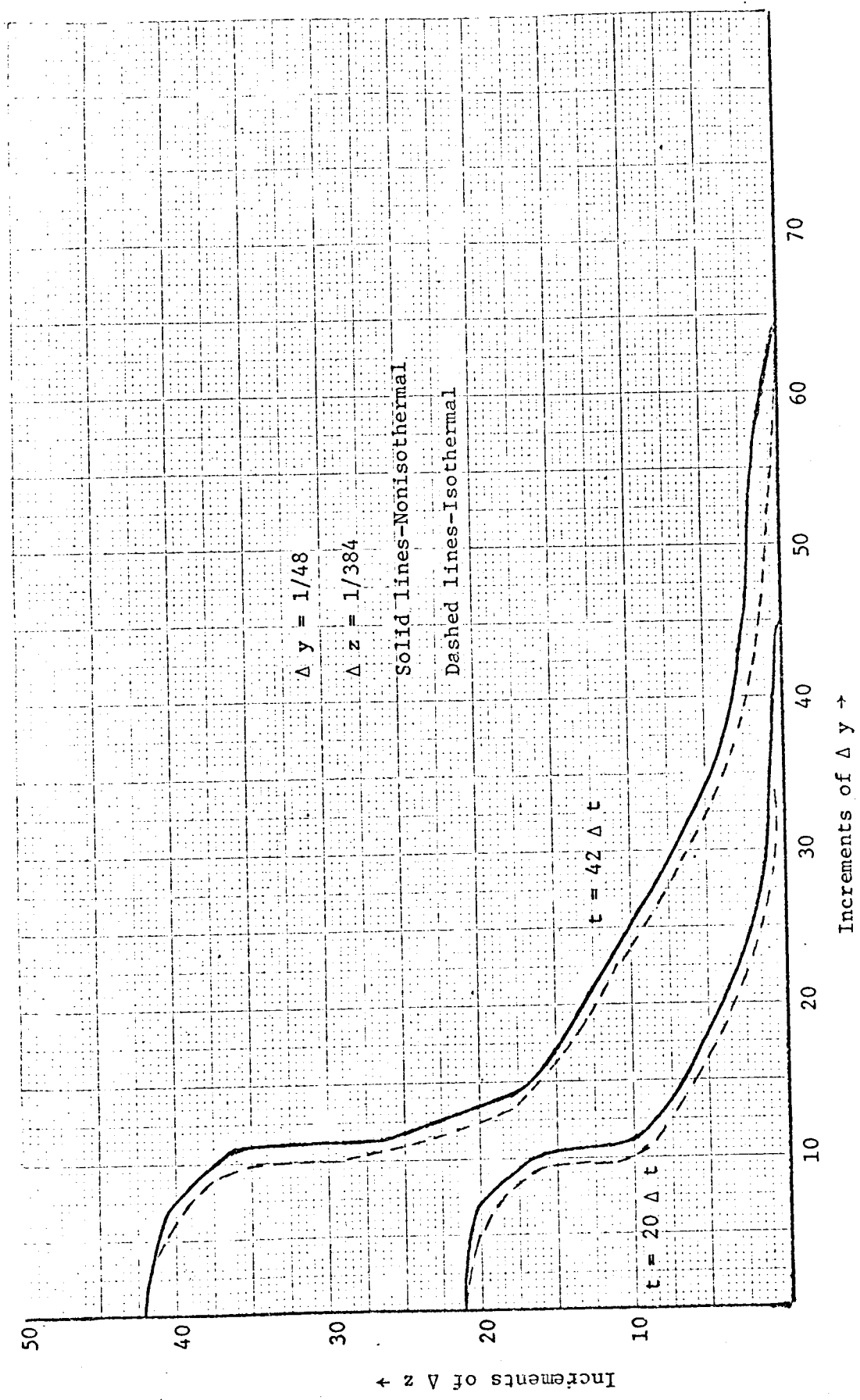Figure 7-1 - Isothermal-Nonisothermal Boundary Comparison No. 1

Figure 7-2 – Isothermal–Nonsiothermal Boundary Comparison No. 2

$\Delta y = 1/48$

$\Delta z = 1/384$

Solid lines—Nonisothermal

Dashed lines—Isothermal

$t = 42 \Delta t$

$t = 20 \Delta t$

Increments of $\Delta y \rightarrow$

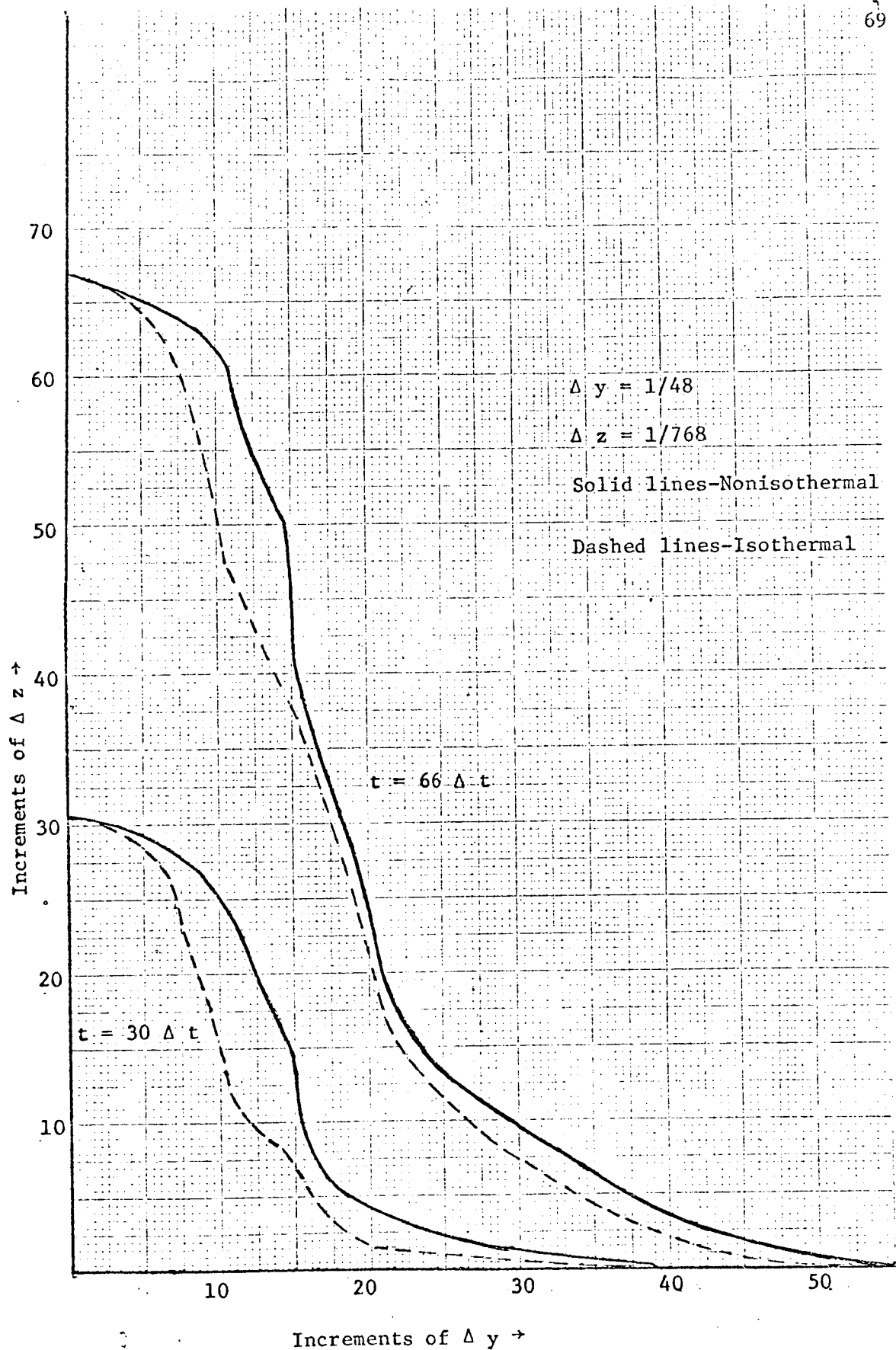Increments of $\Delta z \rightarrow$

Figure 7-3 - Isothermal-Nonisothermal Boundary Comparison No. 3

These show the changes in the boundary position due to vapor condensation.

In addition to the previously mentioned studies of the condensation model, the effect of changes in T_b on the solution was investigated. In the results already presented for this model, T_b was set at 0.8. The effect of increasing T_b from 0.8 up to 0.95 using increments of 0.05 was investigated. It was found that the only difference in the solution was that a small number of the rows contained one less element of fluid. This finding confirmed the consistency of the solution, but the curves for higher temperatures vary only slightly from those at 0.8 so that it is not felt necessary to present them.

As T_b was lowered, it was found that the addition of one increment at several rows occurred. However at a value of about 0.7, the boundary solution breaks down. This probably occurs because the model itself tends to become unrealistic when high temperature gradients are present.

In addition to the results discussed above, the variations in the solution for different values of the constants E_1 and E_4 were checked. These values of course depend on the particular liquid and the general range of temperatures involved.

For E_1, slight variations in the solution occurs for the range 0.1 to 1.0 The constant E_4 is much smaller with a corresponding magnitude of output 0.001. For higher values, the solution breaks down because of the previously discussed sensitivity of the over-all mass balance to changes in the amount of fluid entering the system during a time step.

In general, it was found that the numerical solution is not constrained to one particular liquid or to one set of conditions.

PROGRAM ORGANIZATION

In the preceding chapters, a description of the physical problem was presented along with the finite difference techniques to be used for the numerical solution. The calculations were performed on an IBM 7044 computer using instructions written in FORTRAN IV. Program listings are provided in Appendix B for the two new subroutines developed for the general solution. Listings are also presented for the main program and for the subroutine for the boundary location, since these had some major changes from their use in the original solution.

To provide a clear picture of the overall solution, the general steps which are followed are given below:

1. Computation of w at all rows containing liquid using the WF and COEFF subroutines.

2. Computation of v at the same row using the VF subroutine.

3. Computation of T at the same rows using the TF and TCOEFF subroutines.

4. Calculation of the new boundary position at the new time level for all the previous rows plus one additional row at the top, using the GETJB subroutine.

5. Repetition of the computations for w, v, and T at the grid points in the liquid for the new region.

CONCLUSIONS

The most important conclusions which were drawn from this study were:

1. The study of the original isothermal solution provided better knowledge as to the convergence of iterations procedures used in the moving boundary problem. This could be useful in solving other non-linear problems.

2. A better model for the isothermal drainage problem was sucessfully developed by using boundary layer theory to describe the fluid flow at the surface of the reservoir ($z = 0$). This solution is more physically realistic and has the additional advantage of lasting for longer periods of time.

3. The energy equation was sucessfully incorporated into the solution of the problem. This provided temperature values at all points in time and space in the liquid.

4. A workable model was developed for the overall solution which included mass added to the system due to vapor condensation.

NOMENCLATURE

x	space coordinate
y	space coordinate
z	transformed space coordinate
t	time coordinate
u	x-component of velocity
v	y-component of velocity
w	z-component of velocity
T	temperature
T_s	interface temperature
T_b	wall temperature
S	draining velocity of reservoir
E_1	a constant equal to $k \, / \, \rho c$
E_2	a constant equal to $g \, (\rho - \rho v \,) \, / \, \rho$
E_3	a constant equal to $u \, / \, \rho$
E_4	a constant equal to $k \, / \, h \, \rho$
k	thermal conductivity of liquid
c	heat capacity of liquid
ρ	liquid density
ρ_v	vapor density
μ	liquid viscosity
g	gravitational acceleration

λ	heat of condensation
ν	kinematic viscosity
δ	boundary position of the liquid-vapor interface
JB	boundary position for particular value of i
i	subscript denoting the row number in the z-direction
j	subscript denoting the row number in the y-direction
IM	FORTRAN variable denoting the uppermost row at any time
J	FORTRAN subscript corresponding to i
I	FORTRAN subscript corresponding to i
C_{ij}	coefficients in the tri-diagonal system of equations
D_i	constant vector in the tri-diagonal system of equations

BIBLIOGRAPHY

1. Bird, R. B., W. E. Stewart, and E. N. Lightfoot, <u>Transport Phenomena</u>, John Wiley and Sons, New York (1966).

2. Chung, P. M., "Unsteady Laminar Film Condensation on a Vertical Plate", Journal of Heat Transfer, February, 1963.

3. Douglas, J., A. O. Gardner, and D. W. Peaceman, "Numerical Solution of a Two-Dimensional Moving Boundary Problem", presented to the Association for Computing Machinery, June 19, 1957 in Houston, Texas.

4. Forsythe, G. E., and W. R. Wasow, <u>Finite Difference Methods for Partial Differential Equations</u>, John Wiley and Sons, New York (1960).

5. Kay, J. M., <u>An Introduction to Fluid Mechanics and Heat Transfer</u>, Cambridge University Press, London (1963).

6. Killeen, D. B., personal communication (1967).

7. Killeen, D. B., "The Numerical Solution of Equations Describing an Unsteady Draining Process", a Dissertation, Tulane University, 1966.

8. O'Loughlin, J. R., "Evaporation From a Draining Liquid Form", presented at ASME-AIChE Heat Transfer Conference, Los Angles, California, (1965).

9. Rouse, H. and others, <u>Advanced Mechanics of Fluids</u>, John Wiley and Sons, New York (1965).

10. Schlichting, H., <u>Boundary Layer Theory</u>, McGraw-Hill Book
Company, New York (1960).

11. Sparrow E. M., and Gregg J. L., "A Boundary Layer Treatment
of Laminar-Film Condensation", Journal of Heat Transfer,
Februrary, 1959.

12. Sparrow, E. M., and R. Siegel, "Transient Film Condensation",
Transactions of the ASME, March, 1959.

13. van Rossum, J. J., "Viscous Lifting and the Drainage of Liquids",
Applied Scientific Research, Vol. A-7, August, 1958.

14. von Rosenberg, D. U., Lecture Notes on Numerical Techniques,
Tulane University (1966).

15. von Rosenberg, D. U., personal communications (1967).

Section III

Potential Flow Problems

Numerical Solution for Flux Components in Potential Flow*

By Dale U. von Rosenberg

Abstract. Values of the flux components are often desired in potential flow problems. Second-order correct finite-difference analogs are developed for the differential equations defining these flux components. Two iterative methods of solving the resulting finite-difference equations are presented. Experimental results indicate the most efficient value of the iteration parameter and demonstrate that the number of iterations required is approximately proportional to the square root of the number of points in the grid.

1. Introduction. Many important physical problems can be described by a potential field. Included in these are the flow of heat, the flow of electricity, and the flow of fluids in porous media. For ideal fluid flow problems a potential is defined only to aid in the solution, and the velocity is the dependent variable of interest. Even in cases where the potential corresponds to a real physical variable, such as heat conduction and flow of fluids in porous media, the flux is often the variable of interest.

For two-dimensional Cartesian co-ordinates, the differential equation which defines the potential is

$$(1) \qquad \frac{\partial^2 T}{\partial y^2} + \frac{\partial^2 T}{\partial z^2} = 0 ,$$

where T is the potential, y is one Cartesian co-ordinate, z is the other Cartesian co-ordinate.

The flux components can be defined in terms of the potential as

$$(2a) \qquad v = -k \frac{\partial T}{\partial y} ,$$

$$(2b) \qquad w = -k \frac{\partial T}{\partial z} ,$$

where v is the flux component in the y direction, w is the flux component in the z direction, k is the transport coefficient.

A great number of potential flow problems can be solved by various analytical techniques. However, a numerical solution is required for many boundary conditions. A number of methods have been developed for numerically solving Eq. (1) for the potential. When values of the flux are desired, the flux components must then be determined from the numerical solution for the potential by finite-difference analogs to Eqs. (2a) and (2b).

---

2. Equations Defining Flux Components. The method described in this paper yields a numerical solution directly for the flux components from the defining partial differential equations. Since there are two flux components in the two-dimensional case, two equations are required. The first of these results from the continuity principle and is the equation which yields Eq. (1) in terms of the potential. In terms of the flux components, this equation is

$$(3) \qquad \frac{\partial v}{\partial y} + \frac{\partial w}{\partial z} = 0 .$$

The second of these equations is the irrotationality condition which must hold in order for the potential to be defined by Eq. (2). This relation is

$$(4) \qquad \frac{\partial w}{\partial y} - \frac{\partial v}{\partial z} = 0 .$$

These equations are completely first order, and they contain the first derivative of each dependent variable with respect to each independent variable.

3. Boundary Conditions. Common boundary conditions used in conjunction with Eq. (1) are the specification either of the potential or of the normal derivative of the potential along the boundaries. The most general condition, of course, is specification of a relation between these two along the boundaries. Specification of the potential along a boundary is equivalent to a specification of the tangential flux component along that boundary, while specification of the normal derivative of the potential is equivalent to a specification of the flux component normal to the boundary. The numerical method of solution for the flux components, described herein, has been tested with several types of boundary conditions, including the general type for which a relation between the two flux components is specified.

For purposes of illustrating the numerical method, the boundary conditions used are

$$(5a) \qquad w(z, 1) = f(z) ,$$

$$(5b) \qquad w(0, y) = g(y) ,$$

$$(5c) \qquad v(z, 0) = p(z) ,$$

$$(5d) \qquad v(1, y) = q(y) .$$

These boundary conditions are equivalent to a specification of the potential along the adjacent sides for $y = 1$ and $z = 1$ and of the normal derivative of the potential along the other two adjacent sides where $y = 0$ and $z = 0$.

4. Finite-Difference Equations. A set of grid points with equal increments in the two directions is imposed on the region. This grid is illustrated in Fig. 1. Indices are used to designate location in the grid. These indices are defined by

$$(6a) \qquad z_i = (i - 1)\Delta z \qquad \text{for } 1 \leqq i \leqq R ,$$

$$(6b) \qquad y_j = (j - 1)\Delta y \qquad \text{for } 1 \leqq j \leqq S ,$$

$$(6c) \qquad \text{with } \Delta z = \Delta y .$$

For the case of a square region, $R = S$, but these limits will be used as given in Eq. (6) so that the method can be applied directly to a rectangular region. Two subscripts are used with values of the dependent variables. These are defined as

(7a) $$w_{i,j} = w(z_i, y_j),$$

(7b) $$v_{i,j} = v(z_i, y_j).$$

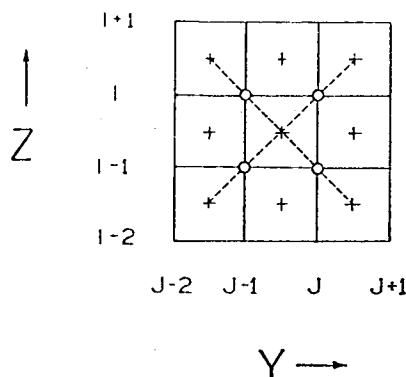The boundary conditions of Eq. (5) are shown in Fig. 1 in terms of the discrete variables.

FIGURE 1. Finite-difference grid

The first derivatives of Eqs. (3) and (4) are replaced by centered differences. These differences are written about the point $z_{i-1/2}, y_{j-1/2}$ which is designated by the cross (+) in Fig. 1. However, only values of the dependent variables on the grid points are used in the finite differences. This method of writing the finite differences has been described previously for equations describing transient, countercurrent flow problems [1]. The analogs for the derivatives of v are

(8a) $$\frac{\partial v}{\partial z} \simeq \frac{1}{2}\left[\frac{v_{i,j} - v_{i-1,j}}{\Delta z} + \frac{v_{i,j-1} - v_{i-1,j-1}}{\Delta z}\right],$$

(8b) $$\frac{\partial v}{\partial y} \simeq \frac{1}{2}\left[\frac{v_{i,j} - v_{i,j-1}}{\Delta y} + \frac{v_{i-1,j} - v_{i-1,j-1}}{\Delta y}\right].$$

Those for w are similar. These analogs are second-order correct. The truncation will be discussed further in the next section.

Two finite-difference equations can be written for each square of four points in the grid. After the space increments and the factor 1/2 have been eliminated, these equations become

(9) $w_{i,j} - w_{i-1,j} + w_{i,j-1} - w_{i-1,j-1} + v_{i,j} - v_{i,j-1} + v_{i-1,j} - v_{i-1,j-1} = 0,$

(10) $w_{i,j} - w_{i,j-1} + w_{i-1,j} - w_{i-1,j-1} - v_{i,j} + v_{i-1,j} - v_{i,j-1} + v_{i-1,j-1} = 0.$

Each equation contains eight values of the dependent variables, two at each of the four points. These equations, together with the boundary conditions, define the values of w and v at all points in the grid. Since the boundary conditions are specified on opposite boundaries in both directions, a simultaneous solution of all the equa-

tions is necessary. Two iterative methods of effecting this solution are presented in later sections.

5. Truncation Error. The complete expressions for the first derivatives are obtained from a Taylor series in two independent variables. The truncation error is obtained by substituting these expressions into the original differential equations. The expressions for the errors can be simplified by use of relations obtained from repeated differentiation of Eqs. (3) and (4). The truncation error for the finite-difference analog to Eq. (3) is

$$(11) \qquad E_3 = -2 \sum_{n=0}^{\infty} \left(\frac{\Delta z}{2} \right)^{4n+2} \left(\frac{\partial^{4n+3} w}{\partial z^{4n+3}} \right) \sum_{r=0}^{2n+1} (-1)^r \frac{1}{(2r)!(4n-2r+3)!}$$

and that for Eq. (4) is

$$(12) \qquad E_4 = -2 \sum_{n=0}^{\infty} \left(\frac{\Delta z}{2} \right)^{4n+2} \left(\frac{\partial^{4n+3} v}{\partial z^{4n+3}} \right) \sum_{r=0}^{2n+1} (-1)^r \frac{1}{(2r)!(4n-2r+3)!}.$$

6. Corresponding Difference Equation in Potential. A finite-difference equation in terms of the potential can be obtained from the finite-difference analog to Eq. (3) and to analogs to Eq. (2). Second-order correct centered difference analogs to Eq. (2) are used to obtain the flux components from the potential. The location of the points used in these analogs are shown in Fig. 2. In order for the flux components at the intersections of the grid lines to be determined from values of the potential by these centered analogs, the potential must be known at the points denoted by the crosses (+). A typical equation for determining a flux component is

$$(13) \qquad v_{i,j} = -k \left(\frac{1}{2} \right) \left(\frac{T_{i+1/2,j+1/2} - T_{i+1/2,j-1/2}}{\Delta y} + \frac{T_{i-1/2,j+1/2} - T_{i-1/2,j-1/2}}{\Delta y} \right).$$

When such analogs for the flux components at the points denoted by circles ($\bigcirc$) in Fig. 2 are substituted into the finite-difference equation for Eq. (3), the finite-
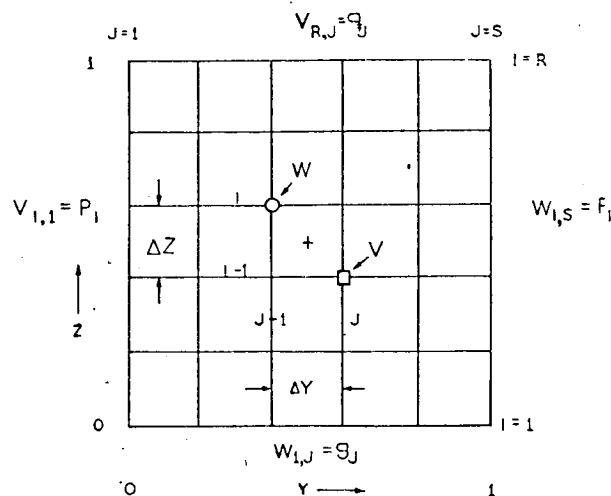

FIGURE 2. Location of points for potential

difference equation for the potential is obtained. This is

$$(14) \quad \frac{T_{i+1/2,j+1/2} + T_{i+1/2,j-3/2} + T_{i-3/2,j+1/2} + T_{i-3/2,j-3/2} - 4T_{i-1/2,j-1/2}}{2(\Delta y)^2} = 0.$$

This equation is the familiar five-point analog to Eq. (1) with the grid lines rotated 45° from those used to define the flux components, as shown in Fig. 2. Furthermore, the increment size is $\sqrt{2}$ times that used in the grid for the flux. When analogs similar to Eq. (13) are substituted into the finite-difference analog to Eq. (4), the irrotationality condition, all terms cancel as they should.

7. Nature of Iterative Methods of Solution. As mentioned previously, two iterative methods of solving Eqs. (9) and (10) will be described. The first method effects the simultaneous solution of the finite-difference equations from a single row in the grid. In the second method, the equations from two adjacent rows in the grid are solved simultaneously. The methods can be formulated and carried out either in the y-direction or in the z-direction. In fact, the convergence is more rapid if the iteration is carried out alternately in the y-direction and then in the z-direction. However, iteration in only one direction is convergent. In the presentation of the methods in this paper, the solution is given for one or two rows of equations in the y-direction.

The iteration procedure is begun at a boundary, where the values of one of the flux components are known for a whole row of points. The other flux component is unknown along this row, as are both components on the second row of points. In the equations presented below, the iteration is begun at the $z = 0$ boundary, where w is given by the boundary condition. See Fig. 1. The finite-difference equations, Eqs. (9) and (10), relate the dependent variables along these two rows of points. However, there are three rows of unknowns and only two rows of equations. It is necessary, therefore, to assume values of v along the second row of points. Values of v on the first row of points and w on the second row are then computed from Eqs. (9) and (10) based on this assumption. These computed values of w are then used with assumed values for v on the third row to compute values of w on the third row and v on the second row. This procedure is continued across the region. For the last row of equations, however, the values of v do not need to be assumed, since they are given by the boundary condition, as shown in Fig. 1, for $z = 1$. The conditions on each boundary are thus introduced once on each sweep across the region. On the next sweep of the region, the values obtained in the first sweep are used in place of the assumed values.

In order to increase the rate of convergence, an iteration parameter, ϵ, is introduced into the Eqs. (9) and (10). These equations become

$$(9a) \quad w_{i,j}^{(m+1)} - w_{i-1,j}^{(m+1)} + w_{i,j-1}^{(m+1)} - w_{i-1,j-1}^{(m+1)} + v_{i,j}^{(m)} - v_{i,j-1}^{(m)} + v_{i-1,j}^{(m+1)} - v_{i-1,j-1}^{(m+1)}$$
$$= \epsilon[(w_{i,j-1}^{(m)} - w_{i,j-1}^{(m+1)}) + (v_{i-1,j}^{(m)} - v_{i-1,j}^{(m+1)})] ;$$

$$(10a) \quad w_{i,j}^{(m+1)} - w_{i,j-1}^{(m+1)} + w_{i-1,j}^{(m+1)} - w_{i-1,j-1}^{(m+1)} - v_{i,j}^{(m)} + v_{i,j}^{(m+1)} - v_{i,j-1}^{(m)} + v_{i-1,j-1}^{(m+1)}$$
$$= \epsilon[-(w_{i,j-1}^{(m)} - w_{i,j-1}^{(m+1)}) + (v_{i-1,j}^{(m)} - v_{i-1,j}^{(m+1)})] .$$

The superscripts denote the level of the iterate. On the left side of the equations, only two values at the old iterate (denoted by m) are used. These are the values of v

on the ith row which were assumed for the initial sweep. The values of w on the $(i - 1)$th row are known at the new iteration level from the computations on the previous row of equations. The values of w on the ith row and v on the $(i - 1)$th row are to be computed from the simultaneous solution of this row of equations. The iteration parameter is introduced into the right sides of the equations as a coefficient of the differences between the old and the new values of one v and one w.

The values of v and w used in this iteration term are not located at the same point in the grid. Reference to Fig. 1 will show that the v appearing in this term is located at the point designated by the square ($\square$) and the w at the point designated by the circle ($\bigcirc$). The location of the v is the one point of the four in the square which is farthest from the boundary conditions specifying v in both the y- and z-directions. The w point is similarly located.

8. Single-Row or Point-Wise Iterative Method. The method in which a single row of equations is solved simultaneously is the simpler of the two. Because of the nature of the equations, the method is actually a point-wise or explicit method. The first step in developing this method is to add Eqs. (9a) and (10a). This resulting equation contains only two of the four values to be computed. When multiplied by one-half and written for j, it is

$$(15) \qquad w_{i,j}^{(m+1)} + (1 + \epsilon)v_{i-1,j}^{(m+1)} = w_{i-1,j-1}^{(m+1)} + v_{i,j-1}^{(m)} + \epsilon v_{i-1,j}^{(m)}.$$

Another equation containing the same two unknowns can be obtained from one-half the difference between these equations written for $j + 1$. This equation is

$$(16) \qquad (1 + \epsilon)w_{i,j}^{(m+1)} - v_{i-1,j}^{(m+1)} = w_{i-1,j+1}^{(m+1)} - v_{i,j+1}^{(m)} + \epsilon w_{i,j}^{(m)}.$$

These equations can be solved simultaneously to yield, for $2 \leq j \leq (S - 1)$,

$$(17) \qquad v_{i-1,j}^{(m+1)} = \frac{(1 + \epsilon)A - B}{1 + (1 + \epsilon)^2},$$

$$(18) \qquad w_{i,j}^{(m+1)} = \frac{A + (1 + \epsilon)B}{1 + (1 + \epsilon)^2},$$

where $A = w_{i-1,j-1}^{(m+1)} + v_{i,j-1}^{(m)} + \epsilon v_{i-1,j}^{(m)}$, $B = w_{i-1,j+1}^{(m+1)} - v_{i,j+1}^{(m)} + \epsilon w_{i,j}^{(m)}$.

The boundary conditions specify $v_{i-1,1} = p_{i-1}$ and $w_{i,s} = f_i$. The value of w at the left boundary can be obtained from Eq. (16) as

$$(19) \qquad w_{i,1}^{(m+1)} = (p_{i-1} + w_{i-1,2}^{(m+1)} - v_{i,2}^{(m)} + w_{i,1}^{(m)})/(1 + \epsilon).$$

Likewise, the value of v at the right boundary can be obtained from Eq. (15) as

$$(20) \qquad v_{i-1,s}^{(m+1)} = (-f_i + w_{i-1,s-1}^{(m+1)} + v_{i,s-1}^{(m)} + v_{i-1,s}^{(m)})/(1 + \epsilon).$$

Eqs. (17)–(20) provide the relations necessary for computing the flux components by the single-row iterative method.

9. Double-Row Iterative Method. The double-row method utilizes the explicit nature of the equations of the single-row method. The values of w on the ith row are expressed in terms of the values of w on the $(i - 1)$th row and v on the ith row by Eqs. (18) and (19) with $\epsilon = 0$. These are substituted into Eqs. (15) and (16) written between the ith and $(i + 1)$th rows. The resulting set of equations can be solved to

yield values of w on the $(i + 1)$th row and values of v on the ith row. The solution of these equations requires values of v at the old iterate on the $(i + 1)$th row and values of w at the new iterate on the $(i - 1)$th row. Values of w on the ith row can then be computed from the values of v at the new iterate on the ith row by Eqs. (18) and (19) with $\epsilon = 0$. Likewise, the values of v on the $(i - 1)$th row can be computed from these values of v on the ith row by Eqs. (17) and (20) with $\epsilon = 0$. In this manner, values of v at the old iterate are required on only every other row of points for each sweep across the region. This method, consequently, converges more rapidly than does the single-row method.

The direct solution of these equations has been effected by separating the complete system into two bi-tridiagonal systems of equations. The general equations of each system are the same, and they are

(21)
$$-\epsilon w_{i+1,j}^{(m+1)} - \tfrac{1}{2}v_{i,j-2}^{(m+1)} + (3 + \epsilon)v_{i,j}^{(m+1)} - \tfrac{1}{2}v_{i,j+2}^{(m+1)}$$
$$= \tfrac{1}{2}[w_{i-1,j-2}^{(m+1)} - w_{i-1,j+2}^{(m+1)}] + v_{i+1,j-1}^{(m)} + v_{i+1,j+1}^{(m)} + \epsilon[v_{i,j}^{(m)} - w_{i+1,j}^{(m)}] ;$$

(22)
$$-(1 + \epsilon)w_{i+1,j-2}^{(m+1)} + 3w_{i+1,j}^{(m+1)} + (4 + 3\epsilon)v_{i,j}^{(m+1)}$$
$$= w_{i-1,j-2}^{(m+1)} + w_{i-1,j}^{(m+1)} + 4v_{i+1,j-1}^{(m)} + \epsilon[2v_{i,j}^{(m)} - w_{i+1,j-2}^{(m)}] .$$

In one system the j index takes on odd values, and in the other system it takes on even values. The boundary equations of each system are obtained from suitable combinations of the original equations.

A number of solution algorithms have been developed for these systems of equations, but all of these develop significant round-off error for grids of 20 points in each direction. Work is continuing in an effort to find satisfactory algorithms.

10. Experimental Study of Convergence Rate. A number of runs were made on an IBM 7044 computer to study the number of iterations required for convergence. The boundary conditions of the test problem are

(23a) $$w(z, 1) = z ,$$

(23b) $$w(0, y) = 0 ,$$

(23c) $$v(z, 0) = 0 ,$$

(23d) $$v(1, y) = -y .$$

The solution to Eqs. (3) and (4) with these boundary conditions is $w = z$ and $v = -y$ for all y and z. Since all derivatives above the first are zero for this problem, the numerical solution will converge to the analytic solution for all grid sizes. Furthermore, this solution is a particularly easy one to check for convergence. The initial guess used in all the test runs was $v = w = 0$ at all points in the grid.

The first purpose of this study was to determine experimentally the most efficient value of the iteration parameter, ϵ. The second was to compare convergence rates for the double-row method and for the single-row method. The third purpose was to compare the effect of grid size on the number of iterations required for convergence.

The runs made to determine the most efficient parameter were made on a square

grid with ten increments on each side. Consequently, there were 200 values of the dependent variables to be determined. The method diverged for the two negative values of the parameter tested, and it converged for all positive values and for zero.

For $\epsilon = 0$, the values of the dependent variables approached the correct values asymptotically from the initial guess of zero. For the three positive values of ϵ tested, namely, $\frac{1}{2}$, 1, and 2, the intermediate values of the dependent variables, in some parts of the grid, increased above the correct values and then converged to those values by a damped oscillation. Furthermore, convergence was more rapid for all three of these values than for $\epsilon = 0$. Of the three positive values, $\epsilon = 1$ was the most efficient. At the end of 20 double iteration steps (one in the y-direction and one in the z-direction) no value of the dependent variables differed from the correct value by more than two in the fourth place. Most values were closer than this. For the other two values of ϵ, some values of the dependent variables differed in the third place after 20 steps.

The double-row method converged in approximately half as many iterations as the single-row method. For $\epsilon = 1$ and a 10×10 grid, the values obtained after ten double steps by the double-row method were approximately the same as those obtained after 20 double steps by the single-row method. After 20 double steps by the double-row method, the values were almost completely converged to six places. Only nine of the 200 values differed from the correct values by more than three in the sixth place. The largest difference was seven in the sixth place.

The number of iterations required for convergence for a square grid is approximately proportional to the number of points along one side of the square or, consequently, to the square root of the total number of points in the grid. For a square grid with 100 points on a side, 200 double steps were required to obtain the same extent of convergence as was obtained by 20 double steps with a 10×10 grid. In both of these test runs, the single-row method was used with $\epsilon = 1$. Similar results were obtained for the double-row method with $\epsilon = 0$ for square grids with 10 and 20 points on each side.

11. Experimental Study of Truncation Error. A study of the truncation error was made for flow near a unit source at the origin. The exact solution for this problem is given by

$$(24) \qquad\qquad w = z/(y^2 + z^2),$$
$$(25) \qquad\qquad v = y/(y^2 + z^2).$$

The flux components were computed in a square region with boundaries at $y = 1/2$, $z = 1/2$, $y = 39/2$, and $z = 39/2$ for increment sizes of 1, 1/2, and 1/4; and the resulting values were compared with the exact solution. The truncation error was approximately 30%, 7%, and 1.5% for the three grid sizes; this variation is in line with the second-order correct nature of the finite-difference analogs. The single-row method of solution was used, and round-off error was negligible even for the largest grid of 77 points per side.

12. Comparison with Alternating-Direction-Implicit Method for Potential. The solution for flux components was compared with the alternating-direction-implicit

method of solution for the potential in a square region for equivalent boundary conditions. The boundary conditions in terms of potential are

(26a)   at $y = 0, \partial T/\partial y = 0$ for all z ,

(26b)   at $z = 0, \partial T/\partial z = 0$ for all y ,

(26c)   at $y = 1, T = 0$ for $z < 1$,

(26d)   at $z = 1, T = 1$ for $y < 1$.

Equivalent boundary conditions in terms of flux components are

(27a)   at $y = 0, v = 0$ for all z ,

(27b)   at $z = 0, w = 0$ for all y ,

(27c)   at $y = 1, w = 0$ for $z < 1$,

(27d)   at $z = 1, v = 0$ for $y < 1$,

(27e)   at $y = 1$ and $z = 1, v = 1$ and $w = -1$.

Numerical solutions were obtained for a grid of 20 increments per side; thus, there were 400 points at which either the potential or the flux components were to be obtained. The initial iterates for each method were essentially equivalent.

For the alternating-direction-implicit method the set of nine iteration parameters which result in most rapid convergence was used. This set of parameters is given by Young [2]. Convergence was obtained in two cycles of the parameters or in 18 iterations.

No analysis has been made to obtain a set of iteration parameters for most rapid convergence in the solution for the flux components. Consequently, this solution was effected using a value of unity for the parameter. Convergence was obtained in 30 iterations when the double-row method of solution was used. This method does not compare unfavorably with the alternating-direction-implicit method, and the use of a set of more efficient iteration parameters for the flux component method should decrease the amount of iterations required.

13. Conclusion. An efficient numerical method for the determination of the flux components in potential flow has been developed. Two iterative methods for solving the resulting finite-difference equations are described. Experimental results which determine the most efficient value of the iteration parameter and evaluate the relative efficiencies of the two iteration techniques are presented. These results also show that the number of iterations required for convergence is approximately proportional to the square root of the number of points in the grid.

Tulane University
New Orleans, Louisiana

1. E. H. Herron & D. U. von Rosenberg, "An efficient numerical method for the solution of pure convective transport problems with split boundary conditions," *Chem. Eng. Sci.*, v. 21, 1966, p. 337.

2. D. Young, *Modern Mathematics for the Engineer*, Second Series, McGraw-Hill, New York, 1961, p. 393. MR **23** #B2205.

An improved method of numerical solution for flux components in potential flow†

W. J. GATES and DALE U. VON ROSENBERG

Tulane University, New Orleans, La. 70118, U.S.A.

Abstract—A numerical method for solution of flux components which is completely superior to a method described previously has been developed. In some cases this method leads to a direct, non-iterative solution of two-dimensional problems. It also has an advantage over the alternating direction implicit method in that much larger space increments can be used in one direction than in the other. Examples are given which show the application of the method to mixed boundary conditions, curved boundaries, and a point source.

1. INTRODUCTION

VALUES of the flux components are often desired in potential flow problems. The flux components can be defined in terms of the potential which in two-dimensional Cartesian co-ordinates is defined by the differential equation

$$\frac{\partial^2 T}{\partial y^2} + \frac{\partial^2 T}{\partial z^2} = 0, \qquad (1)$$

where T is the potential, y is one Cartesian co-ordinate, z is the other Cartesian co-ordinate. For this co-ordinate system, the flux components are defined in terms of the potential by

$$v = -k\frac{\partial T}{\partial y}, \qquad (2a)$$

$$w = -k\frac{\partial T}{\partial z}, \qquad (2b)$$

where v is the flux component in the y direction, w is the flux component in the z direction, k is the transport coefficient.

A great number of potential flow problems can be solved by various analytical techniques. However, a numerical solution is required for many boundary conditions. A number of methods have been developed for numerically solving Eq.

(1) for the potential. When values of the flux are desired, the flux components must then be determined from the numerical solution for the potential by finite-difference analogs to Eqs. (2a) and (2b).

Recently von Rosenberg[1] determined the flux components by solving the differential equations which define them. These are a continuity principle

$$\frac{\partial v}{\partial y} + \frac{\partial w}{\partial z} = 0, \qquad (3)$$

and an irrotationality condition

$$\frac{\partial w}{\partial y} - \frac{\partial v}{\partial z} = 0. \qquad (4)$$

Equation (3) is equivalent to Eq. (1), and Eq. (4) can be obtained by equating the cross-partial derivatives of Eqs. (2a) and (2b).

These equations were solved numerically by using second-order correct analogs based on the grid shown in Fig. 1. Both flux components were determined at all the grid points represented by intersections of the grid lines in Fig. 1. The finite difference analogs to the derivatives were centered about the center of each element; for example, the point $y_{j-1/2}$, $z_{i-1/2}$ in Fig. 1. This

Fig. 1. Physical representation of centered differencing.

ponents being determined at different points. Only one value is determined at each grid point as compared to two values for the normal centered difference approach. The pattern formed on the finite difference grid by these unknowns suggests the name "checkerboard." Figure 2 illustrates this.
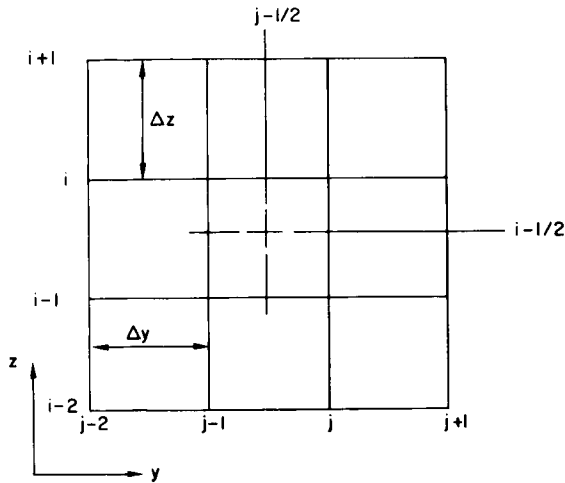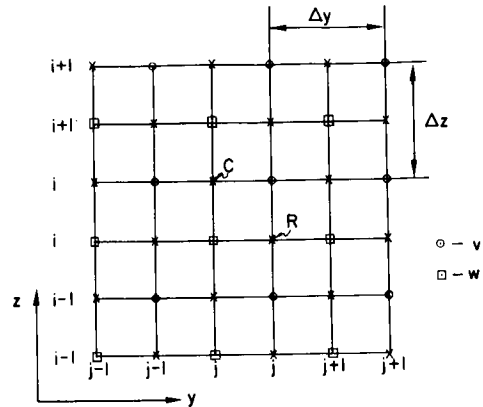

Fig. 2. Physical representation of checkerboard differencing.

original method is termed the centered difference method to distinguish it from the new method described in this paper. The original method is described in detail in Ref. [1].

During the investigations of algorithms for solving the finite difference equations which resulted from this difference scheme, it was discovered that the linear algebraic equations can be reduced to a set of equations which can be solved for one-half of the total unknown flux component values. These remaining equations can be uncoupled to form two independent sets of equations, each of which forms a complete set for one-fourth of the total unknowns. This is the origin of the idea for the "checkerboard" method for determining the flux components.

The "checkerboard" method is a second-order correct differencing scheme with the difference equations for Eqs. (3) and (4) written about different points in the finite difference grid. The name is descriptive of the way the unknown values of v and w appear on the grid.

2. DEVELOPMENT OF THE CHECKERBOARD DIFFERENCE EQUATIONS

In the "checkerboard" method the continuity equations and the irrotationality equations are not centered at the same points on the integration net. This results in the v and w flux com-

The v's are determined at the grid points on Fig. 2 indicated by the symbol $\odot$, and the w's are determined at those grid points indicated by $\square$. The finite difference equations for the continuity equation are centered on the rows with the v's and at the grid points falling between the points where the v's are to be determined. The point indicated by the letter C is an example of one of these points. The finite difference equations for the irrotationality condition are centered on the rows with the w's at the grid points between the points where w's are to be determined. The point indicated by R is one of these points. The space increments, Δy and Δz, are as indicated on the figure. Note that they are the total distance between any two unknowns on any row or column.

The v's and w's have different indexing systems so that if the origin $(z, y) = (0, 0)$ has the subscripts $(i, j) = (1, 1)$ then the variable $w_{i,j}$ will be located at the point given by

$$z_i = (i - 1)\Delta z,$$

$$y_j = (j - 1)\Delta y.$$

The variable $v_{i,j}$ will be located at the point given by

$$z_i = (i - \tfrac{1}{2})\Delta z,$$
$$y_j = (j - \tfrac{1}{2})\Delta y.$$

The finite difference equations are developed by substituting expressions developed from a Taylor series in two independent variables for the continuous derivatives in the differential equations. The checkerboard difference analog for the continuity equation centered at point C of Fig. 2 is

$$\frac{v_{i,j} - v_{i,j-1}}{\Delta y} + \frac{w_{i+1,j} - w_{i,j}}{\Delta z} = 0. \qquad (5)$$

The difference analog for the irrotationality equation centered at point R of Fig. 2 is

$$\frac{v_{i,j} - v_{i-1,j}}{\Delta z} - \frac{w_{i,j+1} - w_{i,j}}{\Delta y} = 0. \qquad (6)$$

These difference equations include only four values of the dependent variables per equation whereas the centered difference analogs[1] include eight values per equation.

3. TRUNCATION ERROR

The truncation error associated with the finite difference equation is that part of the Taylor series truncated in forming the equations. The truncation error for the finite difference analog to Eq. (3) is

$$E_3 = -\sum_{n=1}^{\infty} \left[\frac{1}{(2n+1)!} \left(\frac{\Delta z}{2}\right)^{2n} \left(\frac{\partial^{2n+1} v}{\partial y^{2n+1}} + \frac{\partial^{2n+1} w}{\partial z^{2n+1}}\right) \right] \qquad (7)$$

and that for Eq. (4) is

$$E_4 = -\sum_{n=1}^{\infty} \left[\frac{1}{(2n+1)!} \left(\frac{\Delta z}{2}\right)^{2n} \left(\frac{\partial^{2n+1} v}{\partial z^{2n+1}} - \frac{\partial^{2n+1} w}{\partial y^{2n+1}}\right) \right]. \qquad (8)$$

The expressions for the errors can be simplified by use of relations obtained from repeated dif-ferentiation of Eqs. (3) and (4). Equation (7) can then be expressed as

$$E_3 = -2\sum_{n=0}^{\infty} \left[\frac{1}{(4n+3)!} \left(\frac{\Delta z}{2}\right)^{4n+2} \left(\frac{\partial^{4n+3} w}{\partial z^{4n+3}}\right) \right]. \qquad (9)$$

The truncation error, E_{CD}, for the centered difference analog for the continuity equation is [1]

$$E_{CD} = -2\sum_{n=0}^{\infty} \left[\frac{1}{(4n+3)!} \left(\frac{\Delta z_{CD}}{2}\right)^{4n+2} \left(\frac{\partial^{4n+3} w}{\partial z^{4n+3}}\right) \right.$$
$$\left. (-1)^{n+1} (2)^{2n+1} \right]. \qquad (10)$$

Here Δz_{CD} is the space increment length used on the centered difference grid.

In each of the series, (9) and (10), the first term is much larger than the remainder of the terms. These terms then can be compared to give an approximate relationship between the sizes of the truncation errors for the two methods. This is

$$\frac{E_3}{E_{CD}} = -\frac{1}{2}\left(\frac{\Delta z}{\Delta z_{CD}}\right)^2. \qquad (11)$$

Thus, for the same space increment the checkerboard method has approximately one-half as much truncation error as the centered difference method. The truncation error should be approximately the same when the space increments for the checkerboard are $\sqrt{2}$ times those for the centered difference method.

This analysis was the major reason for the further investigation of the checkerboard method for solving these equations. It was found that the checkerboard solution is relatively much more accurate than this analysis indicates.

4. CORRESPONDING DIFFERENCE EQUATION IN POTENTIAL

It is interesting to see how the checkerboard continuity difference equation looks when the flux components are replaced by their definitions in terms of the potential, Eqs. (2a) and (2b).

On Fig. 2, the symbols x represent the points where the potential is to be determined. Values

of v and w have the same subscripts as before. The subscripts for the potential are such that the variable $T_{i,j}$ will be located at the point given by

$$z_i = (i - \tfrac{1}{2})\Delta z$$

$$y_j = (j - 1)\Delta y.$$

The checkerboard continuity finite difference equation centered at point C is

$$\frac{v_{i,j} - v_{i,j-1}}{\Delta y} + \frac{w_{i+1,j} - w_{i,j}}{\Delta z} = 0. \tag{12}$$

The variables in this expression can be expressed in terms of the potential. An example is

$$v_{i,j} = -k \left(\frac{T_{i,j+1} - T_{i,j}}{\Delta y} \right). \tag{13}$$

These are substituted into Eq. (12) and Δz set equal to Δy to obtain

$$\frac{T_{i+1,j} + T_{i,j+1} + T_{i,j-1} + T_{i-1,j} - 4T_{i,j}}{(\Delta y)^2} = 0. \tag{14}$$

This is the familiar five-point finite difference equation for Laplace's equation. If, similarly, the flux components in the irrotationality difference equation, Eq. (6), are replaced by their definitions in terms of potential, the equation reduces to $0 = 0$ as it should.

5. SINGLE ROW SOLUTION METHOD FOR THE CHECKERBOARD DIFFERENCE EQUATIONS

For purposes of illustrating the numerical method, the model problem used is a rectangular region of length a in the y direction and b in the z direction. The boundary conditions are

$$w(0,y) = f(y) \tag{15a}$$

$$w(z,0) = g(z) \tag{15b}$$

$$v(b,y) = p(y) \tag{15c}$$

$$v(z,a) = q(z). \tag{15d}$$

The boundary conditions are equivalent to specifying the potential on the boundaries at $y = 0$ and $z = b$ and specifying the normal derivative of the potential along the boundaries at $y = a$ and $z = 0$.

The boundary conditions for the model problem are split so that it is necessary either to solve all of the finite difference equations simultaneously for all of the unknown values of the flux components or to perform an iterative solution. Because of the large number of difference equations involved in most practical problems, an iterative solution is the most useful.

The iterative solution developed for the checkerboard difference equations is an implicit, line iterative method. The lengths of the space increments are given by the expressions

$$\Delta y = \frac{2a}{(2S - 1)} \tag{16a}$$

$$\Delta z = \frac{2b}{(2R - 1)} \tag{16b}$$

where

$$1 \leq i \leq R$$

$$1 \leq j \leq S.$$

It was arbitrarily decided to carry out the iteration procedure in the z direction. A row of difference equations for the continuity equation and an adjacent row of difference equations for the irrotationality equation are solved simultaneously for one step of the iteration. This method will be called the single row method for later reference purposes because one row of each set of unknowns is determined per step. The iteration procedure is begun at the boundary $z = 0$ where the flux components $w_{1,j}$ are known for the whole row of points or equivalently for all j. The row of continuity difference equations on the row with the flux components $v_{1,j}$ and the row of irrotationality difference equations on the row with the flux components $w_{2,j}$ are solved simultaneously. These equations involve the flux components $w_{1,j}$, $v_{1,j}$, and $v_{2,j}$. The $w_{1,j}$ are known from the boundary conditions leaving three rows

of unknowns and two rows of equations. The values of $v_{2,j}$ are assumed to start the iteration and the two rows of equations are solved for $v_{1,j}$ and $w_{2,j}$.

For the next step of the iteration, the continuity difference equations on the row with the $v_{2,j}$ and the irrotationality difference equations on the row with the $w_{3,j}$ are solved simultaneously. In order to do this operation, the values of $w_{2,j}$ computed in the first step are used together with guessed values of the $v_{3,j}$; the equations are solved for the $v_{2,j}$ and $w_{3,j}$.

This procedure is continued across the region until the equations adjacent to the boundary at $z = b$ are solved. Here the continuity difference equations on the row with the $v_{R-1,j}$ and the irrotationality difference equations on the row with the $w_{R,j}$ are solved simultaneously for $v_{R-1,j}$ and $w_{R,j}$. For this last step of the iteration the $v_{R,j}$ are known from a boundary condition and the $w_{R-1,j}$ were computed in the preceding step of the iteration.

The boundary conditions on each boundary are thus introduced once in each sweep across the region. On the next sweep of the region, the values obtained in the first sweep are used in place of the assumed values.

The use of iteration parameters to accelerate the convergence was tried, but equally fast convergence was obtained with no parameter. The equations for one step of the single-row method without an iteration parameter are

$$v_{i-1,1}^{(M+1)} + w_{i,2}^{(M+1)} = v_{i,1}^{(M)} + w_{i,1}^{(M)} \qquad (17a)$$

$$-v_{i-1,j-1}^{(M+1)} + w_{i,j}^{(M+1)} + v_{i-1,j}^{(M+1)} = w_{i-1,j}^{(M)} \qquad (17b)$$

$$-w_{i,j}^{(M+1)} + v_{i-1,j}^{(M+1)} + w_{i,j+1}^{(M+1)} = v_{i,j}^{(M)} \qquad (17c)$$

$$-v_{i-1,S-1}^{(M+1)} + w_{i,S}^{(M+1)} = w_{i-1,S}^{(M)} - v_{i-1,S}^{(M)} \qquad (17d)$$

where M indicates the level of the iterate. These equations fit the tri-diagonal matrix form so they can be solved very efficiently with the Thomas Algorithm.

The model problem was solved using this single row method with several different sizes of integration nets. It was determined that the

number of iterations needed for convergence is approximately proportional to N, where N is the number of points on the side in the direction of iteration.

6. MULTIPLE ROW METHODS

The checkerboard finite difference equations have a very simple form when the iteration parameter is omitted. Consequently, a method of solving two rows of each of the two types of equations simultaneously was developed. An advantage of this method over the single row method is that the values of only one-half as many rows of v's need to be assumed in performing an iteration.

The continuity difference equations on the rows with the $v_{1,j}$ and the $v_{2,j}$ and the irrotationality difference equations on the rows with the $w_{2,j}$ and the $w_{3,j}$ and solved simultaneously. The $w_{1,j}$ are known from a boundary condition. These four rows of equations then involve five rows of unknowns; the $v_{1,j}$, $w_{2,j}$, $v_{2,j}$, $w_{3,j}$, and $v_{3,j}$. Values for the $v_{3,j}$ are assumed so that four rows of unknowns and four rows of equations remain.

The $S - 1$ equations on the row with the $w_{2,j}$ yield expressions for the $v_{1,j}$ in terms of the $w_{2,j}$ and $v_{2,j}$. These expressions are used to eliminate the $v_{1,j}$ from the equations on the row with the $v_{1,j}$. The $S - 1$ equations that result from this procedure contain at most five unknowns each. Those equations that involve boundary conditions at the ends of the rows have fewer than five unknowns.

The equations on the row with the $v_{2,j}$ yield expressions for the $w_{3,j}$ in terms of the $v_{2,j}$ and the $w_{2,j}$. These expressions are used to eliminate the $w_{3,j}$ from the equations on the row with the $w_{3,j}$. The resulting $S - 1$ equations contain five unknowns at most. Again, those involving boundary conditions have fewer than five.

The two groups of $S - 1$ equations that have been formed contain the $w_{2,j}$ and the $v_{2,j}$ as the unknowns. The total of $2(S - 1)$ equations when arranged properly and written in matrix form have a penta diagonal matrix of coefficients. An efficient Gaussian reduction algorithm which takes into account the zero elements in the co-

efficient matrix was used for the solution of these equations. After the $v_{2,j}$ and $w_{2,j}$ have been determined, the explicit relations for the $v_{1,j}$ and the $w_{3,j}$ in terms of the $v_{2,j}$ and the $w_{2,j}$ are available for computing these unknowns. This method is termed the double row method because two rows of each set of unknowns are determined per step.

The next and subsequent steps of the iteration procedure follow a pattern very similar to that described for the single row method. A major difference between the two solution algorithms is that with the double row method, the values of only every other row of the v's need be guessed as opposed to the values of every row of v's for the single row method.

The process of solving more than one row of each type of equation simultaneously can be extended to more than two rows. Equations were developed for the simultaneous solution of three rows and of four rows. In the three row method, only one-third of the v's must be assumed to start the iteration procedure; and in the four row method, only one-fourth of these values must be assumed. The band matrix resulting from the three row method contains seven non-zero coefficients, and that from the four row method contains nine.

A pattern developed in the iteration procedures is that each time two more rows of equations are included in a step of the iteration, the coefficient band matrix becomes wider by two elements. The middle two rows of unknowns are determined from the simultaneous solution of the $2(S-1)$ equations in the matrix equation. The other rows of unknowns in the set are computed from explicit expressions as functions of the

values determined from the matrix equation. Details of this procedure are given by Gates[2].

Table 1 contains the values for these coefficients for the general equations discussed above. It also contains the coefficients for the eleven wide band matrix that results from solving five rows of each type of equation in each step of the iteration. The band width is always equal to $2M + 1$, where M is the number of rows of each type of equation in the iteration step.

From Table 1, a pattern was developed for obtaining the coefficients for any band equation from the preceding row of coefficients. The coefficients for the three wide band equation are needed to start the process. Thus, the coefficients for the five wide band equation can be obtained from those for the three wide band, and the seven wide band coefficients can be obtained from those for the five wide band. The absolute value for a coefficient is obtained either as the value of the coefficient immediately above it or as the sum of the absolute values of that coefficient and the two coefficients on either side of it. In order to explain this pattern, it is convenient to define a nomenclature for the general band matrix.

Sets of simultaneous equations that have a band matrix of coefficients are of the general form

$$a_j^{(M)}x_{j-M} + a_j^{(M-1)}x_{j-M+1} + \cdots + a_j^{(2)}x_{j-2}$$
$$+ a_j^{(1)}x_{j-1} + b_jx_j + c_j^{(1)}x_{j+1} + c_j^{(2)}x_{j+2} + \cdots$$
$$+ c_j^{(M-1)}x_{j+M-1} + c_j^{(M)}x_{j+M} = d_j \qquad (18)$$

where the x_j's are the unknowns, the a_j's, b_j, and c_j's are the coefficients, the d_j is the known right-hand-side of the equation, j is the position of the equation in the set of equations and $2M + 1$ is the

Table 1. Coefficients for the band equations

Band width	$a_j^{(5)}$	$a_j^{(4)}$	$a_j^{(3)}$	$a_j^{(2)}$	$a_j^{(1)}$	b_j	$c_j^{(1)}$	$c_j^{(2)}$	$c_j^{(3)}$	$c_j^{(4)}$	$c_j^{(5)}$
3					-1	$+1$	$+1$				
5				-1	-1	$+3$	$+1$	-1			
7			$+1$	-1	-5	$+3$	$+5$	-1	-1		
9		$+1$	$+1$	-7	-5	$+13$	$+5$	-7	-1	$+1$	
11	-1	$+1$	$+9$	-7	-25	$+13$	$+25$	-7	-9	$+1$	$+1$

540

band width of the coefficient matrix. When M equals one, the equation is in the tri diagonal form and when M equals 2, the equation is in the penta diagonal form.

For the 5, 9, 13, etc. wide band equations, b_j and the a_j and c_j coefficients with even superscripts are obtained by the summing operation. For the 7, 11, 15, etc. wide band equations, the a_j and c_j coefficients with the odd superscripts are obtained as the sums. The pattern for the signs of the coefficients is obvious from the table. The pattern for the coefficients of the equations that involve boundary conditions on the sides of the grid and the pattern for obtaining the excitation vector for any multiple row solution method were also developed. Reference [2] includes the recurrence formulas for developing the coefficient matrix and the excitation vector for any multiple row solution method for the model problem.

The development led to a method for the solution of the model problem that includes all of the rows of equations in the integration net in one band matrix. The method does not require the guessing of any of the values of the v's so it is an explicit, non-iterative solution. It involves solving simultaneously a set of $2(S-1)$ equations that have a band matrix of coefficients with the band width equal to $2M+1$, where M is the number of rows of each type of equation included. The remaining unknowns are determined from explicit expressions which give them as functions of the values computed from the matrix equation.

The authors had available the program of an efficient solution algorithm for the band matrix which was developed at the Esso Production Research Company. Given the band width, the band coefficients, and the excitation vector, the solution vector is computed. A computer program for performing the various solution methods for the model problem was written for the IBM 7044 computer.

Table 2 contains the results of solving the model problem for a square region with $S = R = 13$ and $a = b = 1\cdot0$. Each of the solutions was started with the same initial guesses and was converged to the same convergence level.

Table 2. Six solutions of the model problem for the same grid

S	R	Band width	Iterations	Steps/ iteration	Approximate no. of total arithmetic operations
13	13	3	51	12	117,500
13	13	5	29	6	91,900
13	13	7	23	4	88,300
13	13	9	23	3	102,700
13	13	13	23	2	130,300
13	13	25	1	1	9200

The band width values given in the table represent the width of the bands of the coefficient matrices for the different methods. The band width of three means that a single row of each type of equation was solved per step of an iteration and there were then twelve steps per iteration. The band width of 25 means that twelve rows of each type of equation was solved in one step and, therefore, there was no need to iterate to the solution. The solution was obtained in one step.

The number of arithmetic operations for the solution of the simultaneous equations by the general band algorithm was determined. From this value and from the number of iterations required and the number of rows per iteration, the total number of arithmetic operations for each solution was determined. These are included in Table 2.

The results indicate that the number of iterations to reach a desired level of convergence for the model problem is decreased by almost one-half by using the double row method instead of the single row method. Another significant decrease in the number of iterations is accomplished by going to the three row method. The four and six methods give no improvement in the number of iterations required.

Table 2 also shows that the decrease in the number of arithmetic operations required for solution in going from the single row method to the double row method to the three row method is not quite so impressive as the decrease in the number of iterations required. The six row method actually requires more operations than

the single row method. The most impressive figure is that the twelve row method, which for this problem is an explicit, non-iterative method, requires less than one-tenth as many operations as the single row method.

7. EXPLICIT SOLUTION OF THE CHECKER-BOARD EQUATIONS

Table 3 is a summary of the results of explicit solutions for the model problem for several square grids with $a = b = 1 \cdot 0$. The conclusion to be drawn from Table 3 then is that reasonable solutions can be obtained with up to a 41 wide band matrix, but the solution of wider band matrices involves too much round-off error.

Table 3. Summary of explicit solutions of model problems

S	R	Band width	Δy	Maximum per cent error
7	7	13	0·15385	0·000
9	9	17	0·11765	0·000
11	11	21	0·09524	0·001
13	13	25	0·08000	0·005
15	15	29	0·06897	0·052
17	17	33	0·06061	0·129
21	21	41	0·04878	5·038
23	23	45	0·04444	43·936

These results indicate the size of the multiple row method that can be used practically, and they do not impose a limit on the size of grid that can be solved by the checkerboard method. A grid with 41 points on a side was converged very well by the single row method, and a grid with 51 points on a side was converged by the five row method. Other much larger grids were solved with essentially no round-off error by 1, 2, 3, 4, and 5 row methods during the course of the study. Table 3 indicates that the two and three row methods may be the best when the grid is too large to obtain an explicit solution.

8. UNEQUAL SPACE INCREMENTS

Problems sometimes occur in engineering for which it is desirable to use space increments of different lengths in the different co-ordinate

directions. An example is found in oil reservoir studies in which the two co-ordinate directions represent the length and thickness of a reservoir. The thickness may be a few feet and the length a few miles. For this situation, with y representing length and z representing thickness, one would probably want to use a Δy much larger than Δz. When problems of this sort are being solved by the alternating-direction implicit method, a ratio of Δy to Δz of about ten or larger causes convergence problems. This limit is a result of the need to sweep through the region in the direction of the long space increments as well as in the direction of the short space increments.

The iteration procedures developed for the checkerboard difference equations involve sweeping through the region in only one direction, which can be the direction with the shorter space increments, Δz. The single row solution method for the checkerboard difference equations with Δz less than Δy is written very simply from Eqs. (5) and (6). The continuity difference equation is

$$ -v_{i,j}^{(M+1)} + \frac{\Delta y}{\Delta z} w_{i+1,j+1}^{(M+1)} + v_{i,j+1}^{(M+1)} = \frac{\Delta y}{\Delta z} w_{i,j+1}^{(M)} . \quad (19) $$

The irrotationality difference equation is

$$ -w_{i+1,j}^{(M+1)} + \frac{\Delta y}{\Delta z} v_{i,j}^{(M+1)} + w_{i+1,j+1}^{(M+1)} = \frac{\Delta y}{\Delta z} v_{i+1,j}^{(M)}. \quad (20) $$

Solutions of the model problem were obtained by using these equations with the ratio of Δy to Δz having the values of 0·10, 1·0, 10·0, 100·0, 1000·0, and 10,000·0. Exact convergence was obtained for all six cases. The solution with the ratio, $\Delta y/\Delta z$, having the largest value required the fewest number of iterations for convergence and the solution with the smallest ratio required the greatest number of iterations. The same number of points were being determined for all of the cases. These results emphasize the value of making the iteration procedure explicit in the direction with the shorter space increments.

It is possible to develop multiple row solution methods for problems with unequal space

542

increments. When two rows of each equation are solved per step of an iteration, the simultaneous equations fit the penta diagonal matrix form and a general row of the coefficient matrix is

$$-\delta^2 \quad -\delta \quad +(1+2\delta^2) \quad +\delta \quad -\delta^2$$

where δ is the ratio $\Delta y/\Delta z$. When three rows of each equation are solved per step, the simultaneous equations fit the hepta diagonal matrix form and a general row of the coefficient matrix is

$$+\delta^3 \quad -\delta^2 \quad -(2+3\delta^2) \quad +(1+2\delta^2)$$
$$+(2+3\delta^2) \quad -\delta^2 \quad -\delta^3.$$

When δ equals $1\cdot0$ these coefficients reduce to those developed in an earlier section for the situation with equal space increments. The coefficients for multiple row methods with band matrices wider than these becomes very complicated. They were not developed because, as it was mentioned earlier, the two and three row methods are probably the best solution methods, other than the explicit solution method, for a given sized grid.

The checkerboard method then has an important advantage over the alternating-direction implicit method. When the problem to be solved is such that Δy can be much larger than Δz, the checkerboard method can be used.

9. EXPERIMENTAL VERIFICATION THAT THE CHECKERBOARD METHOD IS SECOND-ORDER CORRECT

In an earlier chapter it was demonstrated that the checkerboard method is second-order correct. Thus, the truncation error should be directly proportional to the square of the space increment. If the space increment size is decreased by a factor of one-half, then the truncation error should be decreased by a factor of one-fourth.

The problem used in studying the truncation error was that for flow near a source of strength μ at the origin[1]. The exact solution for this problem is given by

$$w = \frac{\mu z}{(y^2 + z^2)} \qquad (21)$$

$$v = \frac{\mu y}{(y^2 + z^2)}. \qquad (22)$$

In the solution a value of $0\cdot1$ was used for μ. The flux components were computed in a square region with the boundaries at $y = 0\cdot05$, $z = 0\cdot05$, $y = 1\cdot95$, and $z = 1\cdot95$. The boundary conditions specified the exact values of the flux components on the boundaries according to Eq. (13).

Table 4 summarizes the results of solving the problem for four different grid sizes. The conclusion to be drawn is that the checkerboard method is second-order correct since, for both comparisons, the ratio of the errors is approximately equal to the ratio of the square of the space increments.

Table 4. Experimental verification that the checkerboard method is second-order correct

$S \times R$	$(\Delta y)^2$	Ratio of $(\Delta y)^2$	Ratio of average fraction error per value
19 × 19	0·01055		
41 × 41	0·00220	4·80	4·23
25 × 25	0·00601		
51 × 51	0·00142	4·23	3·98

On the basis of Eq. (11), the statement was made that the centered difference method and the checkerboard method should have approximately the same truncation error when the space increments used for the checkerboard method are $\sqrt{2}$ times those used for the centered difference method. The problem of flow near a source at the origin was solved by the centered difference method for a square grid with 28 points on a side. Thus, the space increments were $0\cdot0704$. The converged solution had an average fraction error per flux component of $0\cdot094$.

This solution can be compared to the checkerboard solution for a square grid with nineteen points on a side. The ratio between the space increments for the two solutions was then $0\cdot1025/0\cdot0704 = 1\cdot46$ where $\sqrt{2} = 1\cdot414$. The

checkerboard solution should have been slightly less accurate than the centered difference solution according to Eq. (11). The converged values for the flux components had an average fraction error of 0·026 for the checkerboard method compared to 0·094 for the centered difference solution. Thus, the truncation error for the centered difference method was about 4·5 times that for the checkerboard method where it had been predicted from Eq. (11) that the truncation errors for the two methods should be about equal.

The fact that the checkerboard solution was much more accurate than the centered difference solution cannot be explained in terms of round-off error because the general band algorithm, which is very stable to round-off error, was used for both solution methods. The explanation must lie in the fact that Eq. (11) is a comparison between the truncation error for the derivatives of the function, whereas the values compared in the above study are of the function itself. The checkerboard method gives a much better representation for the function itself than does the centered difference method. This finding is very significant and demonstrates the clear superiority of the checkerboard method. A much larger grid, and thus much less computer time can be used for the checkerboard method. Thus, there is little need to consider further the centered difference method for the determination of flux components in potential flow problems.

10. COMPARISON OF THE CHECKERBOARD AND ADI METHODS

The model problem was solved for the potential by the alternating-direction implicit method. For the ADI method, the set of nine iteration parameters which results in the most rapid convergence for a square grid with twenty increments per side was used.

With twenty increments per side of the grid, the ADI method required 26 iterations to converge the solution to the fifth decimal place. The checkerboard method with the tri diagonal iteration method required 61 iterations to reach the same level of convergence.

Each of the 26 iterations for the ADI method required two sweeps through the grid. Each sweep required that twenty sets of twenty tri diagonal equations each be solved. With approximately eight arithmetic operations per equation, approximately 166,400 operations were required for this optimum ADI solution.

Each iteration by the checkerboard method required the solution of twenty sets of forty tri diagonal equations each. Approximately 390,400 operations were required for the solution, or over twice as many as for the ADI solution.

Table 3 is a summary of the results of solving the model problem for a grid with thirteen points on a side by six different multiple row methods and the approximate number of arithmetic operations required for each solution. The same size grid was solved for the potential by the ADI method with the same set of iteration parameters used previously. This solution required eight iterations to converge the problem to the same level of convergence as those solutions summarized in Table 3. The ADI solution required approximately 18,300 arithmetic operations which is considerably fewer than all of the multiple row solutions, except the explicit solution. That required about 9200 operations or one-half as many as the ADI solution.

The conclusion then is that the ADI method can converge to a solution for the potential with less work than the checkerboard method can converge the equivalent problem for the flux components. However, if an explicit solution can be used for the checkerboard difference equations, then that is the fastest method.

The checkerboard method also has an advantage over the ADI method for problems with grids with unequal space increments as was discussed in an earlier section.

11. MIXED BOUNDARY CONDITION

The example problem for illustrating the treatment of a mixed boundary condition is one with an analytical solution given by Carslaw and Jaeger[3]. The problem is the steady-state temperature in a rectangle with convection into a medium at zero temperature on one boundary.

When the problem is converted from one in temperature, or potential, to one in fluxes the boundary conditions are

$$v(0, y) = -1 \qquad (23a)$$

$$w(b, y) = 0 \qquad (23b)$$

$$v(z, 0) = 0 \qquad (23c)$$

$$\frac{\partial v}{\partial z}(z, a) + hw(z, a) = 0 \qquad (23d)$$

where h is the heat transfer coefficient.

The grid is arranged with unequal space increments for the two co-ordinate directions so that v flux components are to be determined on the boundary at $y = a$. Fictitious points are used for the w flux components in order to write the irrotationality difference equations and finite difference analogs for Eq. (23d) on that boundary.

Figure 3 represents a portion of the boundary at $y = a$. The dotted squares represent the fictitious points. The irrotationality difference

Fig. 3. Boundary with mixed boundary condition.

equation written about the point, p, on Fig. 3 is

$$\frac{v_{i+1,S}^{(M+1)} - v_{i,S}^{(M)}}{\Delta z} - \frac{w_{i,S}^{(F)} - w_{i,S-1}^{(M+1)}}{\Delta y} = 0 \qquad (24)$$

where F indicates a fictitious value, and M represents the level of the iterate. The difference analog for Eq. (23d) is

$$\frac{v_{i+1,S}^{(M+1)} - v_{i,S}^{(M)}}{\Delta z} + h\left(\frac{w_{i,S}^{(F)} + w_{i,S-1}^{(M+1)}}{2}\right) = 0. \qquad (25)$$

The value $w_{i,S}^{(F)}$ is eliminated between Eqs. (24) and (25) to obtain as the last equation in the tri diagonal set for that step of an iteration.

$$\left(2\frac{\Delta y}{\Delta z}\right)w_{i,S-1}^{(M+1)} + \left(1 + \frac{2}{h\Delta y}\right)v_{i+1,S}^{(M+1)} = \left(1 + \frac{2}{h\Delta y}\right)v_{i,S}^{(M)}. \qquad (26)$$

The checkerboard solution was obtained for a grid with 25 points on a side in about 100 iterations. The average percent difference between the values computed from the series and the checkerboard numerical solution was 2·2 percent.

This is a good comparison between the checkerboard numerical solution and the series solution obtained by the classical separation-or-variables technique. The problem illustrates that the method can be easily adapted to problems with mixed boundary conditions.

12. CURVED BOUNDARY AND POINT SOURCE

The boundaries of many problems that occur in engineering are curved. Figure 4 represents one-fourth of an elliptical oil reservoir in which it is desired to find the flow patterns. Fluid is injected in equal quantities at wells in two quadrants of the ellipse and produced in equal quantities from symmetrically placed wells in the other two quadrants. The wells can be considered to be point sources and sinks so that the problem also introduces the problem of handling such points. This problem is one which Douglas and Peaceman[4] solved for the pressure distribution,
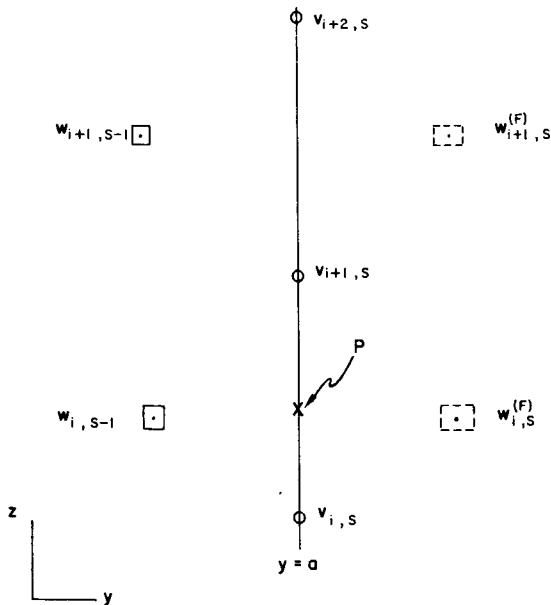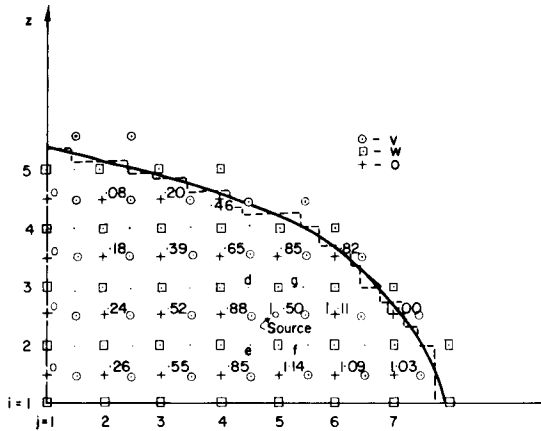
545

Fig. 4. Integration net for elliptical reservoir.

i.e. potential, by using the alternating-direction implicit method.

The wells are located so that the solution is symmetric with respect to z and anti-symmetric with respect to y; thus, it is necessary to consider only the upper right hand quandrant. The boundary conditions specify that the w flux components are zero along both the y and z axes and that there is no flow across the curved boundary.

The no-flow boundary condition on the curved boundary is treated by approximating the curved boundary with a stepped boundary as shown by the broken line on Fig. 4. The points outside the boundary are fictitious but the flux components located there are needed to write the checkerboard difference equations at the usual interior points. The approximate boundary is such that it is vertical when it passes between an interior v flux component and a fictitious v component. There is no flow across the boundary so the v component is zero at the vertical boundary. Likewise, the approximate boundary is horizontal when it passes between an interior and an exterior w flux component. The w component is zero on the horizontal boundary. The interior component, the zero component on the approximate boundary, and the fictitious component all lie on the same straight line so that the exterior component can be expressed as a function of the zero component on the boundary and the interior component by the point-slope formula.

The finite difference equations are written as Eqs. (19) and (20) so that the space increments in the two co-ordinate directions can be adjusted to cause the point source to fall on a point at which the continuity equation would normally be written. The iteration procedure used is the single row method with the tri diagonal sets of equations. Each succeeding step of the iteration procedure has fewer equations to be solved than the previous step.

The solution satisfies Eq. (3) everywhere in the interior of the region, except the point where the fluid is injected. This is because the equation expresses the condition that the net flow into the region around a point is zero. To obtain the correct expression at the point source, one writes a material balance around the source point which is indicated on Fig. 4. The fluid is injected at the rate V. The flow, V_1, across the line d–e is approximately

$$V_1 = - \Delta z \, v_{2,4}^{(M+1)}. \tag{27a}$$

The flow, V_2, across the line e–f is approximately

$$V_2 = - \Delta y \, w_{2,5}^{(M)}. \tag{27b}$$

The flow, V_3, across the line f–g is approximately

$$V_3 = \Delta z \, v_{2,5}^{(M+1)}. \tag{27c}$$

The flow, V_4, across the line g–d is approximately

$$V_4 = \Delta y \, w_{3,5}^{(M+1)}. \tag{27d}$$

Then at steady state $V = V_1 + V_2 + V_3 + V_4$ and the equation to be satisfied is

$$V = \left[\Delta z \left(v_{2,5}^{(M+1)} - v_{2,4}^{(M+1)} \right) + \Delta y \left(w_{3,5}^{(M+1)} - w_{2,5}^{(M)} \right) \right]. \tag{28}$$

This equation fits into the tri diagonal set for that step of the iteration.

The problem was programmed for the grid in Fig. 4. The values of the parameters used were: $a = 1 \cdot 0$, $b = 0 \cdot 643$, $\Delta y = 0 \cdot 147$, $\Delta z = 0 \cdot 155$, and $V = 2 \cdot 0$. The point source was located at the

point $(z, y) = (0.232, 0.589)$. The solution was converged to the fourth decimal place after twenty iterations.

To obtain a check on the solution, the flux components were numerically integrated to obtain the potential which was compared to the solution obtained by Douglas and Peaceman[4]. Equation (13a) was used for the numerical integration with $k = 1.0$. The integration was started at the $y = 0$ boundary where the boundary condition is $T = 0$. The values obtained are shown on Fig. 4 at the points indicated by the +'s. The values cannot be compared exactly to those obtained in [4] because the dimensions of the region used for that solution are not known, but the

potential profiles are generally the same. The method for treating the curved boundary and the point source is satisfactory.

13. CONCLUSION

A numerical method has been described which can lead to a direct solution of some two-dimensional potential flow problems expressed in terms of flux components. This method can be used with one space increment as much as 10,000 times the other, and thus, it has advantages over other methods for the solution of such problems. The method has been demonstrated to be applicable to a variety of boundary conditions and flow configurations.

REFERENCES

[1] VON ROSENBERG D. U., *Maths Comput.* 1967 **21** 620.
[2] GATES W. J., Ph.D. Dissertation, Tulane University 1968.
[3] CARSLAW H. S. and JAEGER J. C., *Conduction of Heat in Solids.* 2nd Edn. p. 166. Oxford University Press 1959.
[4] DOUGLAS J., Jr. and PEACEMAN D. W., *A.I.Ch.E. Jl* 1955 **1** 505.

Résumé—Une méthode, bien supérieure à une méthode décrite précédemment, a été développée pour donner une solution numérique des composants de flux. Dans certains cas, cette méthode conduit à une solution directe, non itérative de problèmes à deux dimensions. Elle présente aussi l'avantage sur la méthode implicite de direction alternée, de permettre d'utiliser des accroissements plus importants dans un sens que dans l'autre. Des exemples sont donnés pour montrer l'application de la méthode aux limites mixtes, courbes et à une source ponctuelle.

Zusammenfassung—Es wurde eine numerische Lösung für Strömungskomponenten entwickelt, die einer früher beschriebenen Methode weit überlegen ist. In manchen Fällen führt diese Methode zu einer unmittelbaren, nicht iterativen Lösung zweidimensionaler Probleme. Sie hat ferner den Vorteil gegenüber der impliziten Methode, mit wechselnden Richtungen dass viel grössere räumliche Zunahmen in einer Richtung verwendet werden können als in der anderen. Es werden Beispiele über die Anwendung der Methode auf gemischte Grenzbedingungen, gekrümmte Grenzen und eine Puhktquelle gegeben.

Chapter 3. The Equations to be Solved

The specific problem which will be used to demonstrate the solution of an elliptic problem is the potential flow of an irrotational, inviscid fluid. At steady state, it is represented in two dimensions as

$$\frac{\partial^2 \phi}{\partial x^2} + \frac{\partial^2 \phi}{\partial y^2} = \phi_{xx} + \phi_{yy} = 0 \tag{3.1}$$

where ϕ is the potential function, representing temperature in heat conduction, pressure in flow through porous media, and concentration in particle diffusion. In these cases,

$$\nabla x \phi = - K \underline{w} \tag{3.2}$$

where K is the dissipation constant, and $\underline{w}$ is the flux or gradient term represented by the heat flux, the velocity, and the mass transfer rate. The parabolic equations can be expressed as

$$\nabla \underline{w} = \nabla^2 \phi = -K_r \frac{\partial \phi}{\partial t} \tag{3.3}$$

where t is time, $\nabla^2 = \partial/\partial x^2 + \partial/\partial y^2$, and K_r represents the capacitance.

In a two-dimensional potential flow problem, the horizontal and vertical flux components can be defined from equation (3.2) as

$$u = - K \frac{\partial \phi}{\partial x} \quad \text{and} \quad v = - K \frac{\partial \phi}{\partial y}. \tag{3.4}$$

By differentiating equations (3.4), one obtains

$$\frac{\partial u}{\partial y} = - K \frac{\partial^2 \phi}{\partial x \partial y} \qquad \frac{\partial v}{\partial x} = - K \frac{\partial^2 \phi}{\partial y \partial x} . \qquad (3.5)$$

Since the two second differentials are equal,

$$\frac{\partial^2 \phi}{\partial x \partial y} = \frac{\partial^2 \phi}{\partial y \partial x} . \qquad (3.6)$$

Then,

$$\frac{\partial u}{\partial y} - \frac{\partial v}{\partial x} = 0. \qquad (3.7)$$

This equation (3.7) is known as the irrotationality equation. In addition to the irrotationality equation, another equation is needed to relate u and v in terms of x and y. Equation (3.3) is the desired equation. When the term $\nabla \underline{w}$ is expanded, this takes the form

$$\frac{\partial u}{\partial x} + \frac{\partial v}{\partial y} = - \frac{\partial \phi}{\partial t} . \qquad (3.8)$$

This unsteady-state potential flow problem as represented by the equations (3.4), (3.7), and (3.8) is one which will be used in the development of new methods for numerical solution.

Boundary conditions may be specified in various ways. The major consideration is that with an elliptic problem, either the potential or a derivative of the potential must be specified along the entire boundary. For example, the boundary conditions may be specified as in Figure 3.1. The specification shown in Figure 3.1 will be used.

$$v = v(x) = -\frac{\partial T}{\partial y}$$

$$u = u(y) = -\frac{\partial T}{\partial x}$$

$$T = T(y)$$
$$v = -\frac{\partial T}{\partial y}$$

$$T = T(x)$$
$$u = -\frac{\partial T}{\partial x}$$

Figure 3.1. Boundary Conditions

Chapter 4. The Finite Difference Equations

Development of Finite Difference Equations

The development of the format for solving the trans-
ient elliptic finite difference equation arises from an
article by von Rosenberg[23] whereby the elliptic equation was
split through the flux definitions, equations (3.4), into
two first-order equations as indicated by equations (3.7)
and (3.10). These equations were then solved by second-order
correct centered difference analogs. Gates[9] later solved
equations of the same type by a checkerboard technique which
he applied to various steady-state elliptic problems.

The unsteady-state potential problem can be solved
similarly. In this method the finite difference analogs of
three equations, the continuity equation, the irrotationality
equation, and a flux definition, are combined in varying
arrangements.

- Consider the elemental arrangement of values displayed
on the lattice shown in Figure 4.1, where i and j index each
double row of values in the z and y directions, respectively.
The v's are determined at grid points indicated by O, the
w's at points indicated by $\square$, and the potential, T, at
points indicated by $\triangle$. This particular arrangement is used
to incorporate the boundary conditions as defined in the
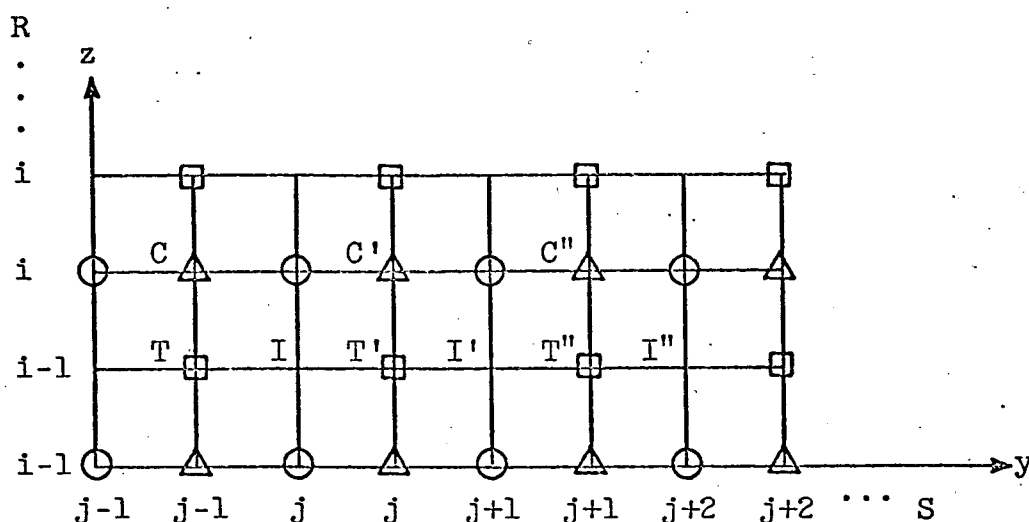model problem.

Figure 4.1. Lattice of C, T, and I.

The finite difference equations are written to tie this block of values together. For instance, if the element shown comprises the total region, then boundary conditions dictate the values of v along column j-1 and row i-1, w along column j+2 and row i, and T along row i-1 and column j+2. Then only the nine values--three groups of the three points in the interior region--are unknown. Therefore nine equations are required to determine the values of the flux components and the potential at each of these points. The finite difference analogs for the continuity equation, (3.11), are written around the points labeled C, C', and C"; those for the irrotationality equation, (3.7), around the points labeled I, I', and I"; and those for equation (3.4), around the points labeled T, T', and T". At C, the finite difference analog for the equation of continuity is

$$\left(\tfrac{1}{2}+\alpha\right)\left[\frac{1}{\Delta y}\left(v_{i,j}-v_{i,j-1}\right) + \frac{1}{\Delta z}\left(w_{i,j-1}-w_{i-1,j-1}\right)\right]_{m+1}$$

$$+ \left(\tfrac{1}{2}-\alpha\right)\left[\frac{1}{\Delta y}\left(v_{i,j}-v_{i,j-1}\right) + \frac{1}{\Delta z}\left(w_{i,j-1}-w_{i-1,j-1}\right)\right]_{m}$$

$$= \frac{1}{\Delta t}\left(T_{i,j-1_m}-T_{i,j-1_{m+1}}\right) \tag{4.1}$$

where α is equal to 1/2, 0, or -1/2 for the backward, centered difference, or forward analog, respectively, and m is the time index.

At time m+1, the potential equation $w = -\partial T/\partial z$ at point T is

$$\dot{w}_{i-1,j-1_{m+1}} = -\frac{1}{\Delta z}\left(T_{i,j-1}-T_{i-1,j-1}\right)_{m+1} \tag{4.2}$$

and the irrotationality equation at point I is

$$\frac{1}{\Delta z}\left(v_{i,j}-v_{i-1,j}\right)_{m+1} - \frac{1}{\Delta y}\left(w_{i-1,j}-w_{i-1,j-1}\right)_{m+1} = 0. \tag{4.3}$$

Truncation Error. In the development of these analogs to continuity, irrotationality, and flux equations, it is important to examine the truncation error in terms of space and time increments. In Appendix B, the truncation errors for the checkerboard arrangement of equations are computed. The truncation errors in each of the three equations are found to be as follows:

In the continuity equation,

$$E_c = -\sum_{n=1}^{\infty}\left\{\frac{1}{(2n+1)!}\left[\left(\frac{\partial^{2n+1}v}{\partial y^{2n+1}}\right)_c\left(\frac{\Delta y}{2}\right)^{2n}+\left(\frac{\partial^{2n+1}w}{\partial z^{2n+1}}\right)_c\left(\frac{\Delta z}{2}\right)^{2n}\right]\right\} \quad (B.11)$$

In the irrotationality equation,

$$E_I = -\sum_{n=1}^{\infty}\left\{\frac{1}{(2n+1)!}\left[\left(\frac{\partial^{2n+1}v}{\partial z^{2n+1}}\right)_I\left(\frac{\Delta z}{2}\right)^{2n}-\left(\frac{\partial^{2n+1}w}{\partial y^{2n+1}}\right)_I\left(\frac{\Delta y}{2}\right)^{2n}\right]\right\} \quad (B.12)$$

And, in the w flux equation,

$$E_T = \sum_{n=1}^{\infty}\frac{1}{(2n+1)!}\left[\left(\frac{\partial^{2n+1}T}{\partial z^{2n+1}}\right)_T\left(\frac{\Delta z}{2}\right)^{2n}\right] \quad (B.18)$$

Each of these errors reveals the fact that the checkerboard analogs are second-order correct.

Method of Sweeping Across the Grid. Letting $\beta = 1/\Delta y$, $\gamma = 1/\Delta t$, $\delta = 1/\Delta z$, $\phi = \beta(\frac{1}{2}+\alpha)$, $\eta = \beta(\frac{1}{2}-\alpha)$, $\theta = \delta(\frac{1}{2}+\alpha)$, and $\zeta = \delta(\frac{1}{2}-\alpha)$, and rewriting, one obtains for equation (4.1):

$$\phi\left(v_{i,j}-v_{i,j-1}\right)_{m+1} + \theta\left(w_{i,j-1}-w_{i-1,j-1}\right)_{m+1}$$

$$+ \eta\left(v_{i,j}-v_{i,j-1}\right)_m + \zeta\left(w_{i,j-1}-w_{i-1,j-1}\right)_m$$

$$= \gamma T_{i,j-1_m} - \gamma T_{i,j-1_{m+1}} \quad (4.4)$$

for equation (4.2):

$$w_{i-1,j-1_{m+1}} = \delta\left(T_{i-1,j-1}-T_{i,j-1}\right)_{m+1} \quad (4.5)$$

and for equation (4.3):

$$\delta\left(v_{i,j} - v_{i-1,j}\right)_{m+1} - \beta\left(w_{i-1,j} - w_{i-1,j-1}\right)_{m+1} = 0. \qquad (4.6)$$

These three equations comprise the set which is repeated for three increments in j in Figure 4.1. In the general case there will be many horizontal groupings by line from boundary to boundary vertically, and there will be many more than three increments in j. At the boundary where z = 0 the flux components $v_{1,j}$ are known for the entire row of points as are the potentials $T_{1,j}$. The values of $w_{2,j}$ are not known unless the boundary z = 1 coincides with i = 2. However, if values for $w_{2,j}$ are assumed, values of $v_{2,j}$, $w_{1,j}$, and $T_{2,j}$ can be computed by the simultaneous solution of equations (4.4), (4.5), and (4.6) for all values of j. The values of $v_{2,1}$, $w_{1,s}$, and $T_{2,s}$ are known from the boundary conditions in the y direction.

For networks larger than two rows, the pattern is similar. Figure 4.2 shows a grid for a four-row format. In this case, for z = 1 along the row coinciding with $w_{4,j}$, the $w_{4,j}$ are defined by boundary conditions, and the initial assumptions are the values of $w_{2,j}$. The $T_{2,j}$, $v_{2,j}$, and $w_{1,j}$ are determined as described above. Then values for $w_{3,j}$ are assumed and $T_{3,j}$, $v_{3,j}$, and $w_{2,j}$ are computed from equations (4.4), (4.5), and (4.6). The values obtained for $T_{2,j}$ and $v_{2,j}$ are used in these equations. Next, with new values of $T_{3,j}$ and $v_{3,j}$ are known values for $w_{4,j}$, the values of $T_{4,j}$, $v_{4,j}$, and $w_{3,j}$ are determined from the same equations. For grids of more than four rows, the values of $w_{i,j}$ are
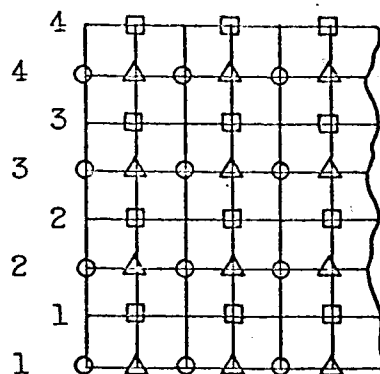
Figure 4.2. Sweep Format Grid

assumed for the calculations of each row until the boundary z = 1 is reached. Henceforth this marching procedure is called "sweeping."

After the first sweep the values of T, w, and v in the interior are not correct since they are based on assumed values for the $w_{i,j}$. Thus a repeat of the entire sweeping process is required. This process of repeating the sweep is termed "iterating." Iterations are continued until successive values of T, w, and v agree within a given tolerance. However, relatively few iterations are required since the values for $w_{i,j}$ at the previous time step can be used as the first assumption. These values are quite near the correct values.

After the values have converged so that all the values are determined at the same time level, the entire process is repeated to obtain values of the dependent variables at an even later time. This procedure is continued until a steady-state is reached or until the solution is obtained for the

desired amount of time.

Solution of Two Rows of Equations Simultaneously

In order to solve equations (4.4), (4.5), and (4.6) simultaneously it is convenient to arrange the terms in a precise way. For the moment, consider that Figure 4.3 is an element of a grid extending in the z direction as in
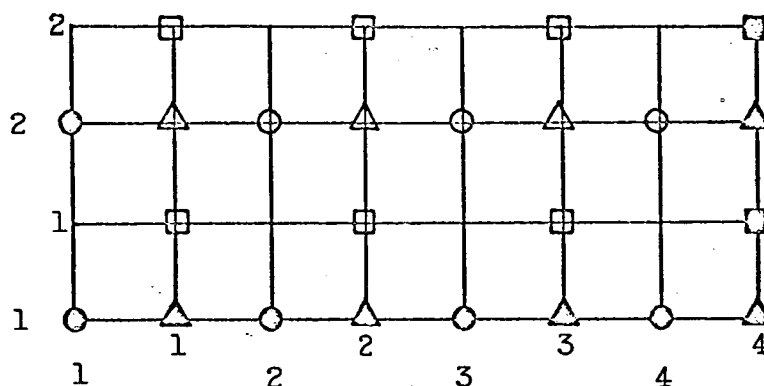
Figure 4.3. Double-Row Grid

Figure 4.1. Then the three values $w_{2,1}$, $w_{2,2}$, and $w_{2,3}$ are assumed, the other boundary values are known, and the nine values in the interior are to be obtained from simultaneous solution of the equations. The three equations may be re-written with the unknown values on the left-hand side and the known or assumed values on the right-hand side. For $j = 2$, the continuity equation becomes

$$\gamma T_{2,1} - {}^\theta w_{1,1} + {}^\phi v_{2,2} = {}^\phi v_{2,1} - {}^\theta w_{2,1} - \eta v_{2,2}$$

$$+ \eta v_{2,1} - \zeta w_{2,1} + \zeta w_{1,1} + \zeta w_{1,1} + \gamma T_{2,1}$$

$$= DP_{2,1} - {}^\theta w_{2,1} \tag{4.7}$$

where $DP_{i,1}$ represents the values known from the previous time step plus $v_{i,1}$ which are known from the boundary conditions. Thus,

$$DP_{i,1} = \eta v_{i,1} - \eta v_{i,2} - \zeta w_{i,1} + \zeta w_{i-1,1} + \phi v_{i,1}. \tag{4.8}$$

The flux equation at $j = 2$ becomes

$$\delta T_{2,1} + w_{1,1} = \delta T_{1,1} \tag{4.9}$$

and the irrotationality equation becomes

$$\beta w_{1,1} + \delta v_{2,2} - \beta w_{1,2} = \delta v_{1,2} \tag{4.10}$$

For $j = 3$, the continuity equation contains two unknown values of $v_{i,j}$ and is

$$\gamma T_{2,2} - \theta w_{1,2} + \phi v_{2,3} - \phi v_{2,2} = -\theta w_{2,2} - \eta v_{2,3}$$

$$+ \eta v_{2,2} - \zeta w_{2,2} + \zeta w_{1,2} + \gamma T_{2,2} = DP_{2,2} - \theta w_{2,2} \tag{4.11}$$

In this instance $DP_{i,j}$ does not contain a boundary value and is

$$DP_{i,j} = \eta v_{i,j} - \eta v_{i,j+1} - \zeta w_{i,j} + \zeta w_{i-1,j} \qquad j \neq 1 \tag{4.12}$$

The flux equation is

$$\delta T_{2,2} + w_{1,2} = \delta T_{1,2}, \tag{4.13}$$

and the irrotationality equation is

$$\beta w_{1,2} + \delta v_{2,3} - \beta w_{1,3} = \delta v_{1,3}. \tag{4.14}$$

The equations at the $y = 1$ boundary are written for $j = 4$ in this simplified case. The continuity equation thus is

$$\gamma T_{2,3} - \theta w_{1,3} + \phi v_{2,4} - \phi v_{2,3} = DP_{2,3} - \theta w_{2,3}, \quad (4.15)$$

the flux equation is

$$\delta T_{2,3} + w_{1,3} = \delta T_{1,3}, \quad (4.16)$$

and the irrotationality equation is

$$\beta w_{1,3} + \delta v_{2,4} = \beta w_{1,4} + \delta v_{1,4}. \quad (4.17)$$

There is only one unknown value of $w_{i-1,j-1}$ in equation (4.17) since the other is given by the boundary condition and is on the right-hand side of the equation.

.In actual problems there will be many more than three and one-half increments in the y direction. In this case, however, the same nine equations are used. The $y = 0$ boundary equations will be the same as (4.7), (4.9), and (4.10), and the equations at the $y = 1$ boundary will be (4.15), (4.16), and (4.17) with j much greater than four. There will be a large number of sets of the interior equations like (4.11), (4.13), and (4.14). By a judicious arrangements of T, w, and v in the left-hand sides of the equations, a diagonal pattern can be obtained in the coefficient matrix. These equations can be written in matrix form as in Figure 4.4, where d_1 through d_9 are the right-hand sides of the equations. The equations enclosed by a dashed line are the general set of equations for the interior points.

$$
\begin{bmatrix}
\gamma & -\theta & \phi & 0 & 0 & & & & \\
\delta & 1 & 0 & \delta & 0 & & & & \\
0 & \beta & \delta & -\beta & 0 & \phi & 0 & & \\
 & -\phi & \gamma & -\theta & \phi & 0 & 0 & & \\
 & 0 & \delta & 1 & 0 & \delta & 0 & & \\
 & 0 & 0 & \beta & \delta & -\beta & 0 & \phi & 0 \\
 & & & -\phi & \gamma & -\theta & \phi & 0 & 0 \\
 & & & 0 & \delta & 1 & 0 & \delta & 0 \\
 & & & 0 & 0 & \beta & \delta & \beta & \delta
\end{bmatrix}
\cdot
\begin{bmatrix}
T_{2,1} \\
w_{1,1} \\
v_{2,2} \\
T_{2,2} \\
w_{1,2} \\
v_{2,3} \\
T_{2,3} \\
w_{1,3} \\
v_{2,4}
\end{bmatrix}
=
\begin{bmatrix}
d_1 \\
d_2 \\
d_3 \\
d_4 \\
d_5 \\
d_6 \\
d_7 \\
d_8 \\
d_9
\end{bmatrix}
\qquad (4.18)
$$

Figure 4.4. Double-Row T, w, v Equations

From equation (4.18), it is noticed that the non-zero terms of the coefficient matrix are in a narrow diagonal pattern with the coefficients γ, 1, and δ of the T, w, and v as the main diagonal. The width of the "band" is five terms.

The equations in this form can be solved simultaneously by using some pentadiagonal algorithm[22] or by a general Peaceman band algorithm.[24] With the Peaceman band algorithm, data to be supplied include the bandwidth, the coefficient vector, and the excitation vector. This algorithm requires approximately N arithmetic operations where

$$N = 7k + 1 + 4 \sum_{n=1}^{k} (n-1). \qquad (4.19)$$

These operations are almost equally divided between addition and multiplication.

Solution of Three Rows of Equations Simultaneously

Let the foregoing procedure be termed the double-row method since the $w_{2,j}$ are assumed and the continuity and irrotationality equations on two rows are solved simultaneously. It is possible to solve equations from three and

four rows of points in a single solution. The continuity, irrotationality, and flux equations may be combined in a variety of ways.

In solving three rows of points simultaneously, the continuity, irrotationality, and flux equations are combined in a certain way. Figure 4.5 shows the points to be considered in the general case; the boundaries are considered
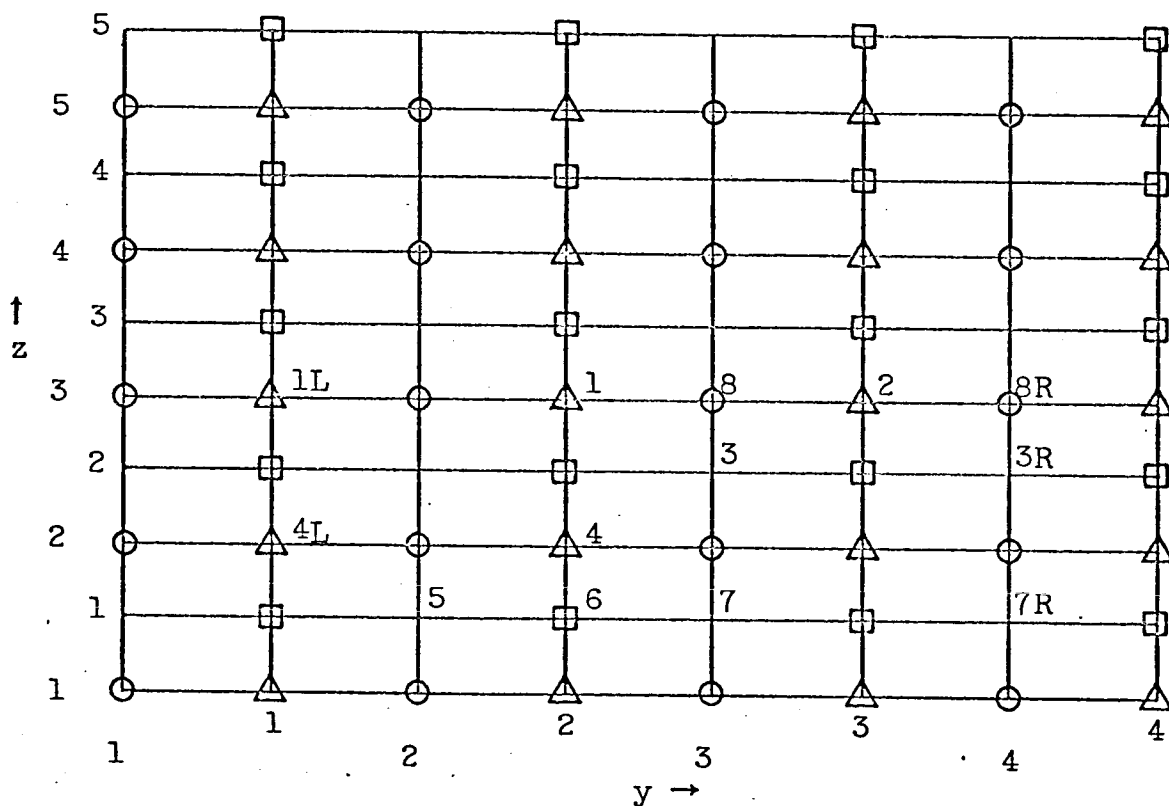

Figure 4.5. Triple-Row Grid

later. The purpose is to tie the $w_{3,j}$ to the $T_{1,j}$ and $v_{1,j}$ in such a way as to require the least amount of computer time to sweep the entire grid solving only for values needed in the sweep and after convergence at a given time level to fill

in the complete lattice with values of T, w, and v from the three equations.

One such method for accomplishing this goal is to write the continuity equation around point 1 in Figure 4.5, the irrotationality equation around point 7, and the flux equation around point 6. In this elemental grid, it can be seen that the three equations may be written only in terms of $T_{3,j}$, $v_{3,j}$, and $w_{1,j}$ so that if the $w_{3,j}$ be assumed, along with the boundary conditions stated along $T_{1,j}$ and $v_{1,j}$, the values of $T_{3,j}$, $v_{3,j}$, and $w_{1,j}$ can be determined. The sweep up the grid can be effected by assuming $w_{5,j}$ and, using the just-determined values of $T_{3,j}$ and $v_{3,j}$, obtain the values of $T_{5,j}$, $v_{5,j}$, and $w_{3,j}$, thereby updating $w_{3,j}$. In this manner the top boundary which is known by boundary conditions can be reached and the procedure begun again until a satisfactory convergence is obtained.

In Appendix C, a system of general equations along with boundary equations are developed. The triple-row, three-variable general equations developed in Appendix C are as follows:

$$\frac{\beta\phi}{\delta} w_{1,1} - \phi v_{3,2} + \gamma T_{3,2} + (-\frac{2\beta\phi}{\delta} - \theta - \frac{\gamma}{\delta}) w_{1,2} + \phi v_{3,3}$$

$$+ \frac{\beta\phi}{\delta} w_{1,3} = DP_{3,2} - \gamma T_{1,2} + DP_{2,2} - \theta w_{3,2}$$

$$+ \phi v_{1,2} - \phi v_{1,3} \qquad\qquad (C.10)$$

$$- \frac{\beta\phi}{\theta} v_{3,2} + \frac{\beta\gamma}{\theta} T_{3,2} + \beta w_{1,2} + (\delta + \frac{2\beta\phi}{\theta}) v_{3,3} - \frac{\beta\gamma}{\theta} T_{3,3}$$

$$- \beta w_{1,3} - \frac{\beta\phi}{\theta} v_{3,4} = \frac{\beta}{\theta}(DP_{3,2} - DP_{3,3}) - \beta w_{3,2}$$

$$+ \beta w_{3,3} + \delta v_{1,3} \qquad\qquad (C.18)$$

$$\beta T_{3,2} + v_{3,3} + \beta T_{3,3} = 0 \qquad\qquad (C.19)$$

Although more computations may be involved in each simultaneous solution of these equations than of the two-row equations, values are assumed so that fewer iterations may be required.

Another reduction in computer time may possibly be realized by incorporating the flux equation into the continuity and irrotationality equations, thereby eliminating the $v_{i,j}$ and leaving equations in terms only of $T_{i,j}$ and $w_{i,j}$. This reduces by one-third the number of equations, although there is an increase in the complication of the remaining equations. The equations are developed in Appendix C; they are presented in Figure C.2. The terms enclosed by a dashed line are the general set, but it must be noted that in equation (C.30), the $T_{3,4}$ term in the general form would be unknown and placed on the left but in this presentation, since $S = 4$ or the maximum j is four terms, it is known. The system of resulting equations is only seven terms wide and the diagonal band is practically full; both of these properties lend this method to a rapid solution compared with previous methods.

$$
\begin{bmatrix} d_1 \\ d_2 \\ d_3 \\ d_4 \\ d_5 \\ d_6 \end{bmatrix}
=
\begin{bmatrix}
(\beta\phi+\gamma) & -\left(\frac{\beta\phi}{\delta}+\theta+\frac{\gamma}{\delta}\right) & -\beta\phi & \frac{\beta\phi}{\delta} & \frac{\beta^2\phi}{\theta} & \frac{\beta\phi}{\delta} \\[4pt]
\left(\frac{\beta\gamma}{\theta}+\beta\delta+\frac{2\beta^2\phi}{\theta}\right) & \beta & -\left(\frac{3\beta^2\phi}{\theta}+\beta\delta+\beta\gamma\right) & -\beta & -\beta\phi & -\beta \\[4pt]
-\beta\phi & \frac{\beta\phi}{\delta} & (2\beta\phi+\gamma) & -\left(\frac{2\beta\phi}{\delta}+\theta+\frac{\gamma}{\delta}\right) & -\left(\frac{3\beta^2\phi}{\theta}+\frac{\beta\gamma}{\theta}+\beta\delta\right) & \frac{\beta\phi}{\delta} \\[4pt]
-\frac{\beta^2\phi}{\theta} & 0 & \left(\frac{3\beta^2\phi}{\theta}+\frac{\beta\gamma}{\theta}+\beta\delta\right) & \beta & (2\beta\phi+\gamma) & -\beta \\[4pt]
0 & 0 & -\beta\phi & \frac{\beta\phi}{\delta} & \left(\frac{2\beta^2\phi}{\theta}+\frac{\beta\gamma}{\theta}+\beta\delta\right) & -\left(\frac{2\beta\phi}{\delta}+\frac{\gamma}{\delta}+\theta\right) \\[4pt]
0 & 0 & -\frac{\beta^2\phi}{\theta} & 0 & \beta & \beta
\end{bmatrix}
\begin{bmatrix} T_{3,1} \\ w_{1,1} \\ T_{3,2} \\ w_{1,2} \\ T_{3,3} \\ w_{1,3} \end{bmatrix}
\qquad (C.33)
$$

Figure C.2. Triple-Row T w Equations.

Solution of Four Rows of Equations Simultaneously

A quadruple-row method, a logical extension of the triple-row method, is developed in Appendix D. Beginning with the equations used in the triple-row method, the continuity, irrotationality, and flux equations are developed incorporating four rows simultaneously. Figure 4.6 aids in understanding the procedure.
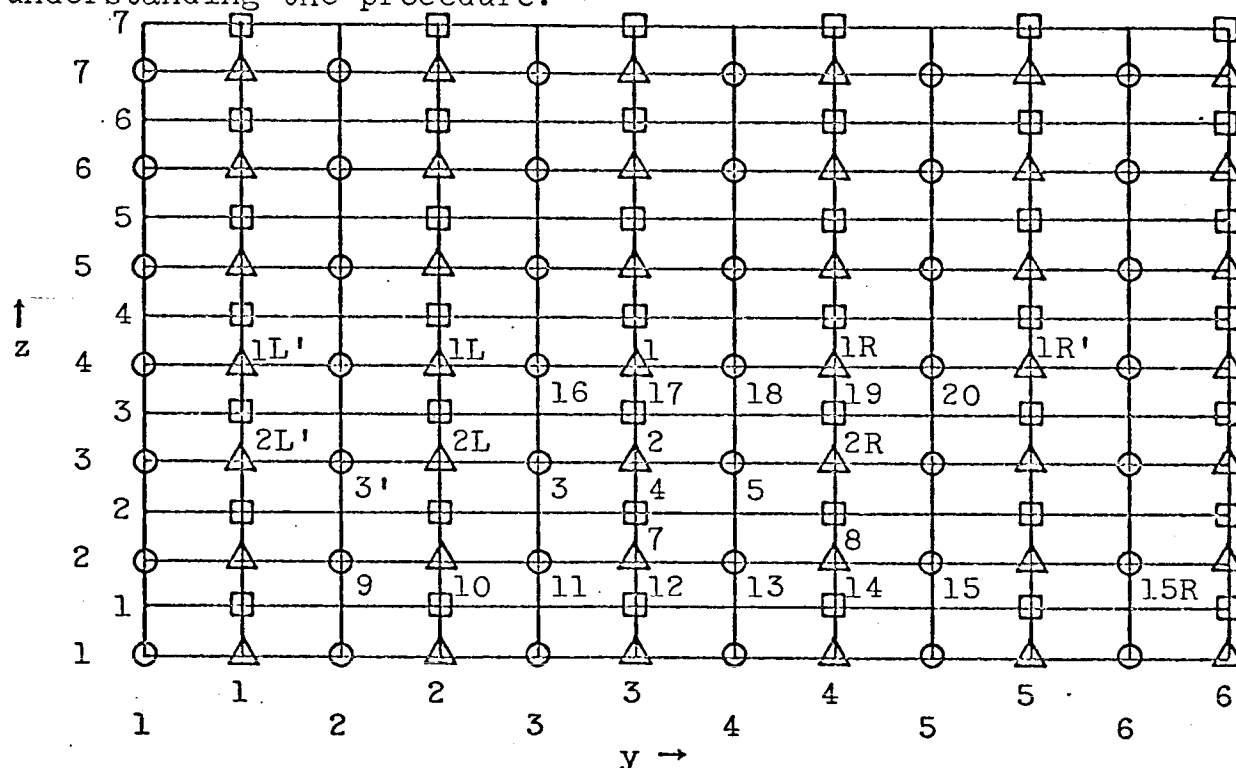

Figure 4.6. Quadruple-Row Grid

The overall plan in this method is generally the same as in the triple-row method. The four rows are tied together by equations in such a manner as to be expressed only in terms of $T_{4,j}$, $v_{4,j}$, and $w_{1,j}$. In this way, the values $w_{4,j}$ may be assumed and with values $T_{1,j}$ and $v_{1,j}$ the

equations solved for $T_{4,j}$, $v_{4,j}$, and $w_{1,j}$. Using the $T_{4,j}$ and $v_{4,j}$ and the assumed values of $w_{7,j}$, the $T_{7,j}$, $v_{7,j}$, and $w_{4,j}$ may be solved and so on up the grid. After repeating this process with the updated $w_{4,j}$, $w_{7,j}$, etc., convergence occurs and the points over the entire lattice may be filled in by equations used to eliminate them before. The complexity of the equations increases markedly, but the elemental pattern is described.

Equations (D.1) through (D.15) can be arranged in diagonal band form similar to that of the triple-row method. The band is 15 terms wide when the equations are listed in the order continuity, followed by irrotationality, followed by flux: C I T. But as was seen in the triple-row method, when the $v_{i,j}$ were expressed in terms of $T_{i,j}$ eliminating one-third of the equations, the time required for solution was reduced. The resulting general equations are presented below.

Continuity:

$$-\frac{\beta^2\phi^2}{\theta\delta^2}w_{1,1} - \beta\phi T_{4,2} + \left(\frac{4\beta^2\phi^2}{\theta\delta^2} + \frac{3\beta\phi}{\delta} + \frac{2\beta\phi\gamma}{\theta\delta^2}\right)w_{1,2} + (2\beta\phi + \gamma)T_{4,3}$$

$$-\left(\frac{6\beta\phi}{\delta} + \frac{6\beta^2\phi^2}{\theta\delta^2} + \frac{4\beta\phi\gamma}{\theta\delta^2} + \theta + \frac{3\gamma}{\delta} + \frac{\gamma^2}{\theta\delta^2}\right)w_{1,3} - \beta\phi T_{4,4}$$

$$+\left(\frac{3\beta\phi}{\delta} + \frac{4\beta^2\phi^2}{\theta\delta^2} + \frac{2\beta\phi\gamma}{\theta\delta^2}\right)w_{1,4} - \frac{\beta^2\phi^2}{\theta\delta^2}w_{1,5} = DP_{4,3} + DP_{3,3}$$

$$+\left(\frac{2\beta\phi}{\theta\delta} + 1 + \frac{\gamma}{\theta\delta}\right)DP_{2,3} - \frac{\beta\phi}{\theta\delta}(DP_{2,2} + DP_{2,4}) - \frac{\beta^2\phi^2}{\theta\delta}T_{1,1}$$

$$+\left(\frac{4\beta^2\phi^2}{\theta\delta} + 2\beta\phi + \frac{2\beta\phi\gamma}{\theta\delta}\right)T_{1,2} - \left(\frac{6\beta^2\phi^2}{\theta\delta} + 4\beta\phi + \frac{4\beta\phi\gamma}{\theta\delta} + 2 + \frac{\gamma^2}{\theta\delta}\right)T_{1,3}$$

$$+ \left(\frac{4\beta^2\phi^2}{\theta\delta} + 2\beta\phi + \frac{2\beta\phi\gamma}{\theta\delta} \right) T_{1,4} - \frac{\beta^2\phi^2}{\theta\delta} T_{1,5} - \theta w_{4,3}$$

$$\text{(D.20)}$$

Irrotationality:

$$\frac{\beta^3\phi^2}{\theta^2\delta} T_{4,1} - \left(\frac{5\beta^2\phi^2}{\theta^2\delta} + \frac{2\beta^2\phi\gamma}{\theta^2\delta} + \frac{3\beta^2\phi}{\theta} \right) T_{4,2} + \left(\frac{9\beta^2\phi}{\theta} + \frac{10\beta^3\phi^2}{\theta^2\delta} \right.$$

$$\left. + \frac{6\beta^2\phi}{\theta^2\delta} + \beta\delta + \frac{3\beta}{\theta} \dotplus \frac{\beta\gamma^2}{\theta^2\delta} \right) T_{4,3} + \beta w_{1,3} - \left(\frac{9\beta^2\phi}{\theta} + \frac{10\beta^2\phi^2}{\theta^2\delta} \right.$$

$$\left. + \frac{6\beta^2\phi\gamma}{\theta^2\delta} + \beta\delta + \frac{3\beta\gamma}{\theta} + \frac{\beta\gamma^2}{\theta^2\delta} \right) T_{4,4} - \beta w_{1,4}$$

$$+ \left(\frac{5\beta^2\phi^2}{\theta^2\delta} + \frac{2\beta^2\phi\gamma}{\theta^2\delta} + \frac{3\beta^2\phi}{\theta} \right) T_{4,5} - \frac{\beta^3\phi^2}{\theta^2\partial} T_{4,6}$$

$$= \frac{\beta}{\theta}(DP_{3,3} - DP_{3,4}) + \left(\frac{2\beta}{\theta} + \frac{3\beta^2\phi}{\theta^2\delta} + \frac{\beta\gamma}{\theta^2\delta} \right)(DP_{4,3} - DP_{4,4})$$

$$+ \frac{\beta^2\phi}{\theta^2\delta}(DP_{4,5} - DP_{4,2}) + \frac{\beta^2\phi}{\theta\delta} w_{4,2} - \left(2\beta + \frac{3\beta^2\phi}{\theta\delta} + \frac{\beta\gamma}{\theta\delta} \right) w_{4,3}$$

$$+ \left(2\beta + \frac{3\beta^2\phi}{\theta\delta} + \frac{\beta\gamma}{\theta\delta} \right) w_{4,4} - \frac{\beta^2\phi}{\theta\delta} w_{4,5} + \beta\delta(T_{1,3} - T_{1,4}) \quad \text{(D.21)}$$

When arranged in diagonal form the two-variable quadruple-row equations present a band of eleven or thirteen terms, depending on the order of writing.

Methods of combining more than four rows are, from Appendix E, extremely unwieldly. The amount of work involved in setting up the coefficient and excitation vectors for a program used to solve any method incorporating more than four rows is prohibitive.

Chapter 5.   Test Problem No. 1

In order to determine the number of iterations required for convergence for the double-, triple-, and quadruple-row methods, tests were conducted on two simple problems. The problem investigated first is that of steady-state potential, T, defined as

$$T = \frac{1}{2}\left[y^2 - (z-1)^2\right] \qquad (5.1)$$

where y and z are the horizontal and vertical coordinates, respectively, normalized from zero to unity in both directions.

The flux definitions at steady state defined in the two equations (3.4) are

$$v = -\frac{\partial T}{\partial y} = -y \qquad w = -\frac{\partial T}{\partial z} = z - 1. \qquad (5.2)$$

The steady-state potential flow situation is shown in Figure 5.1. Solid lines represent the potential flow; and dashed lines, the lines of equal potential. This steady-state condition is approached from initial conditions of $T = w = v = 0$ at every point except at the boundaries at which these are defined as follows:

$$
\begin{aligned}
&w(y,1) = 0 \\
&T(y,0) = -\frac{1}{2}(1-y^2), \quad v(y,0) = -y \\
&v(0,z) = 0 \\
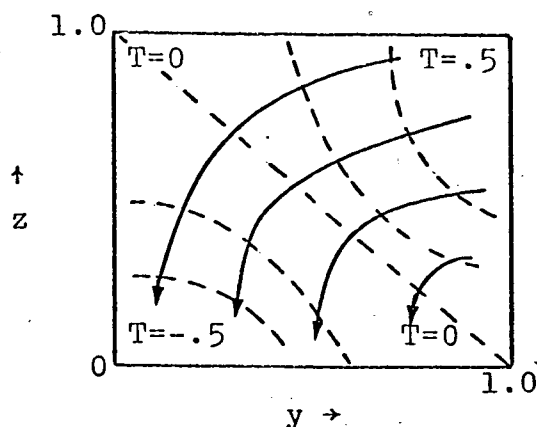&T(1,z) = \frac{1}{2}(2z-z^2), \quad w(1,z) = z - 1
\end{aligned}
\qquad (5.3)
$$

Figure 5.1. Steady-State Potential Flow.

An IBM 7044 computer is used to solve the test problem
with grid sizes (R × S) of 10 × 10 for the double- and quad-
ruple-row methods and 11 × 10 for the triple-row method.
(The z direction must have 2 + i, 3 + 2i, and 4 + 3i sub-
scripts for the double-, triple-, and quadruple-row methods,
respectively.) In Appendix F, computer programs for each of
the three methods are presented. Solutions were obtained
using from one to ten iterations per time step. After each
time step the time increment was increased by 10%.

From the initial conditions, it was found that seventeen
time steps were required to reach steady state. (The values
of T, w, and v for steady-state solution for the grids 10 ×
10 and 11 × 10 are presented in Appendix F in Tables F.1 and
F.2.) To determine the minimum number of iterations required
per time step, the values of the potential at successive time
steps for each run were examined. In each instance it is
seen that the maximum error produced in the calculations was

found at the y = 0 boundary; or at the subscripts (i,1); therefore values of potential at (i,1) were used to compare relative accuracies of computation. In Table 5.1, the values of $T_{2,1}$, $T_{3,1}$, and $T_{4,1}$ are presented for the double-, triple-, and quadruple-row methods, respectively, for two to six iterations per time step at the end of time intervals 15 to 23.

From these results it is seen readily that for four-decimal accuracy, the number of iterations required per time step is five for the double-row method, and only two for both the triple- and quadruple-row methods. In Appendix F, Tables F.3 through F.5 contain results of the potentials determined throughout the lattices at the seventeenth time step for two to six iterations per time step for the three methods.

Of vital interest in selecting the most efficient method is the time required for computer solution of the problem. In Appendix G is presented a method for determining the number of cycles required to perform the calculations, i.e., addition, subtraction, multiplication, and division, for a given grid size and a given number of iterations per time for the various methods discussed. Table 5.2 shows the results of these calculations for the number of cycles required for solving two equations (continuity and irrotationality) for two unknowns (T and w), the v having been eliminated in terms of other T and w values by the flux equation. The

Table 5.1. Potential at Iteration and at Time.

Time Step	2 Iterations	3 Iterations	4 Iterations	5 Iterations	6 Iterations

$$T_{2,1} \quad (\text{S.S.} = 0.39889)$$

Time Step	2 Iterations	3 Iterations	4 Iterations	5 Iterations	6 Iterations
15	-.39885	-.39886	-.39887	-.39888	-.39888
16	-.39882	-.39884	-.39889	-.39889	-.39889
17	-.39895	-.39888	-.39890	-.39890	-.39889
18	-.39874	-.39886	-.39889	-.39889	-.39889
19	-.39906	-.39889	-.39889	-.39890	-.39889
20	-.39866	-.39888	-.39890	-.39889	-.39889
21	-.39915	-.39889	-.39889	-.39889	-.39889
22	-.39860	-.39889	-.39890	-.39889	-.39889
23	-.39919	-.39888	-.39889	-.39889	-.39889

$$T_{31} \quad (\text{S.S.} = 0.32628)$$

Time Step	2 Iterations	3 Iterations	4 Iterations	5 Iterations	6 Iterations
15	-.32568	-.32617	-.32610	-.32611	-.32611
16	-.32583	-.32627	-.32621	-.32621	-.32621
17	-.32593	-.32631	-.32624	-.32625	-.32625
18	-.32601	-.32631	-.32626	-.32630	-.32627
19	-.32607	-.32631	-.32627	-.32681	-.32627
20	-.32612	-.32630	-.32627	-.32723	-.32627
21	-.32617	-.32631	-.32627	-.32736	-.32627
22	-.32620	-.32628	-.32628	-.32757	-.32628
23	-.32623	-.32630	-.32628	-.32764	-.32628

$$T_{41} \quad (\text{S.S.} = 0.23269)$$

Time Step	2 Iterations	3 Iterations	4 Iterations	5 Iterations	6 Iterations
15	-.23212	-.23281	-.23261	-.23266	-.23265
16	-.23226	-.23279	-.23264	-.23269	-.23267
17	-.23235	-.23279	-.23266	-.23269	-.23268
18	-.23244	-.23276	-.23267	-.23269	-.23268
19	-.23251	-.23274	-.23267	-.23269	-.23269
20	-.23256	-.23272	-.23267	-.23269	-.23269
21	-.23260	-.23271	-.23268	-.23269	-.23269
22	-.23263	-.23271	-.23268	-.23269	-.23269
23	-.23266	-.23269	-.23268	-.23269	-.23269

triple-row method effectively reduces the cycles required

by the double-row method by 66% and the quadruple-row method

Table 5.2.   Number of Cycles Required.

Method	Grid Size	Number of Cycles
Double-row	10 × 10	211,800
Triple-row	11 × 10	72,900
Quadruple-row	10 × 10	95,300

reduces it by 57%.   Therefore, the triple-row method, with

only·two iterations per time step is the optimum procedure.

Chapter 7. Test Problem No. 2

The model problem developed in Chapter 5 is purely an ideal representation of an unsteady-state elliptic problem. More realistic is a problem developed to possess certain characteristics present in a particular oil flow through a porous anisotropic medium, an oil reservoir. Such an example is the following problem.

Let Figure 7.1 represent a two-dimensional cross section of a reservoir in the earth where the z axis is vertical and the y axis horizontal. T represents the value of the potential which may in this case be pressure or a linear function
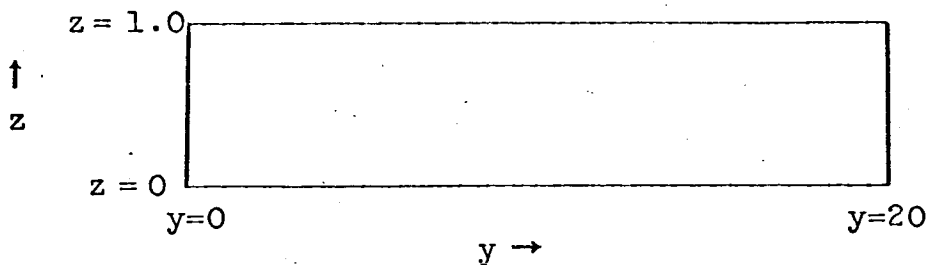

Figure 7.1. Oil Reservoir Dimensions

thereof. The z extends from 0 to unity vertically representing a normalized length and y extends from 0 to 20 representing a reservoir which may possibly be twenty times longer than high in cross section from the outer boundary to the producing oil well. Assuming that immediately above

the oil reservoir (porous medium) there is a salt dome or a gas cap across which no oil flows vertically, the w at the top boundary may be equal to zero. This satisfies the boundary condition along the z = 1 boundary, convenient to the nomenclature used in the model problem. It is also desirable from a realistic point of view for w to be a maximum at z = 0, y = 0, and to approach zero at the well, y = 20. This condition is easily described by the equation

$$w(z,y) = (1-z)(20-y)/20. \qquad (7.1)$$

For the problem to be defined properly, i.e., with enough boundary conditions, T or a derivative thereof must be defined at two boundaries of z and of y. Defining w in equation (7.1) is tantamount to defining T at the two boundaries of z, and since T is defined at the boundary y = 1, either the derivative, v, or the potential itself, T, must be defined at one point along y = 0. (Defining w along y = 0 fixes the T elsewhere along y = 0.) Therefore, assume T = b at y = 0, z = 1. The problem is now defined in accordance with a few characteristics of an oil field reservoir in the vicinity of an oil well. The equations useful for formulating the problem are developed in Appendix I, resulting in a steady-state equation for potential:

$$T = \frac{y^3}{120} - \frac{y^2}{2} - \frac{z^2 y}{40} + \frac{zy}{20} + b(1-y/20) - z$$

$$+ \frac{z^2}{2} + \frac{1}{2} + 6.6416667\, y. \qquad (I.12)$$

In order that v(0,1) = 0, the value of b in equation
I.13 is selected as b = 133.3333. With this value, the
steady-state condition, as shown in Tables J.1 and J.2 for
T, w, and v, for the grids 10 × 10 and 11 × 10 is approached
from initial conditions of T = w = v = 0 at every point
except at the boundaries where

$$w(y,1) = 0$$
$$T(y,0) = y^3/120 - y^2/2 + 133.83333 - 0.025 \, y$$
$$v(y,0) = 0.025 + y - y^2/40$$
$$v(0,z) = z^2/40 - z/20 + 0.025 \qquad (7.2)$$
$$T(20,z) = 0$$
$$w(20,z) = 0.$$

Solutions were attempted using from one to ten iter-
ations per time step. As in the first test problem, Δt, the
time increment, was incremented 10% at the end of each time
step. From the initial condition, it was found that 37 time
steps are required to reach steady state.

From Table 7.1 it is seen again from the values of
$T_{2,1}$, $T_{3,1}$, and $T_{4,1}$ at the end of time intervals 35 to 40,
that five iterations per time step are required when the
double-row method is used, two for the triple- and quadruple-
row methods. In Tables J.3 through J.11 are shown the re-
sults of the potential and the w flux determined throughout
the lattices at the 37th time step for four to six iterations
per time step for the double-row method, and two to four
iterations per time step for the triple- and quadruple-row
methods.

Table 7.1. Potentials for Iterations at Time

Intervals for Test Problem No. 2.

Time Step	4 Iterations	5 Iterations	6 Iterations
	$T_{2,1}$ (S.S. = 133.17)		
35	133.16	133.16	133.16
36	133.16	133.16	133.17
37	133.17	133.17	133.17
38	133.15	133.17	133.17
39	133.19	133.17	133.17
40	133.14	133.17	133.17

Time Step	2 Iterations	3 Iterations	4 Iterations
	$T_{3,1}$ (S.S. = 133.10)		
35	133.00	133.01	133.01
36	133.05	133.06	133.06
37	133.07	133.08	133.08
38	133.09	133.09	133.09
39	133.09	133.10	133.10
40	133.10	133.10	133.10

Time Step	2 Iterations	3 Iterations	4 Iterations
	$T_{4,1}$ (S.S. = 133.01)		
35	132.98	132.97	132.96
36	133.00	132.99	132.99
37	133.01	133.01	133.00
38	133.01	133.01	133.01
39	133.01	133.01	133.01
40	133.01	133.01	133.01

Chapter 8. Conclusion

An efficient numerical method for the solution of un-
steady state elliptic partial differential equations,
particularly advantageous for anisotropic problems, has
been developed. The method was further refined to reduce
the amount of computer time required through an arrange-
ment of multiple groupings of equations describing the given
problem. When two equations, the continuity and irrotation-
ality equations, were solved, the number of cycles required
fell from 211,800 for the double-row method with a grid of
10 × 10 to 72,900 for the triple-row method with a grid of
11 × 10. This was optimum since with the quadruple-row
method, 95,300 cycles were required for a 10 × 10 grid and
further multiple rows were unfeasible. Therefore the triple-
row method effectively reduced the computation time by 66%.
The quadruple-row method reduced the computation time by
57%.

Through an analysis of round-off error it was discovered
that with increased numbers of points in the implicit direc-
tion, the error in calculation increased, but with increased
ratios of implicit to explicit increments ($R = \Delta y / \Delta z$), the
error decreased. Therefore, upon proper selection of incre-
ment size and number, a desired accuracy may be achieved.

The application of the multiple row methods to the oil
reservoir problem produced the same results regarding num-
bers of iterations required per time step for stability. The

double-row method required five iterations per time; the
triple-row and the double-row methods required only two.

Consequently, for unsteady-state problems, especially
those for which the ADI procedure is inefficient, i.e., for
$\Delta y/\Delta z \gg 1$, a stable efficient method has been developed.

Nomenclature

A	Coefficient matrix
a	Constant
a_{ij}	Components of A
B	Point-Jacobi matrix
b	Constant
C	Point-Gauss-Seidel matrix
c^{I-V}	Constants of itegration
c	Constant
D	Diagonal matrix of A
d	Constant
$\underline{d}$	Excitation vector
E	Lower triangular matrix
E_c	Error in Checkerboard analog of continuity equation
E_I	Error in checkerboard analog of irrotationality equation
E_T	Error in checkerboard analog of flux equation
e	Constant
F	Upper triangular matrix
f(x)	Function of x
f	constant
G	I-A matrix
g(x)	Function of x
h	Size of mesh square
I	Identity matrix, number of iterations required
K	Dissipation constant

Nomenclature (Continued)

K_r	Reservoir of potential
k	Index of diagonals parallel to main diagonal.
L	Lower triangular matrix
M	Iteration matrix
m	Time iterate
N	Number of numerical operations required
n	Number of rows, columns, unknowns, or equations
R	Ratio $\Delta y/\Delta z$, number of increments in z direction
R_o	Optimal ratio R
S	Number of increments in y direction
T	Potential
t	Independent variable, time variable
U	Upper triangular matrix
u	Dependent function
v	Horizontal flux
w	Vertical flux
$\underline{x}$	Unknown vector
x	Independent variable
y	Horizontal coordinate, independent variable
z	Vertical coordinate, independent variable
α	Constant
β	$1/\Delta y$
γ	$1/\Delta t$
δ	$1/\Delta z$
ϵ	Error vector

Nomenclature (Continued)

ζ $\delta(\frac{1}{2}-\alpha)$

η $\beta(\frac{1}{2}-\alpha)$, canonical independent variable

θ $(\frac{1}{2}+\alpha)\delta$

λ_e Estimate of eigenvalue

ξ Canonical independent variable

ρ Density

ϕ Potential

ω Relaxation factor

$\#$ Number of cycles of computation required

Subscripts

i   Coordinate in horizontal direction

j   Coordinate in vertical direction

m   Time interate

t   Differential with respect to t

x   Differential with respect to x

y   Differential with respect to y

Superscripts

$\sim$ Auxiliary vector iterate

-1 Inverse of matrix

m   Time iterate

$'$ Error in centered difference as opposed to checkerboard analog

Bibliography

1. Ames, W. F., <u>Nonlinear Partial Differential Equations in Engineering</u>, Academic Press (1965).

2. Churchill, R. V., <u>Fourier Series and Boundary Value Problems</u>, McGraw-Hill (1963).

3. Crichlow, H. G., and P. J. Root, "A Numerical Study of the Effect of Completion Technique on Gas Well Deliverability" (presented at the Second Symposium of Numerical Simulation of Reservoir Performance, Society of Petroleum Engineers of AIME, Dallas, Texas, February, 1970).

4. Culham, W. E., and R. S. Varga, "Numerical Methods for Time Dependent Nonlinear Boundary Value Problems" (presented at the Second Symposium of Numerical Simulation of Reservoir Performance, Society of Petroleum Engineers of AIME, Dallas, Texas, February, 1970).

5. Douglas, J., and Rachford, H. H., "On the Numerical Solution of Heat Conduction of Probems in Two and Three Space Variables," <u>Transactions of the American Mathematical Society</u>, 82, 421 (1965).

6. Forsythe, G. E., and Wasow, W. R., <u>Finite-Difference Methods for Partial Differential Equations</u>, John Wiley and Sons (1967).

7. Fox, L., <u>Numerical Solution of Ordinary and Partial Differential Equations</u>, Addison-Wesley Publishing (1962).

8. Garabedian, P. R., <u>Partial Differential Equations</u>, John Wiley and Sons (1964).

9. Gates, W. J., Numerical Solution for Flux Components in Potential Flow, Ph.D. Dissertation in Chemical Engineering, Tulane University (1968).

10. Gates, W. J., and von Rosenberg, D. U., "Use of a Checkerboard Grid for Numerical Solution for Flux Components" (to be published).

11. Holst, P. H., and K. Aziz, "Numerical Simulation of Three-Dimensional Natural Convection in Porous Media" (presented at the Second Symposium on Numerical Simulation of Reservoir Performance, Society of Petroleum Engineers of AIME, Dallas, Texas, February, 1970).

12. Lapidus, L., Digital Computation for Chemical Engineers, McGraw-Hill (1962).

13. Miller, K. S., Partial Differential Equations in Engineering Problems, Prentice-Hall (1964).

14. Peaceman, D. W., "Fundamentals of Reservoir Simulation: Lecture Notes," Esso Production Research Company (1969).

15. Peaceman, D. W., and Rachford, H. H., "The Numerical Solution of Parabolic and Elliptic Eifferential Equations," Journal of Society of Industrial Applied Mathematics, 3, 28 (1955).

16. Ralson, A., and H. S. Wilf, Mathematical Methods for Digital Computers, Vol. I, John Wiley and Sons (1967).

17. Salvadori, J. G., and M. L. Baron, Numerical Methods in Engineering, Prentice-Hall (1961).

18. Scarborough, J. B., Numerical Mathematical Analysis, Johns Hopkins Press (1966).

19. Sheldon, J. W., "Iterative Methods for the Solution of Elliptic Partial Differential Equations," Mathematical Methods for Digital Computers, Vol. I., ed., Ralston, A., and H. S. Wilf, John Wiley and Sons (1967).

20. Stone, H. L., "Iterative Solution of Implicit Approximations of Multi-Dimension Partial Differential Equations," SIAM Journal of Numerical Analysis, 5, 3 (September 1968).

21. Varga, R. S., Matrix Iterative Analysis, Prentice Hall (1962).

22. von Rosenberg, D. U., Methods for the Numerical Solution of Partial Differential Equations, American Elsevier (1969).

23. von Rosenberg, D. U., "Numerical Solution for Flux Components in Potential Flow," Mathematics of Computation, 21, 100 (October 1967).

24. von Rosenberg, D. U., Personal Communication (1969).

25. Wachspress, E. L., Iterative Solution of Elliptic Systems, Prentice-Hall (1966).

26. Walsh, J., Numerical Analysis: An Introduction, Thompson Book Company (1967).

27. Watts, J. W., "An Interative Matrix Inversion Method Suitable for Anisotropic Problems" (presented at the Second Symposium on Numerical Simulation of Reservoir Performance, Society of Petroleum Engineers of AIME, Dallas, Texas, February 1970).

28. Weinstein, H. G., H. L. Stone, and T. V. Kwan, "Iterative Procedure for Solutions of Systems of Parabolic and Elliptic Equations in Three Dimensions," *Industrial and Engineering Chemistry*, 8, 281 (May 1969).

29. Young, D. M., "Iterative Methods for Solving Partial Differential Equations of the Elliptic Type," *Transactions of the American Mathematical Society*, 76, 1 (January 1954).

Section IV

Compressible Flow Problems

A numerical solution of a transient shock wave problem†

J. W. WATTS‡ and D. U. von ROSENBERG

Tulane University, New Orleans, Louisiana 70118

Abstract – A numerical method for solving one-dimensional, compressible flow problems including locating and following shock waves is described. This method uses a small amount of computer storage, and complete problems can be computed in a few minutes on an IBM 7044 computer. Results of a problem for the discharge of air from a duct are presented.

INTRODUCTION

PHYSICAL systems in which dispersion is small are fairly common. Several examples are compressible fluid flow, water flooding in oil reservoirs, and convective transfer in heat exchangers. A distinguishing feature of these systems is the fact that their describing variables tend to develop regions of steep gradients, called shocks.

When these systems are studied mathematically, it is usually assumed that dispersion becomes zero, causing the describing equations to become hyperbolic. As a result the regions of steep gradients mentioned above become finite discontinuities. There have been several efforts to solve these systems by difference methods, most of which involve smearing the shock over a finite interval[1, 2]. For this reason these methods do not represent the shock very accurately.

Recently several hyperbolic systems have been studied using the centered difference method, originally developed by Wendroff. The results of these studies indicate that the centered difference method is accurate as long as the solutions contain only small discontinuities. As these discontinuities grow, the solutions develop oscillations, making them of little value.

In this paper the centered difference method is modified to yield accurate description of shocks, and the modified method is demonstrated on a typical physical problem.

SYSTEM AND EQUATIONS

The physical system chosen for study is the discharge of an ideal gas from a duct, depicted in Fig. 1. The duct is open at one end, closed at the other. Originally the contents of the duct are at a higher pressure than the surrounding reservoir. At time zero the fluid in the duct is allowed to start flowing into the reservoir.
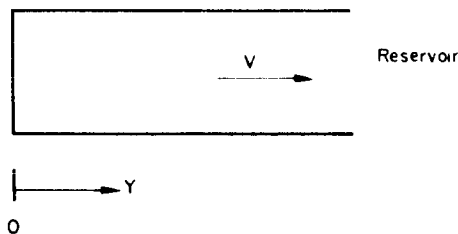

Fig. 1. Schematic of duct.

If flow is assumed one dimensional and isentropic, the following dimensionless equations result.

$$\text{Continuity} \qquad \frac{\partial Z}{\partial W} = -\frac{\partial V}{\partial Y} - \frac{\partial Z}{\partial Y} \qquad (1a)$$

$$\text{Momentum} \qquad \frac{\partial V}{\partial W} = -V\frac{\partial V}{\partial Y} - \exp[Z(\gamma-1)]\frac{\partial Z}{\partial Y} \qquad (1b)$$

Initial conditions $\qquad V(Y, 0) = 0 \qquad$ (2a)

$$Z(Y, 0) = Z_0 \qquad (2b)$$

Boundary conditions $\quad V(0, W) = 0 \qquad$ (3a)

$$Z(1, W) = 0 \text{ for}$$
$$V(1, W) \geqslant 0 \qquad (3b)$$

$$Z(1, W) = \frac{1}{\gamma - 1} \times$$

$$\ln\left[1 - \frac{\gamma - 1}{2} V^2(1, W)\right] \text{ for } V(1, W) < 0 \qquad (3c)$$

where Z = density $= \ln(\rho/\rho_r)$
$\quad V$ = velocity $= u/a_r$
$\quad Y$ = distance $= X/L$
$\quad W$ = time $\quad = a_r t/L$
$\quad \gamma$ = ratio of heat capacities.

When a shock forms, the flow conditions become discontinuous at the point of the shock. The relationships between the dependent variables on either side of the shock are given by the Rankine-Hugoniot equations[3]. These are modified from their usual form to suit the particular definition of the variables.

$$Z' - Z = \ln F \qquad (4a)$$

$$V' - V = \frac{1 - F}{F} A M_s \qquad (4b)$$

where

$$F = \frac{1 + \dfrac{\gamma + 1}{\gamma - 1}\dfrac{p'}{p}}{\dfrac{\gamma + 1}{\gamma - 1} + \dfrac{p'}{p}} \qquad (5)$$

p = pressure
M_s = shock Mach number $= \sqrt{\left(\dfrac{\gamma + 1}{2\gamma}\dfrac{p'}{p} + \dfrac{\gamma - 1}{2\gamma}\right)}$ (6)

$$A = \text{sonic velocity} = \exp\left(\frac{\gamma - 1}{2} Z\right). \qquad (7)$$

Primed variables are evaluated behind the shock; unprimed variables in front of it. The velocity of the shock is given by

W_s = shock velocity
$\quad = V - A M_s$ shock moving left
$\quad = V + A M_s$ shock moving right.

The pressure ratio in terms of dimensionless density is

$$\frac{p'}{p} = \exp[\gamma(Z' - Z)]. \qquad (8)$$

This expression is true for no entropy change across the shock, and shocks are irreversible. However, Rudinger[3] states that Eq. (8) can always be used when the pressure ratio is less than 1·5 and the errors are unimportant in many cases for ratios as high as 2·5. For the problem studied the pressure ratio across the shock did not exceed 1·85; so Eq. (8) was used in all cases.

KNOWLEDGE OF SYSTEM REQUIRED

It would seem that almost complete knowledge of the system to be studied must be known before the problem can be solved. Equations (1a) and (1b) give no indication that a shock will form or that the sonic velocity is of any significance to this problem. However, the formation of and movement of the shock are actually indicated if these equations are solved numerically without a provision for the shock. This occurrence is discussed in an earlier paper[4]. The formation of the shock can be located from this solution by trial and error. To do this, one would compute solution profiles which would indicate the approximate time and location of the shock formation. The moving mesh point would be introduced in the same manner as discussed below, and the profiles recomputed. The initial guess of shock strength and location would probably be slightly incorrect, but these could be refined by trial and error until satisfactory accuracy was obtained.

In most practical cases the initial shock formation and pressure ratio will be either known or easily determined by some simple means. For the problem discussed in this paper, it was determined that the shock formed at the outlet of the duct at

the time when the exit velocity decreased from its initial value. This is the time that the initial characteristic, which started from the exit at the time the flow started, returns to the exit of the duct after being reflected from the closed end.

This same knowledge of the system must be available before any type of solution can be obtained. In the solution of this problem by the wave diagram method, Rudinger[3] requires this knowledge of the system. In fact, Rudinger's solution is much less exact because he shows the shock forming in the interior of the duct at a time later than it actually forms. The numerical solution thus provides an accurate quantitative description of the behavior of the system from a knowledge of the governing equations and the criteria for shock formation.

CENTERED DIFFERENCE METHOD

The centered difference method was originated by Wendroff and was later applied to physical problems by Herron and von Rosenberg and von Rosenberg et al.[4–6] The method is based on second order correct finite difference equations centered in time and space, which for the system studied herein, are the following:

Continuity

$$\frac{Z_{i,n+1}+Z_{i+1,n+1}-Z_{i,n}-Z_{i+1,n}}{2\Delta W}$$

$$=-\frac{V_{i+1,n}+V_{i+1,n+1}-V_{i,n}-V_{i,n+1}}{2\Delta Y}$$

$$-V_{i+1/2,n+1/2}\left[\frac{Z_{i+1,n}+Z_{i+1,n+1}-Z_{i,n}-Z_{i,n+1}}{2\Delta Y}\right] \quad (9)$$

Momentum

$$\frac{V_{i,n+1}+V_{i+1,n+1}-V_{i,n}-V_{i+1,n}}{2\Delta W}$$

$$=-V_{i+i/2,n+1/2}\left[\frac{V_{i+1,n}+V_{i+1,n+1}-V_{i,n}-V_{i,n+1}}{2\Delta Y}\right]$$

$$-e^{(\gamma-1)Z}{}_{i+1/2,n+1/2}$$

$$\times\left[\frac{Z_{i+1,n}+Z_{i+1,n+1}-Z_{i,n}-Z_{i,n+1}}{2\Delta Y}\right] \quad (10)$$

where i is the space index $= Y/\Delta Y$
n is the time index $= W/\Delta W$.

The dependent variables at the centered point are the arithmetic average of their corresponding values at the four surrounding points.

There are two equations associated with each space increment, or a total of $2N$ equations to be solved, where N is the total number of space increments. These equations are nonlinear and must be solved iteratively. First, velocity and density profiles at the new time level are assumed, and the nonlinear coefficients, $V_{i+1/2,n+1/2}$ and $e^{(\gamma-1)Z}{}_{i+1/2,n+1/2}$, are calculated. Then, the $2N$ equations are solved simultaneously using the bitridiagonal matrix inversion algorithm developed by Douglas, Peaceman, and Rachford [7]. This yields improved values of the dependent variables at the new time level, which are used to recalculate the nonlinear coefficients. This process is repeated until convergence is obtained.

REPRESENTATION OF THE SHOCK

When a shock forms, the centered difference method must be modified. In this modification the shock is represented by a grid point which moves with the shock as it travels down the duct. The dependent variables are double valued at this point, one value being associated with conditions immediately behind the shock, the other with conditions immediately in front of it. This shock grid point moves through the mesh of stationary grid points. As a result the finite difference elements on either side of the shock are trapezoidal in shape, whereas the others are rectangular. This situation is shown in Fig. 2.
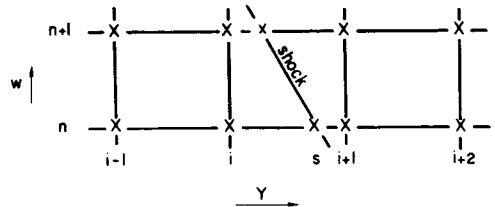

Fig. 2. Finite difference elements near the shock.

Because the finite difference elements adjoining the shock are not rectangular, modified equations had to be derived for these elements. The equations to the left and right of the shock are analogous. The set of equations applying immediately right of the shock is given below.

$$\frac{Z'_{s,n+1} + Z_{i+1,n+1} + Z'_{s,n} - Z_{i+1,n}}{2\Delta W}$$

$$+ \frac{Y_{s,n} - Y_{s,n+1}}{2\Delta W}\left[\frac{Z_{i+1,n} + Z_{i+1,n+1} - Z'_{s,n} - Z'_{s,n+1}}{2Y_{i+1} - Y_{s,n} - Y_{s,n+1}}\right]$$

$$= -\frac{V_{i+1,n} + V_{i+1,n+1} - V'_{s,n} - V'_{s,n+1}}{2Y_{i+1} - Y_{s,n} - Y_{s,n+1}}$$

$$- V'_{i+1/2,n+1/2}\left[\frac{Z_{i+1,n} + Z_{i+1,n+1} - Z'_{s,n} - Z'_{s,n+1}}{2Y_{i+1} - Y_{s,n} - Y_{s,n+1}}\right]. \quad (11)$$

Equation (12) becomes

$$\frac{V'_{s,n+1} + V_{i+1,n+1} - V'_{s,n} - V_{i+1,n}}{2\Delta W}$$

$$+ \frac{Y_{s,n} - Y_{s,n+1}}{2\Delta W}\left[\frac{V_{i+1,n} + V_{i+1,n+1} - V'_{s,n} - V'_{s,n+1}}{2Y_{i+1} - Y_{s,n} - Y_{s,n+1}}\right]$$

$$= - V'_{i+1/2,n+1/2}\left[\frac{V_{i+1,n} + V_{i+1,n+1} - V'_{s,n} - V'_{s,n+1}}{2Y_{i+1} - Y_{s,n} - Y_{s,n+1}}\right]$$

$$- e^{(\gamma-1)Z_{i+1/2,n+1/2}}\left[\frac{Z_{i+1,n} + Z_{i+1,n+1} - Z'_{s,n} - Z'_{s,n+1}}{2Y_{i+1} - Y_{s,n} - Y_{s,n+1}}\right]$$

$$(12)$$

where $Y_{s,n}$ = value of Y on shock point at the old time level

$Y_{s,n+1}$ = value of Y on shock point at the new time level

$$V'_{i+1/2,n+1/2} = \tfrac{1}{4}(V'_{s,n} + V'_{s,n+1} + V_{i+1,n} + V_{i+1,n+1}$$

$$Z'_{i+1/2,n+1/2} = \tfrac{1}{4}(Z'_{s,n} + Z'_{s,n+1} + Z_{i+1,n} + Z_{i+1,n+1}).$$

The relationships between the double values of the variables at the moving mesh point are given by the Rankine–Hugoniot equations.

$$Z'_s - Z_s = \ln F \quad (13)$$

$$V'_s - V_s = \frac{1-F}{F}AM_s.$$

The analogs presented above are written about a point which is centered in time at the time value of $w_n + (\Delta w)/2$. The space position of this point is a distance to the left of Y_{i+1} equal to the average of the space increments at the two time levels. This value is $Y_{i+1} - (Y_{s,n} + Y_{s,n+1})/2$. These analogs were found to be the highest order correct analogs for this trapezoidal area and also the most convenient to use. Several other points, including the center of mass of the trapezoid, were investigated.

As mentioned above, the shock moves across the stationary finite difference mesh. The set of equations associated with the particular increment through which the shock is moving is replaced by three sets, which represent the trapezoidal element left of the shock, the Rankine–Hugoniot equations across the shock, and the trapezoidal element right of the shock. Four unknowns are added to the system—the values of V' and Z' behind the shock and the values of V and Z in front of the shock. The addition of these equations and unknowns does not change the method of solving for the dependent variables at the new time level.

DETERMINATION OF THE SHOCK STRENGTH

The computations described above assume the pressure ratio across the shock to be known. Actually this quantity changes with time and must be calculated at each time step. This calculation requires a determination of the pressure immediately in front of the shock, p. The following rationale is used in this determination.

In compressible flow systems, disturbances are propagated at sonic velocity, whereas shocks move faster than sonic velocity. Therefore, a shock moves faster than the disturbances it propagates and has no effect on flow in front of itself. For this reason the solution to the differential equations in the region of the duct in front of the shock is unaffected by the presence of the shock. In particular, the pressure immediately in front of the shock is independent of

52

the shock. This pressure can be calculated from knowledge of the solution profiles at previous time level and the location of the shock at the new time level.

This calculation can actually be implemented in several ways, and the particular method used is not important. It was chosen to use an adaptation of the method of characteristics as developed by Streeter *et al.*[8]. A detailed description of these calculations is given elsewhere [9].

The calculation of the pressure in front of the shock is used in the following iterative scheme for determining the pressure ratio across the shock.

1. To start the calculations, a pressure ratio across the shock is assumed.
2. The shock velocity and location of the new time level are calculated using the following relationship

$$Y_{s,n+1} = Y_{s,n} + W_s \Delta W.$$

3. Solution profiles at the new time level are calculated using the bitridiagonal algorithm. These profiles include the density behind the shock, from which the pressure behind the shock is obtained.
4. The density in front of the shock is calculated as described above. This calculation is based only on solution profiles in front of the shock at the old time level.
5. An improved pressure ratio across the shock is calculated using the results from Step 3 for the pressure behind the shock and from Step 4 for the pressure in front of it.
6. Steps 2–5 are repeated until the pressure ratio across the shock does not change between successive determinations.

Due to the complexity of the above iteration process, the properties of its convergence cannot be studied theoretically. However, results obtained on the digital computer demonstrate convergence. At first glance the process might appear awkward and time consuming, but this is not actually the case. As mentioned above, the centered difference method requires

iteration on the nonlinear coefficients. When the two iterations are performed simultaneously, only a small increase in computational time is required.

RESULTS

The methods described above were programmed for the digital computer, and a run was made using 80 space increments with $\gamma = 1.4$ and $Z_0 = 0.7409$. The results of this run are presented in the form of velocity profiles at increasing values of time (Figs. 3–5).
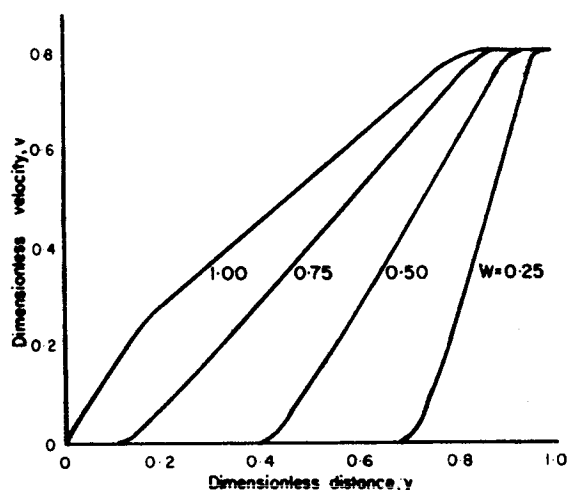

Fig. 3. Velocity profiles $w = 0.25$ to $w = 1.00$.

Soon after the physical process is started, the exit velocity reaches 0.8 and remains at this value until $W = 1.5$. At this time the exit velocity starts to drop and the shock forms at $W = 1.52$. As time goes on, the shock grows in magnitude and moves toward the closed end of the duct, reaching it at $W = 3.0$. The shock is reflected from the closed end and moves toward the open end, leaving the duct at $W = 4.40$.

Although it is not presented here, at $W = 6.08$ a second, weaker shock forms and passes down the duct and back out. Eventually a third, still weaker shock goes through the duct, then a fourth, and so on. The third and successive shocks are weak enough not to require the

53
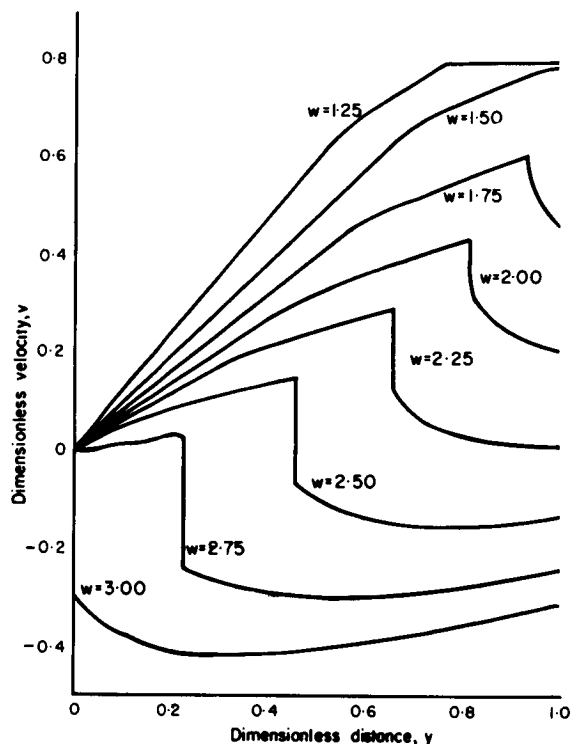
Fig. 4. Velocity profiles $w = 1.25$ to $w = 2.9725$.
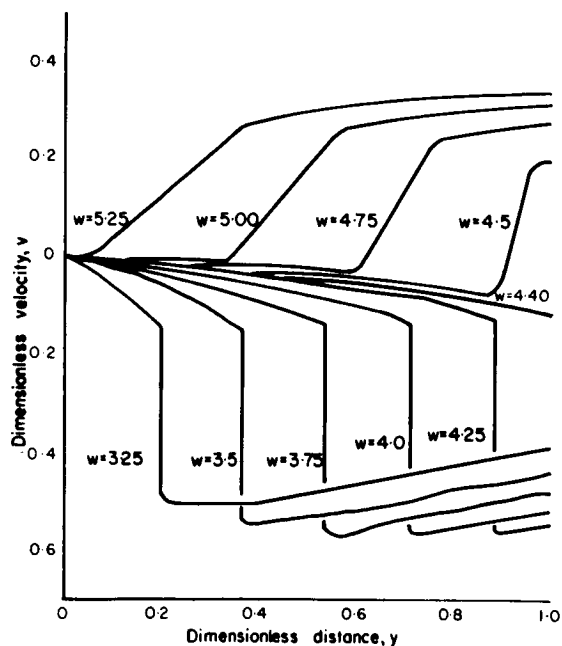
Fig. 5. Velocity profiles $w = 3.25$ to $w = 5.25$.

moving grid point. Good representation of them can be obtained using the unmodified centered difference method.

CONCLUSION

An efficient means has been developed for solving hyperbolic partial differential equations including shocks. In particular, the method developed gives very good representation of the shock. There is no reason this method could not be extended to other sets of equations. The only requirement would be relationships equivalent to the Rankine–Hugoniot equations for the particular system under study.

NOTATION

a speed of sound
A dimensionless speed of sound
F function defined in Eq. (5)
i index in space
L length of duct
M_s shock Mach number
n index in time
p pressure
t time
u velocity
V dimensionless velocity
W dimensionless time
W_s dimensionless shock velocity
X distance from the closed end of the duct
Y dimensionless distance from the closed end of the duct
Z dimensionless density

Greek letters

γ ratio of the heat capacities
ρ density

Subscripts

r evaluated at a reference condition
s evaluated at the shock

Primed variables are evaluated behind the shock.

54

REFERENCES

[1] LAX P. D., *Communs Pure appl. Math.* 1954 **7** 159.
[2] von NEUMANN J. and RICHTMYER R. D., *J. appl. Phys.* 1950 **21** 232.
[3] RUDINGER G., *Wave Diagrams for Nonsteady Flow in Ducts.* Van Nostrand (1955).
[4] von ROSENBERG D. U., BEAUCHAMP D. L. and WATTS J. W., *Chem. Engng Sci.* 1968 **23** 345.
[5] HERRON E. H. and von ROSENBERG D. U., *Chem. Engng Sci.* 1966 **21** 337.
[6] WENDROFF B. J., *J. Soc. Ind. appl. Math.* 1960 **8** 549.
[7] DOUGLAS J., PEACEMAN D. W. and RACHFORD H. H., *Petrol. Trans.* 1959 **216** 297.
[8] STREETER V. L., KEITZER W. F. and BOHR D. F., *Circulation Res.* 1963 **8** 3.
[9] WATTS J. W., A numerical solution of transient compressible flow from a duct. Ph.D. Dissertation in Chemical Engineering, Tulane University 1967.

APPENDIX

A. Initial location of the shock

The method used to determine the pressure ratio across the shock is described above. This method is self-correcting in the following respect. If the grid point representing the shock falls behind the actual location of the shock, the pressure ratio automatically increases, speeding up the grid point and causing it to overtake the shock. Similarly, if the grid point gets ahead of the shock, the pressure ratio decreases and the mesh point is overtaken by the shock.

This feature of the solution was demonstrated experimentally by introducing the moving grid point into the numerical solution a short distance away from the shock. As the numerical solution progressed, this condition quickly corrected itself, with the moving point coinciding with the shock after a few time steps. Thus to introduce the moving point into the numerical solution, it is necessary to know only approximately the time and location of shock formation. Actually these can be accurately determined as described below.

From wave theory it is known that the shock forms at the open end of the duct. It starts off with an infinitesimal magnitude and grows as it moves down the duct. Thus, only the time of formation must be determined.

When the physical process is started by allowing fluid to flow out of the duct, an expansion wave travels from the open end toward the closed end. Upon reaching the closed end, this wave is reflected and travels back toward the open end. The shock forms when this wave reaches the open end of the duct.

To introduce the shock initially, one computes the time that this wave reaches the open end as a part of the numerical solution. The moving point representing the shock is inserted at this time with a unity pressure ratio across the shock. From this point the shock automatically grows and moves into the duct.

B. The crossing of a stationary mesh point by the shock

As the shock moves down the duct, it periodically crosses one of the stationary points. In this situation, the shock is on opposite sides of the stationary mesh point at the old and new time levels. This stationary point is ignored, and the finite difference equations are written about two larger elements, as shown in Fig. 6. Solution profiles at the new time level are computed just as before. Then the values of the dependent variables at the stationary point which was ignored are obtained by interpolating between the points on each side of it. As the shock velocity increases, the shock could cross two mesh points during a single time step. This event is prevented by decreasing the time step size as necessary.
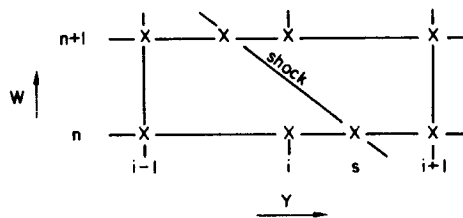

Fig. 6. Shock crossing a stationary mesh point.

C. Reflection of the shock from the closed end of the duct

When the shock reaches the closed end of the duct, it is reflected and starts traveling toward the open end. To get the shock reversed, it is necessary to calculate the pressure ratio across the shock just after reflection.

At the instant the shock reaches the closed end, the velocity left of the shock is known to be zero due to the $Y = 0$ boundary condition. In addition the velocity and density to the right of the shock are known from the solution profiles (the time step is adjusted so as to have the shock exactly at $Y = 0$ at the new time level.) Thus Z, V, V' are known and Z' can be calculated using the Rankine–Hugoniot equations. Using these values of Z and Z', the pressure ratio is calculated by Eq. (8).

After reflection the shock travels back to and out of the open end. Eventually a second, weaker shock forms, then a third, fourth, and so on. The computational procedures are the same for each successive shock.

Résumé — On décrit une méthode numérique pour résoudre les problèmes de courants compressibles unidimensionnés, y compris les travaux de localisation et de poursuite des ondes de choc. Cette méthode n'emploie qu'une faible quantité de données à emmagasinage par ordinateur et les problèmes entiers sont résolus en quelques minutes par un ordinateur IBM 7044. On présente les résultats d'un problème pour la décharge d'air à partir d'une conduite.

55

J. W. WATTS and D. U. von ROSENBERG

Zusammenfassung – Eine numerische Methode zur Lösung eindimensionaler Strömungsprobleme bei komprimierbaren Flüssigkeiten einschliesslich lokalisierter und nachfolgender Stosswellen wird beschrieben. Bei dieser Methode ist die Speicherleistung des Rechners nur zu einem geringen Grad erforderlich, und vollständige Probleme können auf einem IBM 7044 Rechner in wenigen Minuten ausgearbeitet werden. Die Ergebnisse eines Problems hinsichtlich der Luftabgabe aus einem Schacht werden angeführt.

56

NUMERICAL SOLUTION OF CHARACTERISTIC EQUATIONS FOR TRANSIENT, COMPRESSIBLE FLOW

Introduction. The method described by Watts (1) for the numerical solution of transient, compressible flow including shock waves is a satisfactory one. However, it differs somewhat from a solution obtained by the method of Warmbrod and Struck (2). This difference may be caused by the neglecting of entropy variations in Watts' model. Also, since the characteristics are used to follow the shock in the solution by Watts, there is some advantage to solving the characteristic equations rather than the equations in terms of the physical variables.

Development of Characteristic Equations. Three differential equations are needed to describe a polytropic flow. The partial differential equations which describe this flow are well known and are derived from material, force, and energy balances. The properties of the fluid are taken to be those of a perfect gas with constant heat capacity so that the equations will be less complex.

The differential equations are often expressed in terms of the fluid velocity, u, temperature, T, and density, ρ. With the independent variables of length, x', and time, t', the equations are

$$\frac{\partial \ln \rho}{\partial t'} + u \frac{\partial \ln \rho}{x'} + \frac{\partial u}{\partial x'} + Fu = 0 \tag{1}$$

$$\frac{\partial u}{\partial t'} + u\frac{\partial u}{\partial x'} + RT \frac{\partial \ln \rho}{\partial x'} + R\frac{\partial T}{\partial x'} = 0 \tag{2}$$

$$\frac{1}{\gamma-1} \left[\frac{\partial T}{\partial t'} + u\frac{\partial T}{\partial x'} \right] - T\left[\frac{\partial \ln \rho}{\partial t'} + u \frac{\partial \ln \rho}{\partial x'} \right] = 0 \tag{3}$$

The physical properties of the fluid enter the equations through the specific gas constant, R, and the heat capacity ratio, γ. The function F accounts for the geometry of the duct and is defined as

$$F = \frac{1}{B} \frac{dB}{dx'} \tag{4}$$

where B is the cross-sectional area of the duct. Area changes with time are not included in these equations.

When certain types of boundary conditions are imposed, shocks form and move in and out of the duct. Some of the difficulties in obtaining solutions to compressible flow problems lie in determining the time and place of formation of these shocks and in following their motion through the duct. The extent of the discontinuity in each of the dependent variables is related through the appropriate Rankine-Hugoniot equation, which can be found in any text on compressible flow, such as Rudinger (3).

A number of new variables can be defined; one of the more fundamental of these variables is the sonic velocity, a, which is defined as

$$a = \sqrt{\gamma R T} \tag{5}$$

or in dimensionless terms as

$$A = \frac{a}{a_o} \tag{6}$$

where a_o is the sonic velocity at some reference state.
The entropy of the fluid above that at the reference state
is also used. A convenient dimensionless entropy, S, is
defined as

$$S = \frac{S'}{\gamma R} \tag{7}$$

where S' is the dimensional entropy.

Two variables, known as the Riemann variables or
characteristics, are to be utilized in this method of
solution. These are defined as

$$P = \frac{2}{\gamma-1} A + U \tag{8}$$

and

$$Q = \frac{2}{\gamma-1} A - U \tag{9}$$

where the velocity $U = \frac{u}{a_o}$.

The governing equations can be expressed in terms of
these new variables as

$$\frac{\partial P}{\partial t} + (U + A)\frac{\partial P}{\partial x} + FAU - A^2 \frac{\partial S}{\partial x} = 0 \tag{10}$$

$$\frac{\partial Q}{\partial t} + (U - A)\frac{\partial Q}{\partial x} + FAU + A^2 \frac{\partial S}{\partial x} = 0 \qquad (11)$$

$$\frac{\partial S}{\partial t} + U \frac{\partial S}{\partial x} = 0 \qquad (12)$$

The length and time have been made dimensionless in these equations, with

$$x = \frac{x'}{L} \qquad (13)$$

$$t = \frac{a_o t'}{L} \qquad (14)$$

where L is the length of the duct.

The numerical solution of these equations by the centered difference method is much like the method described by Watts. Boundary conditions are known at each end; so the implicit difference method requires the simultaneous solution of all the finite difference equations in the three variables, P, Q, and S. This is accomplished by an algorithm for a tri-tridiagonal set of equations (4).

Alternate Method of Treating Shock. The shock will be represented by a pair of points which move through the fixed grid just as was done by Watts (1). The speed of the shock at the new time level, and, thus, its location, will not be known. However, a value for its speed will be assumed, and its location at the new time will be known subject to this assumption. A series of computations will be made from which

a new value of the shock speed is obtained. This procedure
will be repeated until convergence is obtained.

For weak shocks, the value of the Q characteristic
remains constant as the shock moves in the negative-x
direction, and the value of the P characteristic is constant
across this shock. Consequently, a much simpler method of
computing the characteristics at the shock is proposed.
Since the value of Q is known at the new time level on the
upstream side of the shock, the finite difference equations
upstream of the shock can be solved simultaneously using
this value of Q as a boundary condition. The solution of
these equations will yield the value of P at the upstream
side of the shock. For weak shocks, this is also the value
of P on the downstream side of the shock. With this value
as a boundary condition, the finite difference equations
downstream of the shock can be solved simultaneously.
A value of Q on the downstream side of the shock will result
from this solution; so that values of U and A and the shock
Mach number, M, can be obtained. These values yield a new
estimate for the shock speed, w_s, at the new time level.
If this value agrees, within a pre-set tolerance, to the
assumed value, the computations are completed at the new
time level. If not, this new estimate for w_s is used and
the iteration is continued.

For weak shocks moving in the positive x-direction, the value of P in front of the shock remains almost constant, and the value of Q is almost continuous across the shock. Thus the same procedure can be used.

For stronger shocks the exact equations for the change in P and Q across the shock must be used. The details of the method of treating stronger shocks have not been completed. However, any such method will involve the simultaneous solution of the Rankine-Hugoniot relations with equations from the finite difference grid. Also, some iteration will be necessary.

Progress on Solution. The numerical method has been developed, and a computer program is working for the numerical solution of equations (10), (11), and (12). The program for treating weak shocks is being written at this time. This project should be completed within a few months.

Nomenclature

a - local speed of sound - $\sqrt{\gamma R T}$

a_0 - speed of sound at reference temperature

A - a/a_0

B - cross sectional area of duct

F - $\frac{1}{B} \frac{dB}{dx}$

L - length of duct

M - Mach number of shock $\frac{w_s - U}{A}$

P - $\frac{2}{\gamma-1} A + U$

Q - $\frac{2}{\gamma-1} A - U$

R - specific gas constant

S' - entropy of gas

S - $\frac{S'}{\gamma R}$

T - temperature of gas

t' - time

t - $a_0 t'/L$

u - velocity of gas

U - u/a_0

w_s - speed of shock

x' - length coordinate

x - x'/L

γ - ratio of heat capacities

ρ - density

REFERENCES

(1) Watts, J. W., and D. U. von Rosenberg, *Chem. Eng. Sci.*, 24, (January 1969) 49-56.

(2) Warmbrod, John D., and Heinz G. Struck, *Application of the Characteristic Method in Calculating the Time Dependent, One-Dimensional, Compressible Flow in a Tube Wind Tunnel*, NASA TM X-53769 (August 1968).

(3) Rudinger, George, *Wave Diagrams for Non-Steady Flow in Ducts*, van Nostrand (1955).

(4) von Rosenberg, D. U., *Methods for the Numerical Solution of Partial Differential Equations*, Elsevier (1969).

Section V

Molecular Sieve Adsorption Problem

NUMERICAL SOLUTION OF MICROSCOPIC-MACROSCOPIC SYSTEMS

Introduction. The adsorption of a component from a gas stream by a bed of solid particles is a complex process. Yet, a knowledge of this process is necessary for the design of molecular sieve beds to remove carbon dioxide from the atmosphere of space vehicles and for the prediction of the behavior of these beds. At the request of the Propulsion and Vehicle Engineering Laboratory at Huntsville such a study was undertaken as part of the work performed under contract NAS8-20136.

The processes of adsorption and then desorption to regenerate the bed are carried out under different conditions; so the two processes were described by different models. A most complete description of the adsorption model will be presented first, and then the differences of the desorption model will be discussed.

The Adsorption Models. A mixture of nitrogen, oxygen, and carbon dioxide is flowed through a column packed with molecular sieve beads. During this process the carbon dioxide is adsorbed onto the surface of the beads and diffuses through pores into the interior of the beads. Heat is released onto the solid as the carbon dioxide is adsorbed. The solid and gas are, consequently, at different temperatures; so heat is exchanged between the two, and heat is conducted and convected down the bed.

Although the temperature, pressure, and molecular weight of the gas vary, the effect of these on the gas density is assumed small so that the velocity of the gas is taken to be constant.

For these conditions, a material balance on carbon dioxide in the gas phase yields

$$- \frac{P}{f\rho_g} k \, a(p - p_s) = \frac{\partial p}{\partial t} + u \frac{\partial p}{\partial x} \tag{1}$$

All the symbols are defined at the end of this paper. The first term in this equation represents the transfer of carbon dioxide from the gas phase to the surface of the solid particle under a partial pressure driving force. The term p_s is the partial pressure of carbon dioxide which is in equilibrium with the loading of carbon dioxide on the surface of the solid particle.

A heat balance on the gas phase yields

$$- \frac{1}{f\rho_g c_g} h \, a(T_g - T_s) = \frac{\partial T_g}{\partial t} + u \frac{\partial T_g}{\partial x} \tag{2}$$

The heat balance on the solid phase then yields

$$K \frac{\partial^2 T_s}{\partial x^2} + h \, a(T_g - T_s) + k \, a(p - p_s) \Delta H = \rho_s c_s \frac{\partial T_s}{\partial t} \tag{3}$$

The third term in this equation accounts for the heat released to the solid when the carbon dioxide is adsorbed. It is assumed that each solid bead at any given time and position is at a uniform temperature throughout. However, the diffusion,

by whatever mechanism, of the carbon dioxide into the interior
of the beads is accounted for by allowing the loading of carbon
dioxide on the bead to vary as a function of radial position
inside the bead.

A material balance on carbon dioxide inside the bead is
needed to define this variation: the bead is assumed to be
spherical in shape, with all beads being of the same diameter.
The one-dimensional equation for diffusion into the interior
of the beads is

$$D \frac{1}{r^2} \frac{\partial}{\partial r} \left(r^2 \frac{\partial w}{\partial r} \right) = \frac{\partial w}{\partial t} \tag{4}$$

This equation applies to each bead, and beads are located
throughout the length of the bed. The gas in contact with
each bead contains carbon dioxide at a partial pressure which
varies with both time and position.

This microscopic system must be tied to the macroscopic
gas system by a boundary condition at the surface of the beads.
This condition states that, at the surface where $r = R$,

$$- D\rho_p \left(\frac{\partial w}{\partial r} \right) + kM(p - p_s) = 0 \tag{5}$$

An equilibrium condition relating the loading at the surface
of the bead to the equilibrium partial pressure is also required.
This relation is a function of the solid temperature. For (5A)
sieve this condition is given (1) as

$$p_s = \exp\left[23.823 - \frac{9166.56}{T + 460} + 1.678 \ln w \right] \tag{6}$$

Specification of the initial condition of the bed and of the inlet conditions of the gas stream are sufficient to define the problem.

An efficient numerical method was developed for this complete model. Values of the various parameters were obtained from the report by Airesearch (1), and a number of runs were made with the program. The program did not take a large amount of computer time in the light of the complexity of the model. However, with the numerical values of the physical constants used, it was apparent from these runs that a number of other simplifying assumptions could be made.

The most significant finding was that, because of the high value of the coefficient for diffusion within the beads, the loading inside the beads was almost uniform. Consequently, the microscopic system could be represented by a single equation within the macroscopic system. In effect, the microscopic material balance of equation (4) is combined with the material balance at the surface of the bead to yield this relation, which is

$$\frac{kaM}{\rho_s} (p - p_s) = \frac{\partial w}{\partial t} \tag{7}$$

This macroscopic model is then represented by eqns. (1), (2), (3), (6), and (7). The computer program for the microscopic-

macroscopic system was simplified to describe this simpler system, and the results differed little from those of the complete system with significant savings in computer time.

Two further simplifying assumptions can also be justified. First, it was found that the longitudinal temperature variation was small; so, with the small value of K, the bed thermal conductivity, this term can be eliminated from the equation. Furthermore, h, the heat transfer coefficient between the gas and the solid was large enough that the temperature of the gas and that of the solid differed little. Thus, these two phases were assumed to be at a single temperature and eqns (2) and (3) were combined to yield the relation

$$u\frac{\partial T}{\partial x} + \left[1 + \frac{\rho_s c_s}{f \rho_g c_g}\right] \frac{\partial T}{\partial t} = \frac{ka\Delta H}{f \rho_g c_g} (p-p_s) \tag{8}$$

Equations (1), (6), (7), and (8) thus constitute the simplest model for the carbon dioxide system.

An assumption that mass transfer is rapid enough for equilibrium to exist between the partial pressure of carbon dioxide in the gas phase and the loading of carbon dioxide on the solid beads is not justified. However, the same simplified program was used for the adsorption of water vapor by a molecular sieve. For this system the mass transfer coefficient, k, is much larger than for carbon dioxide, and such an assumption is justified. Eqns. (1) and (7) can be combined to yield

$$\frac{P\rho_s}{f\rho_g M} \frac{\partial w}{\partial t} = \frac{\partial p}{\partial t} + u\frac{\partial p}{\partial x} \tag{9}$$

Equations (8) and (9) together with an equilibrium relation for the water vapor system analogous to eqn. (6) then describe this simplest system for adsorption.

Model for Desorption Process. One proposed procedure for the desorption of the carbon dioxide is to open the bed to the vacuum of deep space. The gas in the voids of the bed will quickly be exhausted, and, after this process is completed, the total pressure of gas in the voids will equal to the partial pressure of carbon dioxide that has desorbed from the bed. For any pressure drop at all, the density of the gas cannot be assumed constant, but it will be related to the temperature and pressure by the ideal gas relationship or other appropriate equation of state. The material balance in the gas phase then becomes

$$-\frac{Ka}{f} (p - p_s) = \frac{\partial \rho_g}{\partial T} + \frac{\partial (u\rho_g)}{\partial x} \tag{10}$$

and the heat balance can be obtained as

$$\frac{Ka}{f} (p-p_s) \left[\frac{\Delta H}{c_g} + T \right] = \rho_g \left[\frac{\partial T}{\partial t} + u\frac{\partial T}{\partial x} \right] + \frac{\rho_s c_s}{fc_g} \frac{\partial T}{\partial t} \tag{11}$$

Equation (7) still applies to this system, and the equilibrium relation of eqn. (6) also applies. However, a relation between the velocity and the pressure gradient is required. The report

by Airesearch ($\underline{1}$) gives an empirical relation of the form

$$u = -\frac{1}{F} \frac{\partial p}{\partial x}$$ (12)

where the coefficient F is given as a function of p. These relations are sufficient to define the problem. A numerical method for the solution of these equations was developed.

The results of this solution showed that, for the boundary conditions developed by Airesearch ($\underline{1}$), the desorption of the carbon dioxide from the beads was much slower than the flow of carbon dioxide out the bed to deep space. Consequently, the partial pressure of carbon dioxide in the void of the bed can be taken as zero for all positions in the bed. The desorption from any part of the bed is then governed simply by

$$-\frac{kaM}{\rho_s} p_s = \frac{dw}{dt}$$ (13)

and the equilibrium relationship. The solid temperature will drop, however, so a relationship to determine it is needed. This is

$$Mc_s \frac{dT}{dt} = \left[\Delta H + c_g T \right] \frac{dw}{dt}$$ (14)

At some time during the desorption process heat may be applied to the bed to increase the rate of desorption. This heating term can be included in eqn. (14). Of course, if the desorption rate is increased greatly, it may be necessary to use the more complete desorption model.

Numerical Method for Solution of Complete Adsorption Model.

The complete adsorption model consists of equations (1), (2),
and (3) to describe the macroscopic system, and equation (4) to
describe the microscopic system. These are related through
eqn. (5). The three dependent variables of the macroscopic
system are the partial pressure of carbon dioxide, p, and the
temperatures of the gas and of the solid, T_g and T_s. The
dependent variable of the microscopic system is the loading
of carbon dioxide on the solid beads, w. The partial pressure
in equilibrium with this loading, p_s is related to w by eqn. (6).

For this system of equations and unknowns a double grid of
points at each time level is set up for the finite difference
solution. These points are arranged as shown in Figure 1.
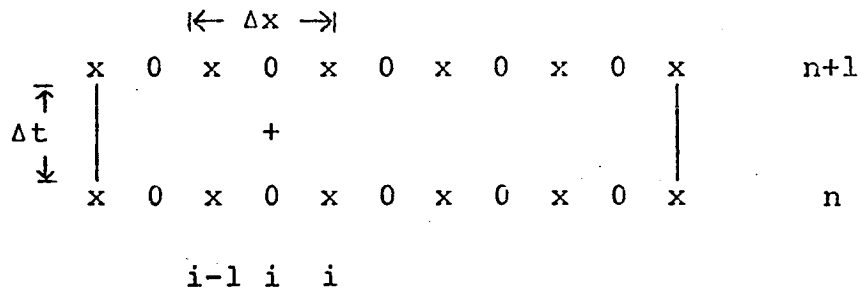The properties of the gas, p and T_g, are determined at the

```
                    |←  Δx  →|
         _    x  0  x  0  x  0  x  0  x  0  x          n+1
         ⊤ |                             |
      Δt   |            +                |
         ↓ |                             |
         _  x  0  x  0  x  0  x  0  x  0  x           n

            i-1  i  i
```

Figure 1. Arrangement of Points

points marked x; and those of the solid, w and T_s, are
determined at the points marked 0, which are half-way between
the points for the gas properties. The finite difference

analogs are written around a point in the center of a box

formed by four points for the gas properties. One of these

points is marked T in Figure 1.

The substantive derivatives of the gas properties require

that $\frac{\Delta x}{\Delta t}$ = u to minimize truncation error ($\underline{2}$).This restriction

requires the time step to be small, but it was found to be a

necessary restriction for the type of process simulated. The

finite difference analog to one of these substantive derivatives

is

$$\frac{\partial p}{\partial t} + u\frac{\partial p}{\partial x} \sim \frac{p_{i,n+1}-p_{i-1,n}}{\Delta t} \tag{15}$$

The time derivatives for properties of the solid are represented

simply as

$$\frac{\partial T_s}{\partial t} \sim \frac{(T_s)_{i,n+1}-(T_s)_{i,n}}{\Delta t} \tag{16}$$

It should be noted that solid properties with the subscript i

are at a point one-half an increment from the point where

properties of the gas phase have the same subscript.

The terms representing the interphase transfer of mass

and heat must be approximated at the centered point marked by +

in Figure 1. The solid properties are represented simply as

$$(T_s)_{i,n+\frac{1}{2}} \sim \frac{1}{2}\left[(T_s)_{i,n} + (T_s)_{i,n+1}\right] \tag{17}$$

The gas properties were originally represented by the average of the values at the four surrounding points as was done by Herron (2). It was discovered during the course of this research that the diagonal analog of

$$p_{i-\frac{1}{2},n+\frac{1}{2}} \approx \frac{1}{2}\left[p_{i,n+1} + p_{i-1,n}\right] \tag{18}$$

led to much better solutions. This discovery was applied to the countercurrent heat exchanger problem (2) and led to a publication (3) which is also a part of Section V of this report.

The solution of this set of equations proceeds first with the computation of the loading, w, and the partial pressure, p, throughout the column at the new time step from eqns. (1), (4), (5), and (6). The temperature of the gas does not appear in these equations, and the temperature of the solid is included only through the equilibrium relation, eqn. (6). The effect of solid temperature on this relation is slight enough that the temperature profile at the old time level can be used. Several runs made with iteration showed there was no discernable effect by improving the values for the temperature in the equilibrium relation.

All the beads within one increment of the bed, between two points marked by x, were assumed to have the same values of temperature and carbon dioxide loading and to be located at the point marked by 0 at the center of the increment. A grid of points in the radial direction within the bead was set up so that the gradient of w within the bead could be computed from

the Crank-Nicolson finite difference equation analogous
to eqn. (4).

The solution was begun by computing the loading distri-
bution within the bead at the point nearest the bed inlet.
The analog to the boundary condition of eqn. (5) contains
the unknown value of p at the point one-half increment beyond
the solid point. However, this value can be obtained in terms
of p_s at the solid point from an analog to eqn. (1). Eqn. (6),
the equilibrium relation, then is the third equation required.
Thus, with a minimum of iteration the loading distribution
within the bead and the carbon dioxide partial pressure at the
next gas point are obtained. This program is used to compute
these values for the entire bed at the new time step.

Once the profile of p as a function of distance at the
new time level is known, the distributions of T_g and T_s with
distance can be computed from the finite difference analogs
to eqns. (2) and (3). Eqn. (3) is second order in T_s, and
there is a boundary condition at each end. Consequently, the
values for both temperatures at all grid points at the new
time level must be determined simultaneously. This solution
is readily performed by the algorithm for bi-tridiagonal
equations ($\underline{4}$).

This method of numerical solution was programmed and gives
very good results. It was discovered from the results of
studies with this program that simplifications in the model

could be made. The first simplification entailed only the replacement of the finite difference grid within a particle by a single value of w at each solid point. This shortened the running time considerably. The simultaneous solution of the entire temperature distributions was still required.

For the simplest model in which the same temperature is assigned to both solid and gas and conduction is neglected, the temperature profile can be computed one point at a time. This model is described by eqns. (1), (7), and (8) together with the equilibrium relation. The program for this model takes only a small amount of computer time and gives results which compare favorably with those obtained from the most complex model. The uncertainty in the values of the various coefficients does not warrant use of a more complex model. Furthermore, for the purposes of the laboratory which requested the program, this simple program is sufficiently accurate. It is important, however, that it was compared with a much more complete model so that the additional simplifying assumptions could be justified.

Numerical Method for Solution for Desorption Model. The numerical solution of the desorption process was more difficult even for the simple case with only one temperature variable and with uniform loading within the beads. The additional variable u, the gas velocity, was determined at the points

marked by 0 in Figure 1, so that the velocity was one-half way between points where pressure was determined. This arrangement was convenient for the numerical solution of eqn. (12). The equations for desorption contain more non-linear terms since the derivatives of gas density, ρ_g, must be expanded to derivatives of p and T_g through the equation of state. Also, the boundary conditions are uncertain. An empirical boundary condition on pressure at the outlet of the bed is presented by Airesearch (1). This relation accounts for pressure drop in the duct connecting the end of the bed to deep space.

As a result of this boundary condition, an initial pressure distribution inside the bed must be assumed to begin the numerical solution. The only assumed distribution which would yield reasonable results with the program was one of zero pressure throughout the bed. Later analysis of the relations and coefficients confirmed this value to be reasonable. Thus, it was determined that the process of desorption was much slower than the outflow of the gas from the duct, at least at the temperatures of the unheated bed.

Status. The computer programs have been made available to the laboratory which requested them. A few comparisons of other simple models of this process with the models discussed above may be made. A most complete description of this work in the form of a doctoral dissertation is being prepared.

Nomenclature

a - surface area of beads per unit volume of bed available for interface transfer

c_g - heat capacity of gas

c_s - heat capacity of solid

D - coefficient of diffusion for adsorbed species inside bead

f - void fraction in bed

h - coefficient of heat transfer between gas and solid

ΔH - heat of adsorption

k - coefficient of mass transfer between gas and solid

K - thermal conductivity of bed

M - molecular weight of adsorbed species

p - partial pressure of adsorbed species

p_s - saturation partial pressure of adsorbed species

P - total pressure

r - radial position inside bead

t - time

T - temperature

T_g - temperature of gas

T_s - temperature of solid

u - gas velocity

w - loading of adsorbed species on solid

x - distance position in bed

ρ_g - gas density

ρ_p - particle density of bead

ρ_s - bulk density of solid in bed

Literature Cited

(1)   A Study on the Properties of Solid Adsorbents for
        the Design of Regenerative CO_2 Removal Systems,
        final report on Contract NAS9 - 3541 prepared by
        Airesearch Manufacturing Division for NASA Manned
        Spacecraft Center, February 1968.

(2)   Herron, E. H., Jr., and D. U. vonRosenberg,
        Chem. Eng. Sci., 21, (April 1966) 337.

(3)   vonRosenberg, D. U. and D. E. Mount,
        Chem. Eng. Sci., 24, (March 1969) 619.

(4)   vonRosenberg, D. U., Methods for the Numerical
        Solution of Partial Differential Equations,
        Elsevier, 1969.

Improved numerical solution of a countercurrent heat exchanger†

(First received 13 September 1968; in revised form 28 September 1968)

Dear Sir:

In a previous paper[1] an efficient numerical method for the solution of pure convective transport problems with split boundary conditions was described. The one shortcoming of this method was an oscillation in the neighborhood of a discontinuity in one of the dependent variables as shown in Fig. 2. Although the oscillation did not remain in the system after the discontinuity had flowed out of the system and later results were not distorted for some applications. it is desirable to obtain a numerical solution without this oscillation. Recently, it was discovered that the oscillation can be eliminated by a minor modification which does not complicate the solution nor decrease its efficiency.

The system used to describe the method is a countercurrent heat exchanger described by

$$\frac{\partial u}{\partial t} = Y_1(v - u) - V_1\frac{\partial u}{\partial x} \tag{1a}$$

$$\frac{\partial v}{\partial t} = -Y_2(v - u) + V_2\frac{\partial v}{\partial x}. \tag{1b}$$

Boundary conditions for the test problem are

$$u(x, 0) = 0 \text{ for all } x$$
$$u(0, t) = 100 \text{ for all } t$$
$$v(x, 0) = 0 \text{ for all } x \tag{1c}$$
$$v(L, t) = 0 \text{ for all } t.$$

Centered difference equations were used to replace Eq. (1) for the numerical solution. Location of the center point for the analogs is shown in Fig. 1. The only analog which was modified from those described in the original paper is the one for $u_{j+1/2,n+1/2}$ used in the interphase heat transfer terms. In the original method, the analog used was

$$u_{j+1/2,n+1/2} \approx \tfrac{1}{4}(u_{j+1,n+1} + u_{j+1,n} + u_{j,n+1} + u_{j,n}). \tag{5}$$

It is this analog which causes the oscillation. For the modified method, this temperature is replaced by the average of the two values lying along the diagonal in the direction of flow; namely,

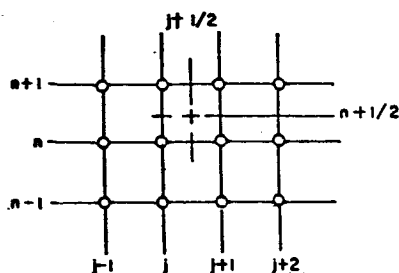$$u_{j+1/2,n+1/2} \approx \tfrac{1}{2}(u_{j+1,n+1} + u_{j,n}). \tag{5a}$$

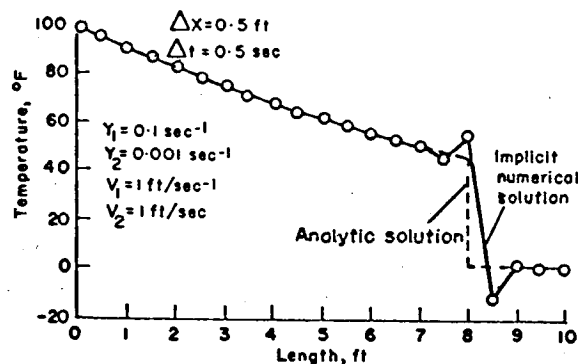Fig. 1. Physical representation of centered differencing.

Fig. 2. Temperature profile of inner fluid for 100°F step change at exchanger inlet after 8 sec. Implicit numerical solution vs. analytic solution.

This analog preserves the second-order-correctness of the method in both space and time. Furthermore, the resulting finite difference equations fit the bi-tridiagonal form and can be solved by the algorithm available. The shifted numbering system described in the original paper should be retained, and the relation between space and time increments that minimizes truncation should also be used.

Results obtained using the analog of Eq. (5a) show no oscillation whatsoever. In fact, these results agree to within 0·01 per cent of the analytic solution for the case shown in Fig. 2 at all points. This close agreement was obtained using twenty increments for the entire exchanger length. There was no distortion whatsoever at the discontinuity. This behavior makes the solution of the modified system useful for representing hyperbolic systems in controller studies.

No detailed analysis of the two analogs has been made. However, it is apparent that the four-point analog of Eq. (5) introduces into its equation a value of the dependent variable, $u_{j+1,n}$, which is ahead of the discontinuity. Actually, the function u is double valued at the discontinuity, and the inclusion of the value at this point gives rise to the oscillation. The diagonal analog of Eq. (5a) does not contain values on both sides of the discontinuity, so no oscillation occurs.

A number of analogs for the unperturbed temperature, v, were used in conjunction with analog of Eq. (5a) for u. The four-point analog of Eq. (5) for v gave the best results, although results using the diagonal analog Eq. (5a) were satisfactory. As a general rule. the four-point analog can always be used if there is no discontinuity in the dependent variable, but the diagonal analog should be used when a discontinuity is introduced into a variable.

Tulane University   D. U. VON ROSENBERG
New Orleans, Louisiana, U.S.A.   D. E. MOUNT

REFERENCES

[1] HERRON E. H. and VON ROSENBERG D. U., *Chem. Engng Sci.* 1966 21 337.